Universidad de Oviedo

Ph.D. Programme in Energy and Process Control

Dissertation Thesis

Study of the Cooling of Steel Mills Lamination Coils

Ph.D. Candidate: Doddy Irawan

Advisor: Jorge Luis Parrondo

Supervisors: Antonio José Gutiérrez Trashorras

Eduardo Álvarez Álvarez

This doctoral thesis in an outcome of a full-time doctoral study program at the Department of Energy
University of Oviedo

Doctorando:Doddy Irawan

Tutor:Jorge Luis Parrondo

Directors: Antonio José Gutiérrez Trashorras

Eduardo Álvarez Álvarez

Those who are persistent will succeed
Those who are patient will be fortunate
Those who follow God`s path will reach the goal

ACKNOWLEDGEMENT

I would like to express my gratitude to peoples at Department of Energy for the Support and encouragement given to me in recent years, without which it would have been impossible for me to carry out this work. In particular, I would like to acknowledge for the help and knowledge provided.

I would also like to immensely thank my supervisors, Prof. Dr. Antonio José Gutiérrez Trashorrass, Prof. Dr. Eduardo Álvarez Álvarez, and Prof. Dr. Eduardo Blanco Marigorta, for the patient guidance, encouragement, and advice they have provided throughout my time as his their student. I have been incredibly lucky fortunate to have supervisors who cared so much about my work, and who responded to my questions and queries so promptly.

My sincere thank also goes to my tutor, Prof. Dr. Jorge Parrondo, who accepted me as a doctoral student at the Department of Energy at Universidad de Oviedo. In addition to his being a tutor, he has offered me the greatest assistance that he is like a father to me during my stay in Spain.

I am also indebted to Erasmus Mundus Swap and Transfer (SAT) who has funded my doctoral studies for 34 months, and this has been an amazing experience for me.

I must express my gratitude to my family, especially my mother, my wife, my son, my daughters, my brother and sister for their continuous support and encouragement. In addition, a special thank should go to my wife for her patience in facing the hardship during my study.

I would also like to thank Professor in Fluid Mechanics and Thermal Engine, and Machine, as well as my best friends Andreas and Irene for being helpful during my study. My thanks also go to Celia, Ana, Luis, Li, and Frank for their warm friendships. I love you all.

RESUMEN:

En los procesos de producción de acero laminado en caliente el control del enfriamiento después de terminar el laminado juega un papel importante en la microestructura final y en las propiedades mecánicas del producto. La bobina de acero producida en una planta de acero después de la laminación debe ser enfriada desde una temperatura alta hasta la temperatura ambiente, para ser transportada y vendida. El enfriamiento de la bobina dura entre cuatro y seis días, dependiendo de las condiciones climáticas. Normalmente, la bobina se almacenará en una nave industrial hasta que alcance la temperatura ambiente.

En este trabajo se ha desarrollado una nueva metodología para obtener la ley de enfriamiento de las bobinas. Se utilizaron modelos numéricos para simular y estudiar la velocidad de enfriamiento de la bobina y calcular los valores de los parámetros involucrados en la ley de enfriamiento. La geometría de la bobina consiste en un cilindro con una altura entre 1,6 m y 1,8 m, y un diámetro exterior de 0,9 m. Las bobinas también tienen un hueco coaxial de pequeño diámetro. Las simulaciones del proceso de enfriamiento de la bobina se realizaron mediante técnicas de CFD con el software ANSYS FLUENT en condiciones de régimen transitorio para geometrías 2D (bidimensionales) y 3D (tridimensionales) para obtener la tasa óptima de disminución de la temperatura.

Se simularon diferentes geometrías correspondientes a una única bobina en posiciones horizontal y vertical, y sus combinaciones en grupos de varios niveles de altura. Específicamente, se utilizaron modelos 2D de simetría axisimétrica y 3D para estudiar el enfriamiento natural de las bobinas de acero. Ambos modelos son consistentes y los resultados obtenidos son bastante similares. Se tarda cinco días en que una bobina de acero se enfríe desde 673,15 K a temperatura ambiente, y la función que relaciona la temperatura promedio de las bobinas con el tiempo es prácticamente idéntica para ambas posiciones de la bobina. También se estudió el efecto de la capacidad calorífica específica variable y de la conductividad térmica Cilíndrico-ortotrópica con diferentes temperaturas y presiones entre capas..

Finalmente, se obtuvo una ecuación (ley de enfriamiento) basada en términos logarítmicos y arctangentes para cada uno de los casos estudiados. Esta ecuación describe los efectos de conducción, convección y radiación y se ha definido y verificado teniendo en cuenta las restricciones límite del problema.

ABSTRACT:

In the hot-rolled steel production processes the cooling control after finishing rolling plays an important role on the final microstructure and mechanical properties of the product. Steel coil produced at a steel mill after the lamination must be cooled from a high temperature to the ambient temperature, to be transported and sold. Coil cooling takes between four and six days depending on weather conditions. Usually, the coil will be stored in a warehouse until it reaches the ambient temperature.

In this work, a new methodology to obtain the coils cooling law has been developed. Numerical models were used to simulate and study the rate of the coil cooling and to calculate the values of the parameters involved in the cooling law. The geometry of the coil is a cylinder with a height between 1.6 m and 1.8 m and an outer diameter of 0.9 m. The coils also have a coaxial hollow of small diameter. The simulations of the coil cooling process were performed by using CFD techniques with ANSYS FLUENT software in transient conditions for 2D (two-dimensional) and 3D (three-dimensional) geometries to obtain the optimal rate of temperature decrease.

Different geometries corresponding to a single coil in horizontal and vertical positions and their combinations in groups of various height levels were simulated. Specifically, 2D axisymmetric and 3D simulation models were used to study the steel coils natural cooling. Both models are consistent and the results obtained are quite similar. It takes five days for a steel coil become cooled from 673.15 K to ambient temperature, and the relationship between average coils temperature and time is nearly equal. The effect of variable specific heat capacity and Cyl-orthotropic thermal conductivity with different interlayer pressures and temperatures was also studied.

Besides, an equation (cooling law) based on logarithmic and arctangent terms was obtained for all cases. This equation describes conduction, convection and radiations effects and has been defined and verified considering the boundary restrictions of the problem.

TABLES OF CONTENTS

LIST OF FIGURES

LIST OF TABLES

NOMENCLATURE

List of Symbols
Alphanumeric Symbols

A	Area
A_2, A_3	profile type
a	acceleration, the speed of a pressure wave
a_x, a_y, a_z	acceleration components
B	Bulk modulus of elasticity, free surface width
b	Channel bottom width
C	Centroid, Chezy coefficient
C_1, C_3	Drag profile type
C_D	Drag coefficient
C_d	Discharge coefficient
C_f	Skin-friction coefficient
C_H	Head coefficient
C_L	Lift Coefficient
C_P	Pressure recovery factor, pressure coefficient
C_{NPSH}	Net positive suction heat coefficient
C_Q	Flow rate coefficient
C_V	Velocity coefficient
$C_{\dot{W}}$	Power coefficient
c	Specific heat, speed of sound, chord length, celerity
c_f	Local skin-friction coefficient
c_p	Constant pressure specific heat
c_v	Constant volume specific heat
c.s.	Control surface
c.v.	Control volume
D	Diameter
Dt	Substantial derivative
d	Diameter
dx	Differential distance
$d\theta$	Differential angle
E	Energy, specific energy, coefficient
E_c	Critical energy
EGL	Energy grade line
Eu	Euler number
e	The exponential, specific energy, wall roughness height, pipe wall thickness
exp	Exponential
$\mathbf{F}$	Force vector
F	Force magnitude
F_B	Buoyant force
F_H	Horizontal force component
F_V	Vertical force component

F_W	Body force equal to the weight
f	Friction factor, frequency
G	Center of gravity
$\overline{GM}$	Metacentric height
$\mathbf{g}$	Gravity vector
g	Gravity
H	Enthalpy
H_D	Design head
H_P	Pump head
H_T	Turbine head
HGL	Hydraulic grade line
h	Distance, height, specific enthalpy
h_j	Head loss across a hydraulic pump
I	Second moment of an area
$\bar{I}$	Second moment about the centroidal axis
I_{xy}	Product of inertia
$\hat{\imath}$	Unit vector in the x-direction
$\hat{\jmath}$	Unit vector in the y-direction
$\hat{k}$	Unit vector in the z-direction
K	Thermal conductivity, flow coefficient
K_c	Contraction coefficient
K_e	Expansion coefficient
K_{uv}	Correlation coefficient
k	Ratio of specific heats
L	Length
L_E	Entrance length
L_e	Equivalent length
ℓ	Length
ℓ_m	Mixing length
M	Molar mass; Mach number; Momentum function
M	Mach number
M_1, M_2, M_3	Profile type
m	Mass, side-wall slope, constant for curve fit
$\dot{m}$	Mass flux
$\dot{m}_r$	Relative mass flux
$\dot{m}_a$	Added mass
m_1, m_2	Side-wall slopes
$\dot{mom}$	Momentum flux
N	General extensive property, an integer, number of jets
NPSH	Net positive suction head
n	Normal direction, number of moles, power-law exponent, Manning
$\hat{\boldsymbol{n}}$	Unit normal vector
P	Power, force, wetted perimeter
p	Pressure
Q	Flow rate (discharge), heat transfer

Q_D	Design discharge
$\dot{Q}$	Rate of heat transfer
q	Source strength, specific discharge, heat flux
R	Radius, gas constant, hydraulic radius, radius of curvature
Re	Reynolds number
Re_{crit}	Critical Reynolds number
R_u	Universal gas constant
R_x, R_y	Force components
r	Radius, coordinate variable
$\mathbf{r}$	Position vector
S	Specific gravity, entropy, distance, slope of channel
S_1, S_2, S_3	Profile type
S_c	Critical slope
St	Strouhal number
$\mathbf{S}$	Position vector
S_0	Slope of channel bottom
s	Specific entropy, streamline coordinate
$\hat{\mathbf{s}}$	Unit vector tangent to streamline
sys	System
T	Temperature, torque, tension
t	Time, tangential direction
U	Average velocity
U_∞	Free-stream-velocity away from a body
u-x	Component velocity, circumferential blade speed
u'	Velocity perturbation
$\tilde{u}$	Specific internal energy
$\bar{u}$	Time average velocity
u_τ	Shear velocity
V	Velocity
V_c	Critical velocity
V_{ss}	Steady-state velocity
$\mathbf{V}$	Velocity vector
$\bar{V}$	Spatial average velocity
$\forall$	Volume
V_B	Blade velocity
V_n	Normal component of velocity
V_r	Relative speed
V_t	Tangential velocity
v	Velocity, y-component velocity
v'	Velocity perturbation
$v_r v_z\, v_\theta\, v_\phi$	Velocity components
W	Work, weight, change in hydraulic grade line
$\dot{W}$	Work rate (power)
$\dot{W}_f$	Actual power
We	Weber number
$\dot{W}_S$	Shaft work (power)

ω - z	Component velocity, velocity of hydraulic bore
X_T	Distance where transition begins
x	Coordinate variable
x_m	Origin of moving reference frame
$\tilde{x}$	Distance relative to moving reference frame
$\bar{x} - x$	Coordinate of centroid
Y	Upstream water height above top of wier
y	Coordinate variable, flow energy heat
y_c	Critical depth
z	Coordinate variable
α	Angle, angle of attack, lapse rate, thermal diffusivity, kinetic-energy correction factor, blade angle
β	Angle, momentum correction factor, fixed jet angle, blade angle
Δ	A small increment
∇	Gradient operator
∇^2	Laplacian
δ	Boundary layer thickness
$\delta(x)$	Dirac-delta function
δ_d	Displacement thickness
δ_v	Viscous wall layer thickness
ε	A small volume
ε_{xx}, ε_{xy},ε_{xz}	Rate-of-strain components
ϕ	Angle, coordinate variable, velocity potential function, speed factor
Γ	Circulation, vortex strength
γ	Specific weight
η	A general intensive property, eddy viscosity, efficiency, a position variable
η_P	Pump efficiency
η_T	Turbine efficiency
λ	Mean free path, constants, wavelength
μ	Viscosity, double strength
ν	Kinematic viscosity
π	A pi term
θ	Angle, momentum thickness, laser beam angle
ρ	density
Ω	Angular velocity
Ω_P	Specific speed of a pump
Ω_T	Specific speed of s turbine
Ω	Angular velocity vector
σ	Surface tension; Cavitation number. Circumferential stress
σ_{xx}, σ_{yy},σ_{zz}	Normal stress component
τ	Stress vector

$\bar{\tau}$	Time average vector
$\tau_{xy}\,\tau_{xz}\,\tau_{yz}$	Shear stress components
ω	Angular velocity, vorticity
$\boldsymbol{\omega}$	Vorticity vector
ψ	Stream function
$\frac{\partial}{\partial x}$	Partial derivative

CHAPTER I. INTRODUCTION

1.1. Steel Industry

1.1.1. Steel industry in the world

The history of the global steel industry development was remarkable. Steel industry is a strategic industry in the world. Asian countries began to develop the steel industry so that the western nations no longer take control of it because many factors have changed such as the cost of materials and technology. Government regulations in Asian countries are very influential and profitable for the companies and the higher growth of the steel industry.

The industrial revolution that occurred in the 19th century was the processing of real steel at great or small scale. The significant change took place with the latest steel processing technology such as Bessemer process. In 1854, the Bessemer process was developed by the English industry for the production on a large scale and eventually was spread throughout Europe and the United States.

The increase in production is high during the 20th century with the technology of large size Blast furnaces to melt iron ore. In 1954, Austria developed steel technology to become efficient. In Asia, Japan and South Korea improved casting continuous molten steel, and the plants sited in the ports that rely on large ships for the transportation of raw materials (imports and exports), so the price of steel products fell down.

In general, the steel plants should be close to the availability of minerals such as coal and iron ore. American coalmines located in Pennsylvania, Ohio, New York, and New Jersey were also pig iron mines. Birmingham area provided iron ore and coal. In late 19th century, America had mines in Minnesota and Michigan. East Asian countries such as South Korea, Taiwan, and Japan do not have the raw materials, but they provided the location of the source of raw materials for steel export to the world economy.

After World War 2, technological change was slow and there were nonexistence of competition in the world of industry. At that time, the US companies dominated the market of the world steel industry. The steel industry supported the US economy.

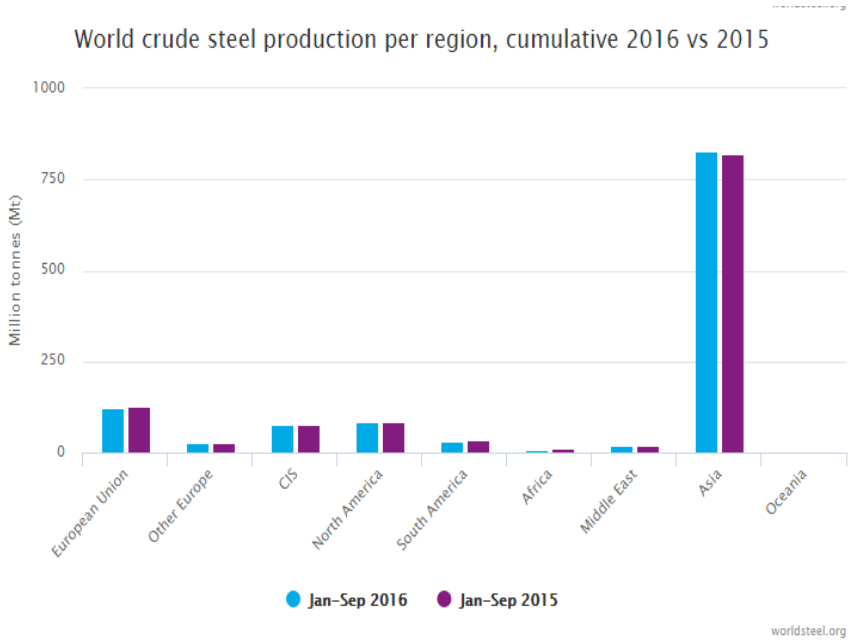

Fig.1. World crude steel production per region
(*Source: worldsteel.org*)

From fig.1 about world crude, steel production per region from cumulative 2015 and 2016 is presented. Asia had the biggest crude steel production in the world and the European Union in the second position.

1.1.2 Steel Industry in the EU

The Steel Industy is a strategic industry for economic growth, latest innovation, and full employment for the EU. Big demand of steel after the financial crisis was favorable for this sector, so the European Commission continuously encouraged their members to improve the steel industry. Steel was needed for a variety of industries such as automotive, construction, electronic and renewable energies.

Regarding steel production China was first and the EU second. EU steel production is over 177 million tons per year or 11% of world steel production. The process of the steel industry was need by downstream sectors, especially the automotive, construction, electronics, etc. So that the EU tried to boost the production of GDP in order to reach 20% in 2020. The European Union has 500 locations of steel production plants spread across 23 countries.

The policy undertakes in improving the EU steel industry, which officially formed high-level steel group to improve the competitiveness of the steel sector in 2013. The EU is providing structural funds, research funds for coal and steel, as well as policies and horizon 2020 with the aim of maintaining the competitiveness of the industry's future.

The challenge for the EU steel industry, among others, are the availability of raw materials and energy, environmental regulations and climate change, as well as the competition from Asian countries, Africa, and others.

Matters affecting the competitiveness of the steel industry in the European Union divide into six points, namely:

1. The precise rules of steel production. It is essential for sustainable development, and the internal market instrument can work well, as investors' expectations.
2. The improved market mainly in the construction and automotive fields by increasing steel demand and efficiency so that sustainable growth-oriented EU economy.
3. Restriction of trade done by non-EU countries can provide benefits for the EU member state. The European Union seeks to negotiate trade barriers by implementing market access strategy.
4. The access to raw materials is crucial for the steel making industry.
5. The EU through the WTO (world trade organization) supports the liberalization of international trade.

6. The price of energy is high, because it is up to 40% of total production costs. [1]

Steel is part of an industrial cycle that is closely related to various fields such as automotive, construction and electronics, mechanical and electrical. The economic crisis has led to a significantly decline in manufacturing activity and steel demand by 27% from before the financial crisis. [2]

Steel is an essential material in construction and manufacturing. However, some trends in steelmaking technology and steel use could affect steel demand. Design and innovation process innovation can be expected to be the key drivers for such trends. That is an area where Europe can lead as steel making technology.

About the demand, construction of power stations, including on- and off-shore wind farms, energy transmission, housing and the transport sector will continue to provide new opportunities for innovative steel products.

The improvement of competitiveness must increase the value-added steel products as a differentiator from competitors. Studies of OECD value added steel products is still limited to the share of steel demand due to intense competition. Regularly steel production costs are very high and require substantial investments in research and development (R&D). [3]

According to the study of N. Pardo, J.A. Moya, K. Vatopoulos in 2012, energy prices fluctuate significantly influencing energy prices in the future, and this is a challenge for policy makers. [4]. A second study by the global commission on the economy and climate shows the efficient cost recovery in 2030 and the payback period is two years, with a margin increase in CO_2 emissions of approximately 20%. Meanwhile, in 2030, for a payback period of six years, the margin improvement in CO_2 emissions is the range between 50% and 65%. [5]

Reduce input costs, due to the high investment required energy efficiency and policies must take into account the impact on competitiveness. EU Commission will monitor the consequences or impacts caused by CO_2

emmisons to contribute to a sustainable development (Directive on Energy Efficiency). [6].

The success of technology in reducing CO_2 emissions is crucial. The challenge is the high cost and public awareness and acceptance that has been presented at on the Commission's Communication on the Future of Carbon Capture and Storage in Europe. [7].

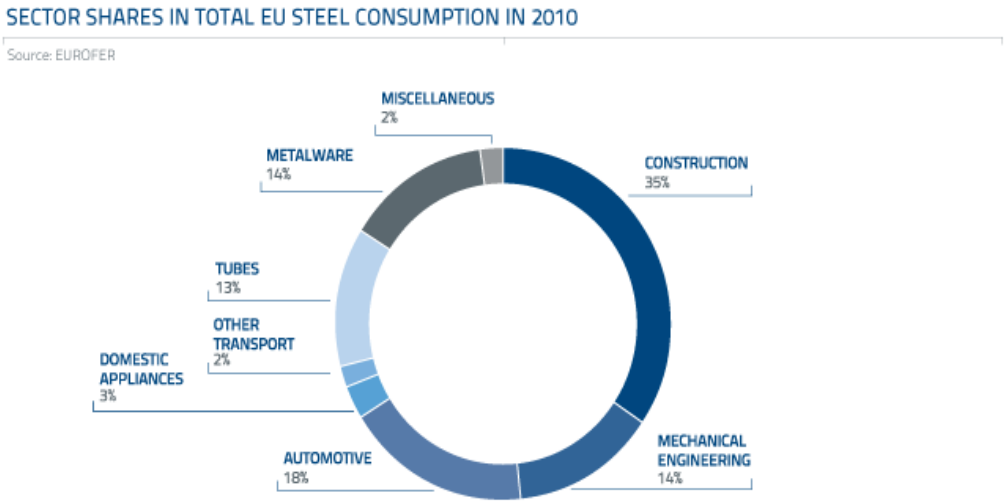

Fig.2. Total EU Steel Consumption in 2020
(*Source: http://www.eurofer.org*)

Figure 2 is a chart of total EU steel consumption forecasted for 2020. It shows that the consumption of steel will be: construction sector 35%, automotive 18%, mechanical engineering 14%, metal ware 14%, tubes 13%, domestic appliances 3%, and other transport 2%, miscellaneous 2%.

Europe's steel industry is essential for employment, innovation, added value creation and sustainable development within the Union.

Figure 3 shows a European steel map. The red color indicates the primary steelmaking (blast furnace and blast oxygen furnace) countries or cities. The blue color, secondary steel making (electric arc furnace) and the yellow color, processing of steel.

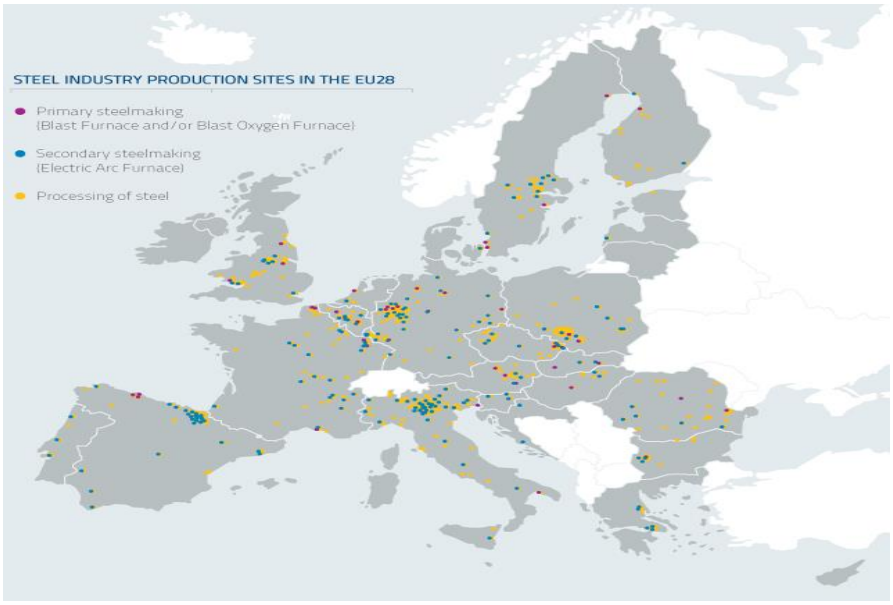

Fig.3. European Steel Map
(*Source: http://www.eurofer.org*)

1.1.3 Steel Industry in Spain

Vizcaya, Cantabria, Asturias, and Sagunto (Valencia) are the main provinces that have a steel industry in Spain. In 1960, the Spanish steel production reached 1.9 million tons and 11.1 million tons in 1975. It made the Spanish manufacturer is the fifth in Europe and thirteenth in the world ranking. The economic crisis in steel consumption nearby 50% but the early 80s fixed production reached 13 million ton reached 14 million tons in 1985. Spain reduced the overall production capacity. In 1986 it decreased by 16% to just 11.8 million tons and dropped lower in 1987. The Spanish government was restructuring the steel industry in 1980. [8]

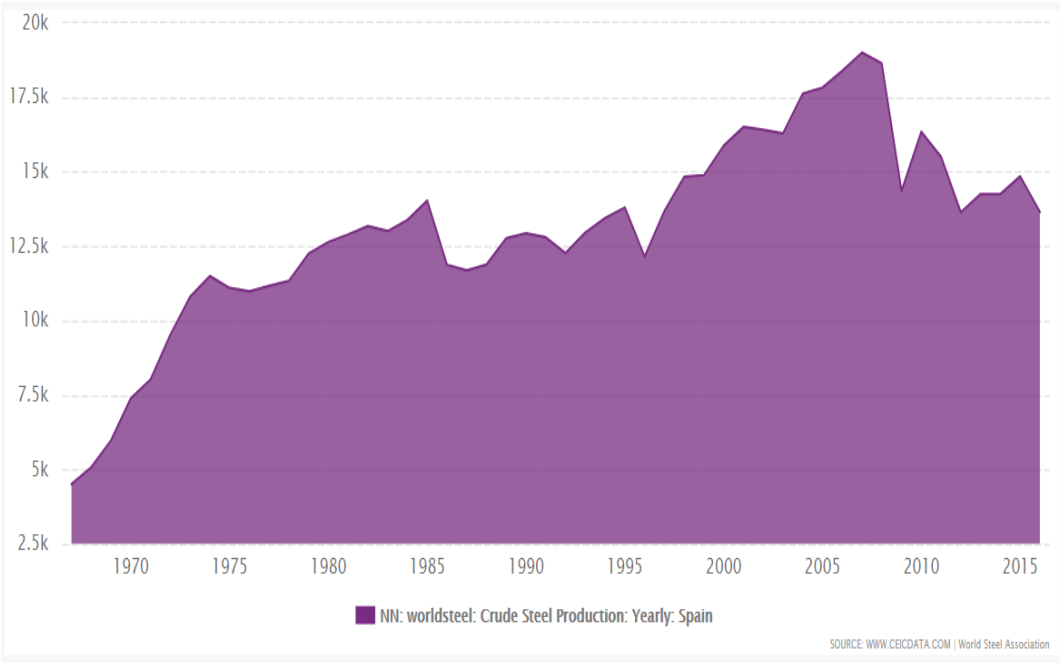

Fig.4. Total Production Crude Steel
(https://www.ceicdata.com/en/indicator/spain/crude-steel-production)

Figure 4 is shown Spain's crude steel production was reported at 13,654.41 tons in December 2016. It recorded a decrease of the previous number of 14,845.00 tons for December 2015. Spain's crude steel production data is updated yearly, averaging 13,093.50 tons from December 1967 to 2016. The data reached highest value of 18,999.00 tons in 2017 and a record low 4,512.00 tons in 1967. Spain's crude steel production data remains active status in CEIC and is reported by World Steel Association. [9]

The Basque region plays the main role in the Spanish steel industry, providing one-third of the country's entire steel production. In particular, liquid steel production by the Basque region in 2013 accounted for 29 percent of overall Spanish liquid steel production, while total steel output capacity in the Basque country was 39.1 percent of Spanish steel production capacity. Spanish production includes both blast furnace and electric arc furnace (EAF) facilities, with EAF mills accounting for the majority share (10.6 million tons in 2013) and the remainder produced by blast furnaces (3.1 million tons in 2013).

Crude steel production in Spain grew 0.7 percent on year in 2013, resulting in a total of 13.7 million tons of carbon steel production, while in February 2014 Spanish crude steel producers reached a total output of 2.30 million tons, 10.6 percent higher than the 2013 February level. Spanish production of stainless steel and special steel totaled 13 million tons and 14 million tons respectively in 2013, maintaining the levels reached in 2012. Flat products accounted for 12 million tons of overall Spanish finished steel production in 2013, while great product output amounted to 8 million tons in the given year. However, total steel exports from Spain in 2013 reached 9.7 million tons in 2013, exceeding the steel import volume of 7.6 million tons for the same year. These figures compare with exports of eight million tons and imports of over 14 million tons in 2007. Currently, Spain has enough capacities to produce and cover steel needs in the domestic market, and, following European market trends and demand, mainly focused on export supplies, mainly to other EU countries as well as to Latin America.

The focus on export is a common tendency for Spanish suppliers, and it is caused not only by modest demand in the local market but also by the energy reform in Spain that was initiated by the government in July 2013 and which canceled subsidies for electricity costs. According to this reform, the costs of electricity have increased several times, so higher electricity costs have affected production costs, and as a result, steel prices have become stable at high levels.

International steel suppliers are interested in the Spanish market and keep stock volumes at their service and warehousing facilities. For instance, a distributing service center is Tata Steel Layde Steel. The company functions as a warehouse. Tata's products are distributed in the Spanish market and the EU. At the same time, it operates as a processor of cold rolled products.

Steel plant equipment producers, as well as research and innovation centers, occupy another notable part of the Spanish steel market, with 75 companies. Including ATHADER S.L., JAURE S.A, TALLERES JACO INDUSTRIALS S.L., GLUAL HIDRAULICA S.L., TECNALIA Research,

and Innovation Center, and INGETEAM POWER TECHNOLOGY S.A. Due to fulfilled capacity potential in the Spanish market, many of these companies highly focused on the export of their services and machines, with exports making up 45-85 percent of their sales volumes in total. [10]

1.2 Energy requirements in steel industry

Nowadays, almost all-human activity is highly dependent on energy. Many support tools, such as engine, household appliances, and industrial machines cannot operate without power. Utilization of non-renewable energy in excess can cause an energy crisis. Energy has become an important component for human survival because almost all activities of human life rely heavily on the availability of sufficient energy. The next few years, humanity will still depend on fossil energy sources. It is necessary to meet the energy require of humans with energy resources on a large scale. Renewable energy sources are difficult to manage on a large scale because of fluctuations in the potential and the economic level that can´t compete with conventional energy.

Energy scarcity occurs in many countries because of human population continue to grow year after year, and consequently, energy demand for is also increasing. Energy sources can classify into two groups, namely renewable energy and non-renewable energy. Renewable energy will utilized continuously as the wind, water, the sun. [11] Humans cannot consume this energy throughout time. Renewable energy is environmentally friendly energy or "green energy." This energy has no impact on global warming.

The iron and steel manufacturing is one of the most energy and carbon-intensive industries in the world. Iron and steel making processes are still mostly coal-based and thus highly dependent on fossil fuels, releasing a substantial amount of CO_2 [12,13]. It is the second largest consumer of industry, consuming around 616 Mtoe (million tons of oil equivalent) (25.8 EJ) and is recognized one of the biggest industrial sources of direct CO_2 emissions (2.3 Gt in 2007) [14]. According to the Intergovernmental Panel on Climate Change (IPCC), the steel industry accounts for 4–5% of the total world CO_2 emission. International Energy

Agency (IEA) reported that CO_2 emissions from manufacturing industry account for approximately 40% of the total CO_2 emissions worldwide [4] and iron and steel manufacturing sector contributes the biggest share of around 27% of the global manufacturing sectors [15].

However, steel is considered to be one of the most important and useful metals in the world, and it continues to be the dominant global metal production [16]. The rate of steel output and consumption in the world has been increasing considerably for the last ten years, from 850 million tons (Mt) in 2000 to 1537 Mt in 2011 and has accelerated since 2002[17]. In 2013, the steel industries produced 1606 Mt of crude steel worldwide [18] with an average annual growth rate of around 5% [19].This significant increase in steel production for human needs will drive a significant intensification in the total industrial energy use and CO_2 emission. Therefore, to address the global warming and climate change issues are strategically important for the steelmaking industry to reduce significantly CO_2 emission. The reduction of carbon dioxide emissions from the steel mill can achieve in three areas: reducing steel demand by increasing steel recycling and innovating in steel manufacturing technologies [20]. Due to the consistent growth in steel consumption and the shortage of available high-quality and low price of steel scraps to meet the demand, development, and implementation of new CO_2 breakthrough technologies seems to be the only way to reduce substantial emissions[21,22]. Consequently, researches and developments of carbon reduction programs and technologies are necessary for steel industry as a solution to mitigating the climate change, despite iron and steel making processes are complex in nature [23].

Industry accounts for about 30% of global final energy use and almost 40% of global emissions attributed to industrial activities (IEA 2010). Rising energy prices and requirements to reduce CO_2 emissions are a great concern for energy efficiency measures are there for an important issue. Energy efficiency measures include, for example, 1) production planning; 2) investment in energy-efficient equipment, 3) recycling of energy in the industrial manufacturing process; and 4) recovery of excess energy and subsequent utilization in another process. Heat

recovery can use in its original form or converted into other energy forms. Recently, technologies for the recovery and use of excess industrial heat have gained increased attention because they offer an opportunity for the industry to be more energy efficient and, at the same time, reduce its CO_2 emissions. The iron and steel industry is an intensive energy consumer. In Europe, it means 19% of the final energy consumed in an industry [24].

In recent years, the iron and steel industry has done efforts to reduce the energy consumption and to recovery heat loss. Some of the technologies under research can have an important impact on the reduction of CO_2 emissions in European industry, according to the bottom-up model presented by [25]. The production of steel divided in integrated steelmaking and electric steelmaking. The first route produces steel from iron ore in blast furnaces and in the second route, an electric arc furnace melts scrap. The integrated steelmaking route consumes five times the primary energy consumed for electric steelmaking according to [26]

The energy intensive in iron and steel industry often conducts production processes at high temperatures. The steel industry has experienced significant advances in the development of new technique for the emissions reduction and the energy efficiency. One of the possible events is the energy recovery from coils process. The goal was to analyze an innovative heat recovery solution for heat recovery solution to accomplish energy efficiency opportunities, increase the sustainability, synergies with industrial [27]. The iron and steel industry faced with a broad range of environmental concern that fundamentally related to high-energy requirements, material usage, and the by-products associated with generating enormous quantities of steel. Steel produced after several processing steps, including iron making, primary and secondary steelmaking, casting, and hot rolling. These processes followed by various fabrication processes: cold rolling, forming, forging, joining, machining, coating, and heat treatment. Steel industry produces steel from raw materials (e.g. iron ore, coal, and limestone) or recycling steel scrap. High-temperature waste heat from the iron and steel industry, as shown in figure 5, is mainly stored in products, molten slag, and waste gas [28].

Molten slag, as a kind of by-product during the steelmaking process, exhausted in extremely high temperature and thus, it carries a great deal of high-grade heat accounting for 10% of waste energy in the steel industry and 35% of high-temperature waste heat (figure 5). Unfortunately, this amount of heat is one of the few high-temperature waste heat resources that have not well recycled in the entire steelmaking industry due to immature heat recovery technologies [29].

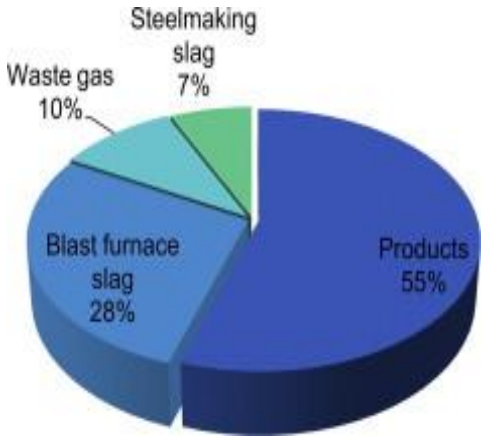

Fig.5. Distribution of steel industry high-temperature waste heat

The slag products have an equivalent value: the indirect reduction of CO_2 emission in different industrial processes. [30] For example, It estimated that 2002, the use granulated and pelleted slags instead of limestone ($CaCO_3$) in the cement industry, reduce CO_2 emissions to 22 millions of tons [31].

1.3 The procedure of making coils steel.

Hot rolled in the form of coil and plate is a type of steel product produced from [32] the hot rolling process. Plants and users of this type of steel normally call this product ‘black steel’ to differentiate it from the cold rolled commonly known as ‘white steel’. [33]

Hot rolling is a metalworking process that occurs above the recrystallization temperature of the material. After the grains deform during processing, they recrystallize, which maintains an equiaxed microstructure and prevents the metal from work hardening. The starting material is usually large pieces of metal, like

semi-finished casting products, such as slabs, blooms, and billets. If these products came from a continuous casting operation, the products usually fed directly into the rolling mills at the proper temperature. In smaller operations, the material starts at room temperature and must heat [34]. The process does in a gas- or oil-fired soaking pit for larger work pieces and smaller work pieces induction heating used. As the material worked, the temperature must monitor to make sure it remains above the recrystallization temperature. A finishing temperature defined above the recrystallization temperature; and temperature range 50 to 100°C (90 to 180°F) under the recrystallization temperature. If the temperature drops below this temperature, the material must re-heated before hot rolling. [35]

Hot rolled metals have little directionality in their mechanical properties and deformation induced residual stresses. However, in some cases, non-metallic inclusions will impart some directionality and work pieces less than 20 mm (0.79 in) thick often have some directional properties[36]. Besides, non-uniform cooling will induce many residual stresses, which usually occurs in shapes that have a non-uniform cross-section, such as I-beams. While the finished product is of high quality, the surface covered in mill scale, which is an oxide that forms at high temperature. It usually removed via pickling or the smooth, clean surface process, which reveals a flat surface [37]. Dimensional tolerances are 2 to 5% of the overall dimension.

Hot rolled mild steel appears to have a wider tolerance for the total of included carbon than doe's cold rolled steel. The similar metals, hot rolled products seem to be less costly than cold-rolled ones. [38]

Hot rolling used to produce sheet metal or simple cross sections, such as rail tracks. Other typical uses for hot rolled metal includes truck frames, automotive wheels, pipe and tubular, water heaters, agriculture equipment, strappings, stampings, compressor shells, railcar components, wheel rims, metal buildings, railroad hopper cars, doors, shelving, discs, guard rails, automotive clutch plates. [39].

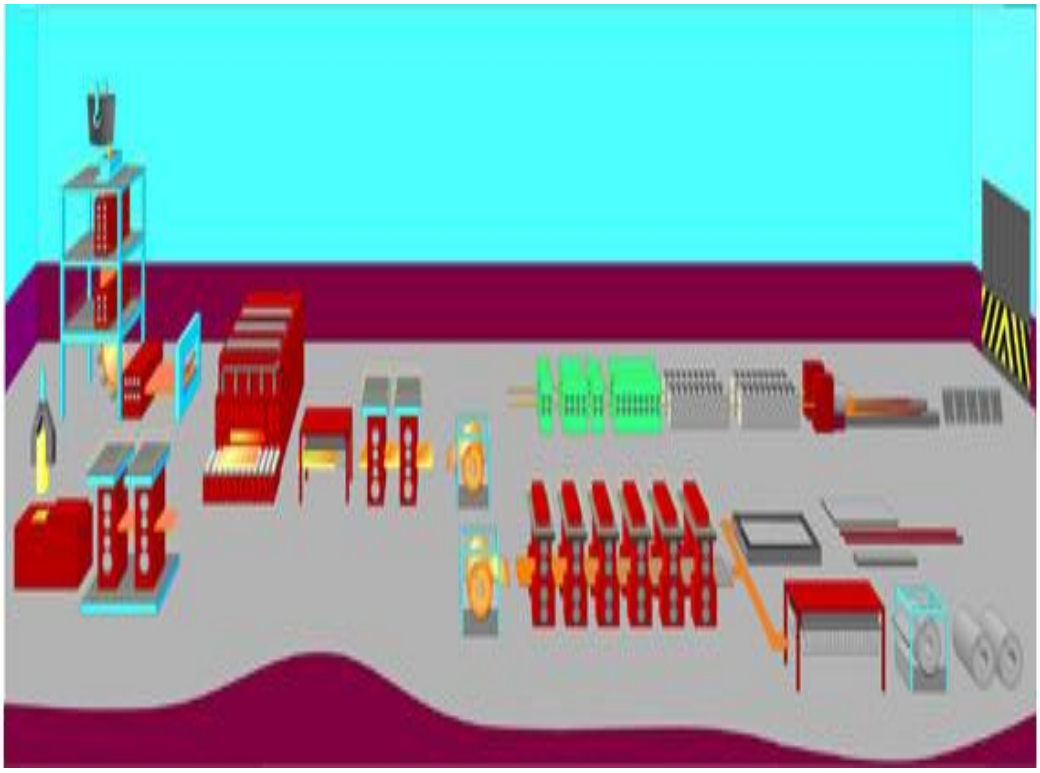

Fig.6. Hot rolling mill production

Figure 6 shown about hot rolling mill production where ingots of heated metal are passed between rollers to produce sheets or bars of a required cross section and form like coils.

The schematic diagrams detailed on the following pages illustrate the principal features of a modern rolling mill.

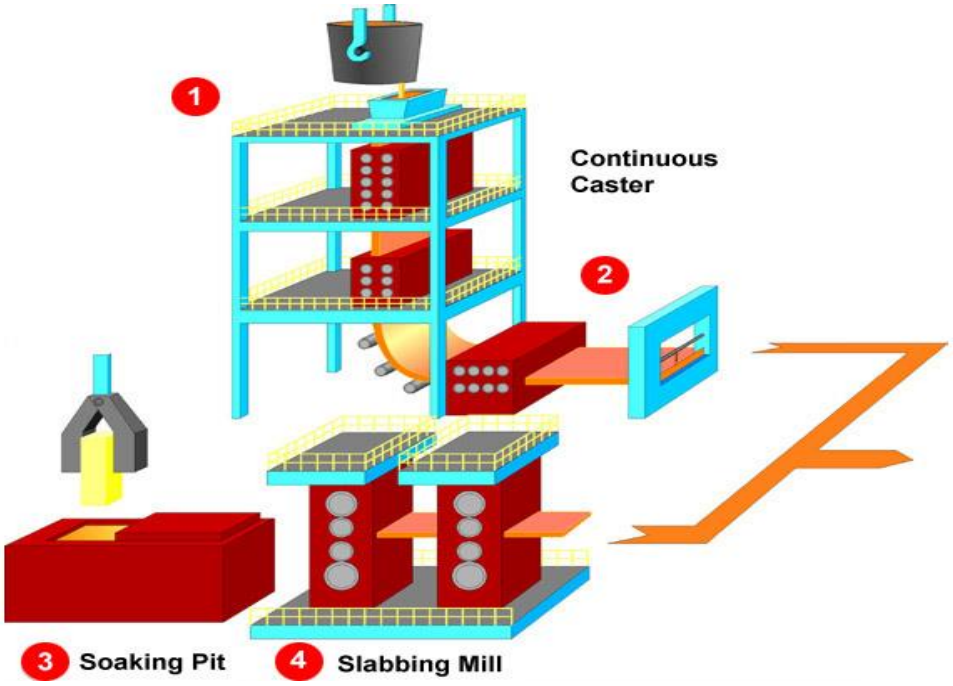

Fig.7. Stage one hot rolling mill

Figure 7 shown systematic hot rolling mill production, step 1 and 2 are a continuous caster, also called strand casting, and is the process whereby molten metal solidify into a "semi-finished" billet, bloom, or slab for subsequent rolling. Stage 3, Soaking Pit is a deep furnace in which a steel ingot allowed to stand until its temperature equalizes throughout in preparation for forging or rolling. Moreover, stage 4, Slabbing Mill is a steel rolling mill that produces slabs.

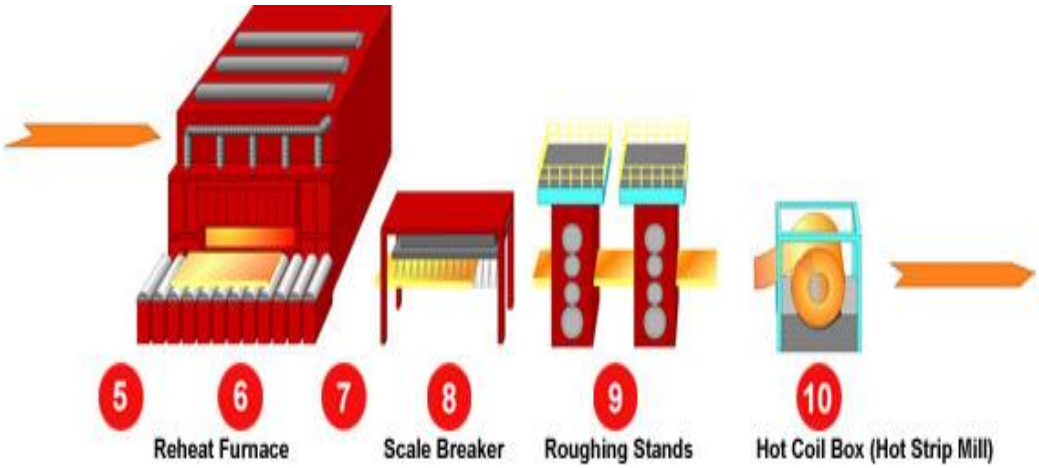

Fig.8. Stage two hot rolling mill

Stage 5 and 6, reheating furnaces used in hot rolling mills to heat the steel stock (Billets, blooms or slabs) to temperatures of around 1200ºC which are suitable for plastic deformation of steel and hence for rolling in the mill. The heating process in a reheating furnace is a continuous process where the steel stock charged at the furnace entrance, heated in the furnace and discharge at the furnace exit. Heat transferred to the steel stock during its traverse through the furnace mainly using convection and radiation from the burner gases and the furnace walls. After reheating furnace is scale breaker in stage 7 and 8. The slab passes through a descaling unit, an enclosure employing two pairs of spray headers that blast the intensely hot slab with 1,500 psi pressurized water to remove the 1/8-inch thick layer of oxide iron that forms at the surface of the slab in the oxygen rich atmosphere of the reheat furnace. Stage 9 is roughing stands; the roughing mill is make up of six independent rolling mill stand, the last four of which incorporate small vertical rolling mills called edgers. Slabs heated in the furnace until they glow bright orange –yellow are rolled through one stand at a time to produce so called transfer bar suitable for finishing rolling. Stage 10 is hot coil box (hot strip mill), which the process before finishing stands. Because hot rolling mill can be two product that is coil strip and wire/rod.

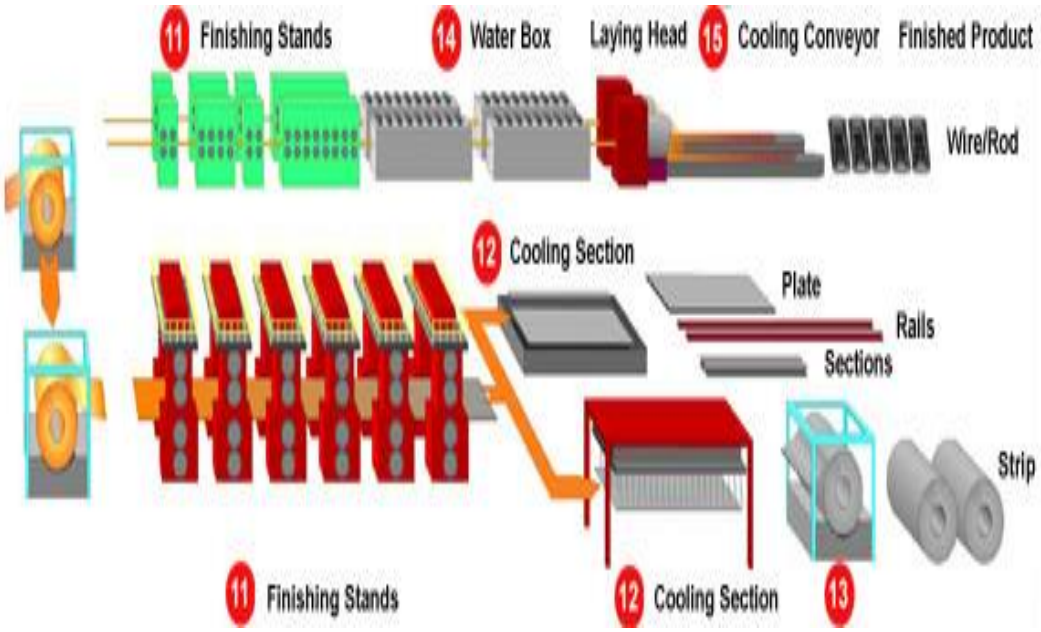

Fig.9 Stage three hot rolling mill
(Source: *https://www.landinst.com/industries/hot-rolling-mill*)

Stage 11 finishing stands have two part because output products are coil strip and wire/rod. Stage 12 is cooling section for strip coil, plate, and rails. Stage 14 is water box process for wire/rod product. Stage 13 output product that is strip. Stage 15 is cooling conveyor before finished product wire/rod.

1.4 Cooling Process

The rolling processes, cooling the steel are a critical factor. The speed at which the rolled product cooled will affect the mechanical properties of the steel. The cooling rate usually controls by spraying water on the steel as it passes through and leaves the mill, although occasionally the rolled steel is air-cooled using large fans.

After hot rolling, many steel product undergoing to further processing in the cold state. This stage of processing may not necessarily alter the shape of the steel product, but it does reduce it in thickness and significantly improve its performance characteristics. Hot rolled coil commonly cold rolled (also known as cold reduced). The strip is first de-coiled (uncoiled) and then passes through a series of rolling mill stands which apply pressure to the strip and progressively reduce its thickness - down to as little as 0.15 mm.[40]

Cold rolling processes also used to improve the surface quality of the steel. Cold Rolling also has the effect of hardening steel, so cold reduced strip subsequently annealed: a process of very carefully controlled heating and cooling to soften it. Cold compressed strip and sheet can withstand subsequent forming and pressing operations without the steel cracking. [41]

In metalworking, rolling is a metal forming process in which metal stock passed through one or more pairs of rolls to reduce the thickness and to make the thickness uniform; the concept is similar to the rolling of dough. Rolling classified according to the temperature of the metal rolled. If the temperature of the metal is above its recrystallization temperature, then the process known as hot rolling. Regarding usage, hot rolling processes more tonnage than any other

manufacturing process, and cold rolling processes the most tonnage out of all cold working procedures.[42]

In hot-rolled steel production processes, controlled cooling after finishing rolling plays an important role on the final microstructure and mechanical properties of the product. Stelmor air-cooling process is the most successful controlled cooling process to produce the steel wire with the sizes ranges from 5 mm to 20 mm. In this process, after passing through the water cooling boxes in which the temperature reduced to approximately 800 °C, the rolled wire is placed, using laying head, into circle loops on the conveyor, where the forced air cooling performed by a series of fans below.

Considerable researchers have devoted to studying the thermal and microstructural behaviors of steel in the controlled cooling process. For instance, Nobari and Serajzadeh [43] developed a mathematical model to predict temperature variations and austenite phase transformation in steel during controlled cooling. Shivpuri and co-workers [44] presented a computational approach to grain size evolution and mechanical properties of hot rolled rod. Yu et al. [45] developed an online Stelmor controlled cooling system for the stabilization of process operation. These numerical models have successfully applied to controlled cooling process for realizing stable operation and improving product quality. Thus, in industrial practice, with more and more manipulated variables under control, the fact that the product quality varies with season and climate is more and more outstanding.

However, up to now, it is no available in the literature to describe the quantitative analysis of the impacts of ambient temperature and humidity upon the cooling process of hot rolled steel. Fortunately, some investigations in the similar treatment reported, Brenn [46] discussed the effects of ambient conditions on the drying process of liquid coatings on round metal wires. [47] reported a model to analyze the effects of environmental conditions during air treatment operations of food. These research results provide the base for the study of the effects of ambient conditions on the controlled cooling of the hot-rolled wire rod of steel.

Steel Mills Lamination Coils Cooling, an integrated model for describing the effects of ambient conditions on the cooling performance of hot-rolled steel wire after rolling presented. The effects of moist air on heat transfer have derived from the theoretical and empirical models with the involved ambient conditions, and the results used to calculate the temperature evolution and phase transformation of high-carbon steel, SWRH82B, by the numerical approach. Then the predicted values of ultimate tensile strength compared with the industrial trials to validate the model. Additionally, the inverse solution of wind speed also discussed for realizing stable production process under different ambient conditions. [48]

Fig.10 Storage of Steel Coils
(source: *http://www.steelorbis.com*)

Figure 10. Sample storage of steel coil is in multi-stack storing in warehouse. Usually, the coil is arranged 2 or 3 levels, depending on warehouse area and coil size.

1.5 Objective

The steel coils produced in steel plants after lamination must be cooled from temperatures of 400ºC or 673.15 K to ambient temperature, to be transported for sale. Its geometry is cylindrical with heights between 1.6 m and 1.8 m. The outside diameter of the coil is 0.9 m. They have a central hollow coaxial of several diameters (approximately of 0.18 m). Coils cooling takes between four and six days depending on weather conditions, because usually they are let cool in a workshop virtually weatherproof. The cooling by liquids is not allowed because it could change the mechanical properties of the coils.

The study of coil cooling encloses several difficulties such as the fact that the geometries are not simple and usually stored in stacks of two or three levels; it is an unsteady phenomenon, with long cooling times, involving convection, radiation, etc. The knowledge of the coil cooling law by conduction, natural convection and radiation has not been deeply study in the literature and it is fundamental to widen the understanding of the cooling mechanisms to be able to control the cooling process.

The main objective of this thesis is to obtain a methodology to calculate the cooling law of a coil. This cooling law will be expressed by a mathematical equation depending on a few number of parameters. The parameters can be obtained by simulations or experimentally, allowing to obtain the general cooling law that can be extrapolated for other cases with different geometries and conditions; and avoiding to simulate o perform the experimental studies that depend on a large number of parameters.

The specific objectives are:

- Develop a numerical model to calculate the cooling law of coils under different circumstances.
- Study of the heat transfer mechanisms involved in the cooling of coils, to characterize the temperature distributions inside the coil, as well as the temperature and velocity distributions around the coils.

- The temperature decrease along time during the cooling process and the analytical equations of temperature inside the coil versus time, under different configurations: one vertical coil, one horizontal coil, rows of coils, etc.
- The influence of the variation of the thermal conductivity and specific heat with temperature and different interlayer pressures in the conduction heat transfer and therefore in the cooling process of coils.

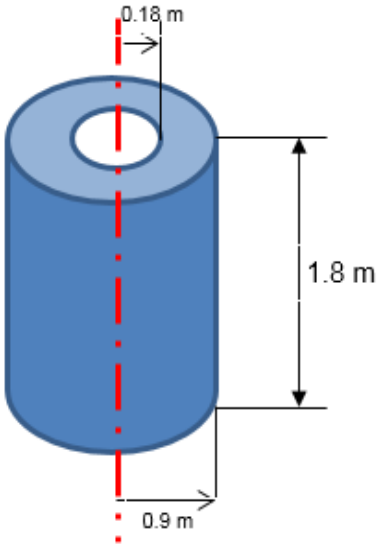

Fig.11. Geometry of the steel coil

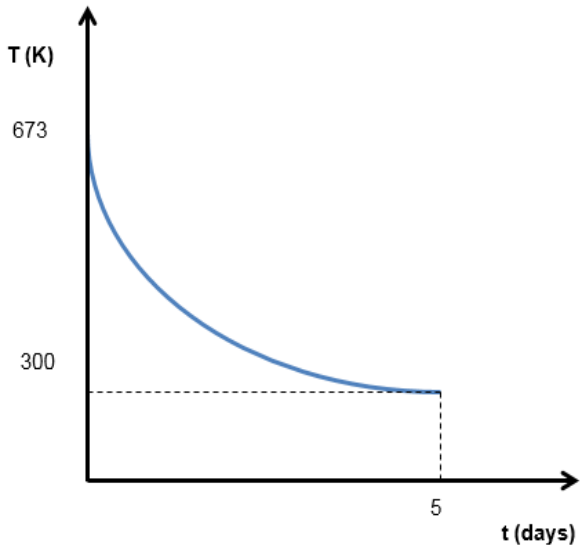

Fig.12. Graph of the coil cooling

CHAPTER 2. LITERATURE REVIEW AND THEORY

2.1 Literature Review

According to Souza [49], a computational algorithm is developed in case of tube cooling in continuous bed. The mathematical models are essential for calculating the coordinates of the radial position coordinates, the angular and axial coordinates, the equation for conservation of energy in cylindrical coordinates is using the finite volume method with an addition expression referring to the effect of axial tube rotation. [50]

The Equivalent thermal conductivity can be given as a function of material properties, strip thickness, surface characteristic of pieces, average compressive stress, and temperature. The finite element analysis for cooling of hot rolled coil has been carried out under various cooling conditions by using the equivalent thermal conductivity radial direction. The calculated result has been compared with data calculated using isotropic thermal conductivity and orthotropic stress independent conductivity and with experimental data. The final temperature of the hot rolling process is between 400ºC and 750ºC. In general, longer coil cooling steel takes between 5 and 9 days. The result was the cooling curve between isotropic conductivity shows the higher temperature than orthotropic conductivity. The cooling curves calculated from the equivalent thermal conductivity as the radial thermal conductivity show reasonable effects of radial thermal stress and are in good agreement with experimental data. [51]

According to Mats Karlberg, it has always been of greatest importance to control the temperature distribution of the products throughout the hot strip rolling process including the last coiling operation. The coil cooling process is crucial to decide the heat flux from the coil by an accurate description of the boundary condition to predict the cooling rate. [52].

In the hot coil box, the middle billet in the form of strip coil existence, there is a hollow gap between layered cylindrical coils of the continuous steel strip. The inside thermal conductivity of coils belongs to internal heat source axisymmetric

transient thermal conductivity. Axial thermal conductivity is mainly through the steel heat; radial can think of as cyclically alternate by steel layer and interface cascade formed. The coil of the temperature of the outside corner downs the fastest, followed by the outer surface than the inside surface, and the finally the inside steel coil. [53]

According to S.C. Baik, the model of equivalent radial thermal conductivity and the experiment of cooling show that temperature of hot rolled coil with a function of time during air cooling, along with the test result. The resulting of air cooling and water cooling in the coil, the surface temperature decreased rapidly after was sprayed. When the water spraying stopped, the remaining water on the coil evaporates within 10 minutes, and the surface temperature increased again. Finite element analysis indicates that that the cooling time decreases from 32 ~ 53 hours to 6 ~ 13 hours for spray water cooling. [54]

The distribution of airflow through many convectors or the convector plates (‘C′ insert) in the stacked coil is near different input flow rates. The distribution is, therefore, independent of the flow rate entering the base. The velocity of air on top and bottom of any coil increase if 'C' inserts replace standard convectors. Therefore, it results in increased heat transfer coefficients and makes the cooling process faster. Besides, an effective heat transfer area is higher in the 'C' insertion case. The mathematical model can be used to predict the temperature profile any coil provided the heat transfer coefficient are properly tuned. The empirical equation used for computation of the heat transfer coefficient give reasonably good values. The cooling time is expected to be brought down by the use of ‘C’ inserts. The operators will get an idea about the actual time taken for the cooling of a particular coil, having an appropriate grade and dimension, with the application of the mathematical model [55].

Air plus water cooling is the best way of cooling approach compared to natural air cooling and forced air cooling. Air cooling plus cooling water efficiency is around 3 up to 4 times forced air cooling and 5 up to 6 times natural air cooling. Uneven temperatures along steel lines before circular have an effect on the thermal evolution of the rolled steel, which is primarily the position of the

coil near the inner wall and outer wall. Both dimensional changes in the radial direction of the steel coil and the width change affect the thermal wall and outside the steel coil. Under the same initial conditions, steel grades are also an influential factor affecting the temperature distribution of steel coils [56].

According to Baskiyar, The simulation result of coil cooling the 6 mm rod shows a lower temperature difference between the surface and the interior.The total of heat transfer coefficient applied can influence the coolant of rolling-rod and cooling induces the temperature difference between interior and surface. The phase-wise cooling scheme can decrease temperature difference during achieving desired temperature reduction. [57]

Several factors affect the cooling of hot-rolled coils such as coiling temperature, oxidized layer thickness, the pressure between layers of a coil and varying the ambient temperature. The research is investigating the effect of different factors i.e. coiling temperature, ambient temperature, cooling method and storing position on the cooling time. The effect of coiling temperature (initial temperature) and ambient temperature on the cooling time of typical coil (strip width=1200 mm, strip thickness = 4 mm, weight = 18,000 kg) in single and multi-stack configurations as predicted by simulation and experiment. The result are The coiling temperature had less effect, but the ambient temperature had the strong effect on cooling times. [58]

Cold rolled coils can be through an annealing process to improve their formability and mechanical ability. A mathematical model of the thermal of the coils during the heating cycle has developed. This model allows us to determine the coldest point of the coil and the end time of the furnace operation. The model used to analyze the effect of strip thickness on the required heating time. Thin strips lead to prolong heating time and larger temperature differences inside the coil. [59]

The importance of coil cooling condition on mechanical properties uniformity of HSLA and AHSS steel grades demonstrated. It also shows that the roll of hot roll coils under current industrial production can cool uniformly. That is why to predict steel microstructure correctly, and mechanical properties after

hot rolled rolling the accurate description not only of ROT condition but also of coil cooling should do. Two solutions to provide accurate data of coil cooling tested. First, one is to use coil-cooling abacuses from 2D finite element model. Based on the FE abacus the TACSI simulation is very well suited to that reported in the industry literature data well with an accuracy of 15-20 MPa for both tensile and yield stresses. However, this approach recognized to be cumbersome and time-consuming. The second solution, a new 2D coil-cooling model incorporated in TACSI model showed similar performances. Author to describe the evolution of temperature and phase transformation during circular and cooling and would enable the evaluation of better mechanical properties. [60]

Temperature uniformity of steel in high-performance hydrogen bell-type annealing furnace has a significant effect on their quality and production. The hot rolled coil can be considered as a periodically laminated material composed of steel layers and interface layers in the radial direction. The radial effective thermal conductivity has been proposed, which is based on surface characteristics, strip thickness and compressive stress of the rolled coil. The annealing calculated by using the radial thermal conductivity and measured inside and the surface of rolled coils in HPH furnace, and compared the experimental data with the numerical prediction results are satisfactory. [61]

The cooling time of cold rolled coil has calculated using an algorithm, and it takes approximately 20-22 hours to become ambient temperature. The crown of strip type model needs a lot of time about 2 hours, to cool off the flat strip profile design. Compared with the top strip profile model, the flat strip profile model neglects the pressure press effect due to the coil tension and indicates the temperature distribution. It is not suitable to apply to flat type models to the analysis of steel coil processes. So the crown strip type recommended for more accurate determination analysis. [62]

According to Chen G, The result obtained show that the increase of equivalent radial thermal conductivity leads to shortening of annealing time, while the growth of the steel coil outside diameter and the strip steel width will result in an extension of annealing time. The temperature within the coil predicted during

the annealing cycle, including the heating process and cooling process and the theoretical fundamental and an effective means to be aware online control and optimal production to secure the quality of heat treatment and increase productivity.[63]

The hollow cylinder approach cannot be an accurate, sufficient assumption due to the appearance of spaces between the layers of a hot-rolled strip in the coil. The coil was assumed to be a series of thin-walled, concentric cylinder. In this condition, lower values are estimated for thermal stress throughout cooling than those under the hollow, solid cylinder approach. The thinner layer thickness cause, the less thermal value, probably because of a vast number of interface spaces in the coil. According to the cylinder solid cylinder approach, strip thickness has a bit effect on the value of term tension estimation, leads by the temperature divergence in time history. The thin-walled concentric cylinder method causes the highest amount of stress to create in the shortest time intervals after the beginning of cooling.[64]

During annealing, heat transfer within steel coils complicated by different conductivity in radial and axial directions. Due to small air gaps between the steel layers in the radial direction. The time lag, the time for coldest point to reach a critical temperature is of importance to an annealing operator. Determining the dependence of this time lag on coil dimensions, radial diffusivity, gas temperature, and boundary conditions will help the steel industry to optimize production.[65]

According to Saboonchi, The use of a water basin can reduce the cooling time of hot rolled coil by 6-8 times in complete water-immersion cooling. Immersion in water for a short period is efficient than longer storage in the water basin. It is proposed to position the nozzle that faces the two end surfaces of the coil. This option guarantees a restricted temperature gradient, lower energy and water consumption, and higher time-saving. Water spray on the outer surface of the coil, and increased spray rate will have the effect on cooling time. [66]

2.2 Theory

2.2.1 Computational Fluid Dynamics (CFD)

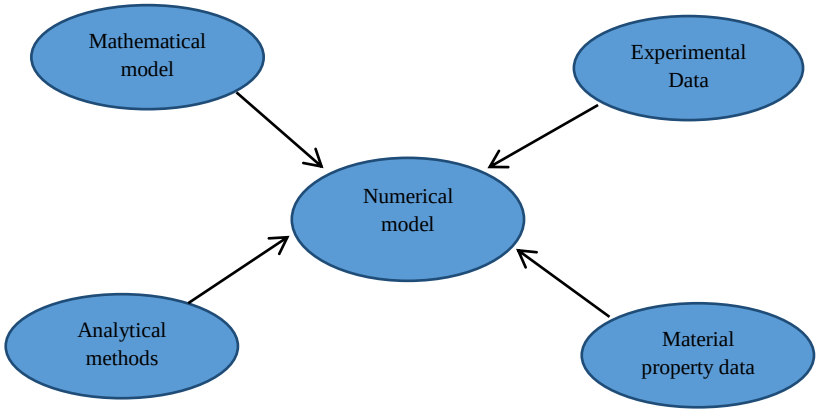

Fig.13.Various inputs and component that constitute a typical numerical model in CFD

The main advantages of numerical simulation using CFD modeling followed:

- Fast and low-cost 2D and 3D steady or unsteady-state for studies of cooling of steel mills lamination coils.
- Optimization of the process conditions of laminated coils cooling.
- Scale-up for process of coils steel cooling,

One of the questions that still needs to addressed in numerical simulation of heat and mass transfer is which CFD model should utilize, either two or three-dimensional? What are the differences between their predictions of flow patterns? Are the computational costs justified in the case of 3D numerical simulation? How to answer these questions, a deep study of the cooling of steel mills lamination coils by using CFD modeling of the process is needed. In the present work, 2D and 3D CFD models of cooling laminated steel coils develop.

The mathematical description of a fluid as a continuum medium required almost one century to mature in the form that uses today. Euler gave the breakthrough point in 1759, which established the differential equations

that govern compressible flow in ideal fluids. He pioneered the description of fluids using local thermodynamic properties and the macroscopic velocity found at fixed points of space and wrote conservation equations for mass, momentum, and energy in cases for which the surface interaction between liquid particles was everywhere perpendicular to the surface element. He correctly identified the intensity of this interaction with the thermodynamic pressure and obtained a closed system of differential equations, known as the Euler equation, which describes ideal fluids, characterized by negligible viscous effects. About sixty years later, in 1822, Navier extended the incompressible Euler equations to include real fluid effects, where the surface interaction departs on the purely surface normal response. In 1845, Stokes generalized the Navier proposal to include compressible flow cases. The resulting laws, known as the Navier-Stokes equations, constitute a set of five differential equations that exhibit strong nonlinear behavior except at very low flow velocities or in certain very rapidly changing conditions. The non-linear character precludes finding general solutions to the equations and is at the root of the broad range of fluid flow responses.

The complexity attached to flow analysis; the equations often exhibit a significant disparity in the characteristic value of key terms. The implication is that fluid response often involves the presence of multiple spatial and temporal scales showing the large difference between them. Besides, the non-linear terms propel an instability mechanism that can lead to a chaotic fluid response known as turbulent flow. Because of all these complexities, experimental studies have been and still are fundamental in the flow analysis process. That is also not surprising to find that one of the first applications of computers for the simulation of physical phenomena was in the solution of the Navier-Stokes equations, initiating the discipline of computational fluid dynamics (CFD). In a practical sense, the starting point can place in the early 1950's, when first computers used for flow analysis during the H-bomb development. Benefiting from these initial computations, research at Los Alamos National Lab in the USA produced during the 1950's and 1960's

numerical codes to first solve incompressible flow using some auxiliary flow variables known as the stream function and vorticity. During the 1970's, efficient numerical schemes developed to solve incompressible flow using the first flow variables (pressure and velocity). These methods incorporated a numerically implicit formulation of the equations, with pressure or velocity coupling strategies. [67].

About the same time two-equation based, comprehensive turbulence models proposed. These advances resulted in the development of control volume formulations for the resolution of laminar and turbulent incompressible flows in complex geometries.

By the end of the 1960s, the aerospace industry was also actively seeking efficient numerical schemes to solve incompressible and compressible Euler flow. In the first group, three-dimensional panel solvers developed which, for two -dimensional cases, complemented with boundary layer codes to determine the complete performance of aerodynamic profiles. The compressible case first engaged through the potential flow equations, which can apply to describe weak forms of flow discontinuities known as shock waves. Difficulties encountered when trying to capture these discontinuities were resolved in 1970[68]when innovative spatial discretization schemes which depended on the local flow properties introduced. This strategy allowed the first computation of transonic flow with weak shock waves. The development of potential solvers virtually halted by the mid-1970s when the assault to the compressible Euler equations took place. It culminated in the early 1980s [69,70-71], as efficient finite volume, schemes to solve the compressible Euler equations in complex geometries became available. The success of these projects was so impressive that in 1985 the computation of the transonic Euler flow over a full aircraft achieves. In the following years, the extension to include the viscous terms in the laminar Navier-Stokes equations and the turbulent terms in the Reynolds averaged Navier-Stokes equations accomplished.

During the past two decades, both incompressible and compressible flow solving schemes have improved by introducing more efficient algorithms to speed up and increase the solver performance. Besides, extensions of the proposed turbulence models to account for more complex flow physics have incorporated. At the same time, the available computer power has drastically increased. The incorporation of advanced turbulence models such as Reynolds stress or large scale resolving descriptions to routine CFD analysis. All these advances have prompted the extension of CFD users from the pioneering work of aerospace and nuclear engineering researchers to the automotive, chemical, naval, processing, or bioengineering industries. The success of flow analysis based on CFD tools has also led to the development of commercial CFD packages in the last three decades.

In spite of the advances achieved in numerical flow simulation and considering the present and near future computer capabilities, the analysis of technological flows through CFD tools still involves simplifications that limit the full potential that can achieve with its use. Specifically:

a) Flow physics modeling. Technological flows often incorporate complex flow physics, including transition and turbulent regions, chemical reactions, multiphase, and three-dimensional, unsteady evolution. Some of these aspects require modeling that often includes drastic simplifications. For example, the simulation of turbulent flow requires selecting a turbulence model. Although more models that are sophisticated have been developed and incorporate in CFD solvers, most of them are still crude approximations to the complex, underlying flow physics. The predictive capability of CFD simulations strongly hinges on the ability of the physical models to reproduce the correct flow behavior. It is important to have an assessment of the limitations [72] that the simplified flow physics may introduce in the simulation results.
b) Boundary conditions simplifications. The numerical simulation of technological flows often requires limiting the computational domain in which the flow solved. This implies that non-trivial boundary conditions

must established in regions where the computational domain boundary placed. The accuracy of the imposed boundary conditions may significantly affect the results. It is important to estimate the sensitivity of results to errors in the specification of the boundary conditions and to set realistic boundary conditions values when this sensitivity can affect the accuracy of the results.

c) Discretization issues, the numerical resolution of fluid flow involve the discretization of the equations governing the flow evolution. As a previous step, the formulation in which the fluid equations cast must select. For the numerical simulation of fluid flow, three formulations have mostly used finite differences (FD), finite elements (FEM), and finite volume (FVM) methods. When solving general, complex geometry flows the finite volume approach is the most widely used choice. Its popularity results from its superior ability to discretize complex geometry in flow problems based on unstructured meshes and complex flow physics. The formulation has selected, the discretization of the equations must accomplish. The high non-linearity and coupling characterizing the flow equations imply that their discretization can highly affect the solution convergence and accuracy. In addition, because of the characteristics mentioned above, the mesh properties often determine the quality of the obtained solution. These aspects stress the importance of having knowledge on how the discretization of the different terms included in the flow equations accomplished.

d) Convergence aspects, for a given CFD problem, complete problem convergence can sometimes compromised by the solver implementation details, the mesh geometry, the complexity of the underlying flow physics, and constraints imposed in the available computation time. The lack of convergence translates in additional errors in the numerical solution. Measures to speed up the problem convergence include solver optimization methods, mesh quality improvement, and convergence acceleration strategies.

Solving specific flow problems with CFD techniques involves different steps that summarized in figure 12.

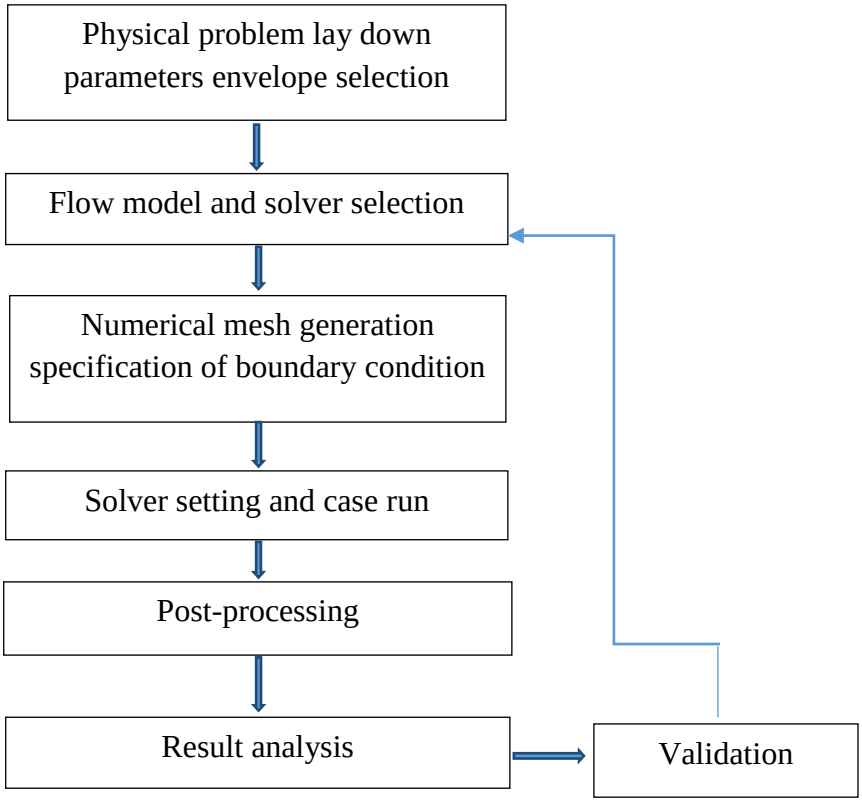

Fig.14. Flowchart of numerical simulation procedure

The description of the physical problem to be resolved should first clearly stated. If the problem requires solving for different values of parameters that appear in its specification, a non-dimensional problem description can help selecting the minimum number of simulations that need to perform to cover the sought parameter envelope. Next, a decision about the flow model and solver type should take. In complex flow on physics scenarios, simplification of the equations to focus on the flow controlling terms can be important to optimize available computational resources and to speed up problem convergence. In this sense, the solving strategy often involves including models that are more complex as long as the simulation proceeds. The construction of the numerical mesh in which the discretization

will base is a critical aspect of the simulation process. As will be recursively seen in this course, the grid quality and density can determine the accuracy and convergence speed of a CFD simulation. In this respect knowledge of the solver and of the flow physics expected to occur in the simulation are relevant during the mesh definition stage. As the grid constructed, the preparation of the boundary conditions to impose should engage. When the computational domain split to control its size, non-trivial boundary condition specification must propose. In some cases, this aspect can have a significant impact on the solution accuracy, and therefore it should handle with care. The mesh and boundary conditions prepare, the selection of the solver parameters to use in the simulation should perform. The optimal choice often involves adaptive parameter setting as the simulation proceeds towards convergence. After convergence has achieved, result post-processing carried out to extract the desired information. A validation stage can also be included, comparing obtained results to available experimental data or previously available, validated simulations. The conclusions of the validation exercise can lead to modifications in different choices of the complete simulation process. [73]

2.2.2 Heat Transfer

The subject of heat transfer is of fundamental importance in many branches of engineering. A mechanical engineer may be interested in knowing [74] the mechanism of heat transfer involved in the operation of equipment, for example, boilers, condensers, air pre-heaters, economizers, and so on, in a thermal power plant in order to improve their performance. The study of heat transfer provides economical and efficient solutions for critical problems encountered in many engineering items in equipment. It is important to quantity the amount of energy transferred per unit time and for that, we require the use of rate equation.

Heat transfer is that section of engineering science that studies the energy transport between material bodies due a temperature different

(Bejan1993; Holman 1989; Incropera and Dewitt 1990; sukhatme 1992). The three modes of heat transfer are:

1) Conduction

   Conduction is the mode of heat transfer in [75] which energy exchange takes places from the region of high temperature [76] to that of low temperature by kinetic motion or direct impacts molecules. To understand its fundamental principles, let us concentrate on the case of a gas at rest, which turns out to be the easiest example to understand the fundamentals of conduction despite the initial feeling of the opposite.

For Heat conduction, the rate equation known as Fourier´s law, which is expressed for one dimension as

$$q_x = -k\frac{dT}{dx} \tag{2.1}$$

Where q_x is the heat flux in the x direction *(W/m^2)*, *k* is thermal conductivity *(W/m-K)*, a property of material) and $\frac{dT}{dx}$ is the temperature gradient *(K/m)*. Heat transfer-conduction steady state one-dimensional involve

a) Flat surface (x, y, z)
b) Cylinder (r, z, θ)
c) Sphere (r, θ, ϕ)

Coordinate Cartesian

Line x:

$$q_x = -kA\frac{dT}{dx} \tag{2.2}$$

Line y:

$$q_y = -kA\frac{dT}{dy} \tag{2.3}$$

Line z:

$$q_z = -kA\frac{dT}{dz} \tag{2.4}$$

Coordinate cylinder:

Line r:

$$q_r = -kA\frac{dT}{dr} \tag{2.5}$$

Lineθ:

$$q_\theta = -\frac{k}{r}A\frac{dT}{d\theta} \tag{2.6}$$

Line z:

$$q_z = -kA\frac{dT}{dz} \tag{2.7}$$

Coordinate Sphere:

Line r:

$$q_r = -kA\frac{dT}{dr} \tag{2.8}$$

Lineθ:

$$q_\theta = -\frac{k}{r}A\frac{dT}{d\theta} \tag{2.9}$$

Lineϕ:

$$q_\theta = -\frac{k}{rsin\theta}A\frac{dT}{d\theta} \tag{2.10}$$

Heat transfer-conduction in hollow cylinder

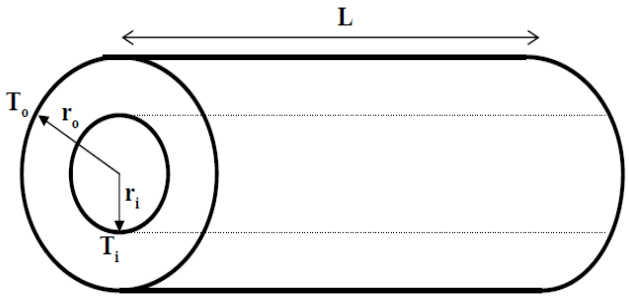

Fig.15.The shape of hollow cylinder

Electric equation

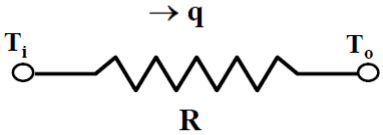

Heat flow toward to the radial direction (line r). Wide areas of heat flow to the cylinder system are:

$$A = 2\pi r^2 \tag{2.11}$$

Moreover, Fourier laws to be:

$$q = kA_r\left(-\frac{dT}{dr}\right) = -k2\pi rL\frac{dT}{dr} \tag{2.12}$$

Boundary condition

$$r = r_i \rightarrow T = T_i$$
$$r = r_o \rightarrow T = T_o$$

Equation of heat flow q for coordinate cylinder is:

$$q = \frac{2\pi Kl(T_i - T_o)}{\ln(\frac{r_0}{r_i})} \tag{2.13}$$

$$or$$

$$q = \frac{2\pi Kl(T_i - T_o)}{2.3\log(\frac{r_0}{r_i})} \tag{2.14}$$

A typical composite hollow cylinder with both inside and outside experiencing convection shown in Fig.14 The figure includes the thermal network that represents the system.

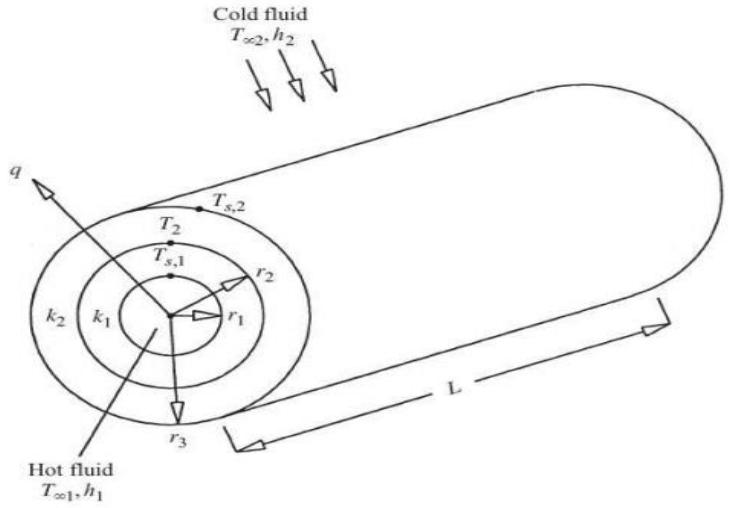

Fig.16.The shape of composite hollow cylinder

Equation:

$$\frac{1}{h_1 2\pi r_1 L}\frac{ln\left(\frac{r_2}{r_1}\right)}{2\pi k_1 L}\frac{ln\left(\frac{r_3}{r_2}\right)}{2\pi k_2 L}\frac{1}{h_2 2\pi r_3 L} \tag{2.15}$$

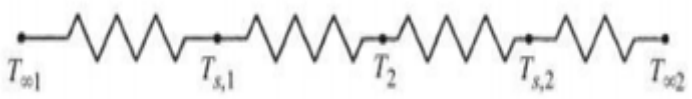

The rate of heat transfer q given by

$$q = \frac{T_{\infty,1} - T_{\infty,2}}{\frac{1}{h_1 2\pi r_1 L} + \frac{ln\left(\frac{r_2}{r_1}\right)}{2\pi k_1 L} + \frac{ln\left(\frac{r_3}{r_2}\right)}{2\pi k_2 L} + \frac{1}{h_2 2\pi r_3 L}} \tag{2.16}$$

2) Convection

Natural convection

Heat transfer mechanism in natural convection, consider a body at initial temperature T_∞ where $T_0 > T_\infty$owing to the temperature difference, heat begins to flow from the body to the fluid. Heat transfer will take place first by pure conduction, and a temperature gradient will establish in the fluid. The temperature variation within the fluid will generate a density gradient, which, in a gravitational field, will give rise in turn, to a convective motion because of buoyancy force called free convection or natural convection.

Newton´s law of cooling as gives the rate equation

$$q = h(T_w - T_a) \tag{2.17}$$

Where q is the convective heat flux; *(W/m^2)*; *(Tw - Ta)* is the temperature difference between the wall and the fluid and *h* is the convection of heat transfer coefficient, *(W/m K)*.

The convection of heat transfer coefficient frequently appears as a boundary condition in the solution of heat conduction through solids. Alternatively, for heat transfer from the hot fluid to the cold wall equation written as

$$q = h(T_a - T_w) \tag{2.18}$$

When heat added to a fluid and the fluid density varies with temperature, a flow can induce due to the force of gravity acting on the density variations. The importance of buoyancy troops in a mixed convection flow can measured by the ratio of the Grashof and Reynolds numbers:

$$\frac{G_r}{{R_e}^2} = \frac{g\beta\Delta TL}{v^2} \tag{2.19}$$

When this number approaches or exceeds unity, you should expect strong buoyancy contributions to the flow. Conversely, if it is [77] minuscule, buoyancy forces may ignore in your simulation. In pure natural convection, the Rayleigh number measures the strength of the buoyancy-induced flow:

$$R_a = \frac{g\beta\Delta TL}{\mu\alpha} \tag{2.20}$$

Whereβ is the thermal expansion coefficient:

$$\beta = -\left(\frac{\partial \rho}{\partial T}\right) \tag{2.21}$$

α(Alpha) is the thermal diffusivity.

$$\alpha = \frac{k}{\rho C_p} \tag{2.22}$$

Rayleigh numbers less than 10^8 indicate a buoyancy-induced laminar flow, with the transition to turbulence occurring over the range of $10^8 < Ra < 10^{10}$.

3) Radiation

Radiative heat transfer is a mode of energy transfer where the energy transported via electromagnetic waves. The emission or absorption of radiation energy by a body is a bulk process [78] that is, radiation originating from the interior of the body emitted through the surface.

$$q = \sigma {T_w}^4 \tag{2.23}$$

Where q is the radiative heat flux *(W/m^2)*, σ is the Stefan-Boltzmann constant (5.6669 x 10^{-8}), in *(W/m^2K^4)*. If a radiation flux, q_{inc} is incident on a blackbody, it completely absorbed by the blackbody. However, if the radiation flux q_{inc} is incident on real body, then the energy absorb q_{abs} by the body is given by

$$q_{abs} = \alpha q_{inc} \tag{2.24}$$

Where the absorptivity, α lies between zero and unity, for all real bodies it is always less than unity.

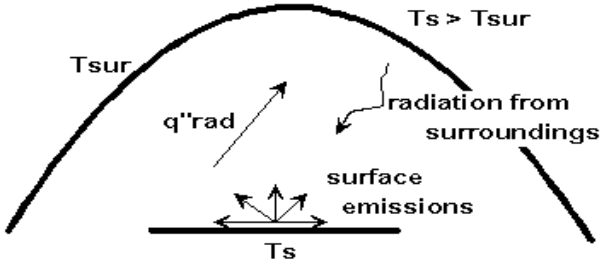

Fig.17. Radiation energy is exchange between a surface and the surrounding. (Source: *http://aml.engineering.columbia.edu*)

The large surrounding area can approximate as a blackbody about the small surfaceA_1. Then, the radiation flux emitted by the area $\sigma T_2^4$is also the radiation flux incident on the surface A_1. Hence, the radiation energy absorbed by the surface A_1 is

$$A_1 \alpha_1 \sigma T_2^4 \tag{2.25}$$

2.2.3 Theory of the Simulation

2.2.3.1 Pressure Based Solver

The pressure-based solver employs an algorithm, which belongs to a general class of methods called the projection method. In the projection method, the constraint of mass conservation (continuity) of the velocity field is achieved by solving a pressure (or pressure correction) equation. The pressure equation [79] derived from the continuity and the momentum equations in such a way that the velocity field, corrected by the pressure, satisfies the continuity. Since the governing equations are nonlinear and coupled to one another, the solution process involves iterations wherein the entire set of governing equations solved repeatedly until the solution converges.

In this section, specific practices related to the discretization of the momentum and continuity equations and their solution using the pressure-based solver addressed. These unusual methods easily described by considering the steady-state continuity and momentum equations in integral form:

$$\oint \rho \vec{v} \,.\, d\vec{A} = 0 \tag{2.26}$$

$$\oint \rho \vec{v}\, \vec{v} \,.\, d\vec{A} = -\oint pI \,.\, d\vec{A} + \oint \bar{\bar{\tau}} \,.\, d\vec{A} + \int_V \overrightarrow{F}\, dV \tag{2.27}$$

Where,I is the identity matrix,$\bar{\bar{\tau}}$ am the stress tensor, and $\vec{F}$ am the force vector.

$$R_a = \frac{g\beta \Delta T L^3 \rho}{\mu \alpha} \tag{2.28}$$

The 2D energy equation is as follows:

$$\frac{\partial}{\partial x}\left(k\frac{\partial T}{\partial x}\right)+\frac{\partial}{\partial y}\left(k\frac{\partial T}{\partial y}\right)+\dot{q}=\rho C_p\frac{\partial T}{\partial t} \quad (2.29)$$

Where, *T* and *t* are temperature and time.

The 3D solves the energy equation in the following form:

$$\frac{\partial y}{\partial t}(\rho E)+\nabla.\left(\vec{v}(\rho E+p)\right)=\nabla\left(k_{eff}\nabla T-\sum_j h_j\vec{J}_j+(\bar{\bar{\tau}}_{eff}.\vec{v})\right)+S_h \quad (2.30)$$

Where k_{eff} is the sufficient conductivity ($k+k_t$ where k_t is the turbulent thermal conductivity, defined according to the turbulence model used), and$\vec{J}_J$ is diffusion flux of species, *j*. The first three terms on the right-hand-side represent energy transfer due to conduction, species diffusion, and viscous dissipation, respectively. S_h Includes the heat of chemical reaction, and any other volumetric heat sources:

$$E=h\frac{p}{\rho}+\frac{v^2}{2} \quad (2.31)$$

Where sensible enthalpy *h* defined for ideal gas as

$$\boldsymbol{h}=\sum_{\boldsymbol{j}}\boldsymbol{Y_j}\,\boldsymbol{h_j} \quad (2.32)$$

And for incompressible flow as

$$\boldsymbol{h}=\sum_{\boldsymbol{j}}\boldsymbol{Y_j}\,\boldsymbol{h_j}+\frac{\boldsymbol{p}}{\boldsymbol{\rho}} \quad (2.33)$$

Y_j The mass fraction of species *j* and

$$h_j=\int_{T_{ref}}^{T}C_p.jdT \quad (2.34)$$

The value used for T_{ref} in the sensible enthalpy calculation depends on the solver and model in use.

For transport equations model we using the standard$k-\varepsilon$, the turbulence kinetic energy *k* and its rate of dissipation, ε obtained from the following transport equations:

$$\frac{\partial}{\partial t}(\rho k)+\frac{\partial}{\partial x_i}(\rho k u_i)=\frac{\partial}{\partial x_j}\left[\left(\mu+\frac{\mu_t}{\sigma_k}\right)\frac{\partial k}{\partial x_j}\right]+G_k+G_b-\rho\varepsilon-Y_M+S_k \quad (2.35)$$

$$\frac{\partial y}{\partial t}(\rho\varepsilon)+\frac{\partial}{\partial x_i}(\rho\varepsilon u_i)=\frac{\partial}{\partial x_j}\left[\left(\mu+\frac{\mu_t}{\sigma_\varepsilon}\right)\frac{\partial\varepsilon}{\partial x_j}\right]+C_{1\varepsilon}\frac{\varepsilon}{k}+(G_k+C_{3\varepsilon}G_b)-C_{2\varepsilon}\rho\frac{\varepsilon^2}{k}+S_\varepsilon \quad (2.36)$$

Standard wall function, Momentum boundary condition based on launder-Spaulding law-of-the-wall velocity yields:

$$U^* = \frac{1}{k}\ln(Ey^*) \tag{2.37}$$

Where,

$$U^* \equiv \frac{U_p C_\mu^{1/4} K_P^{1/2}}{\tau_w/\rho} \tag{2.38}$$

$$y^* \equiv \frac{\rho C_\mu^{1/4} K_P^{1/2} y_P}{\mu} \tag{2.39}$$

The equation for radiation model (DO) is:

$$\nabla.(I(\vec{r},\vec{s})\vec{s}) + (a+\sigma_s)I(\vec{r},\vec{s}) = an^2\frac{\sigma T^4}{\pi} + \frac{\sigma_s}{4\pi}\int_0^{4\pi} I(\vec{r},\vec{s}')\Phi(\vec{s},\vec{s}')d\Omega' \tag{2.40}$$

2.2.3.2 Steady-State Flow Solution Methods

In the explicit scheme, a multi-stage, time stepping algorithm [80] is used to discretize the time derivative in equation

$$\Gamma\frac{\partial}{\partial t}\int_V QdV + \oint[F-G]dA = \int_V HdV \tag{2.41}$$

The solution advanced from iteration *n* to iteration *n+1* with *m* stage Runge-Kutta scheme, given by

$$Q^0 = Q^n$$

$$\Delta Q^i = -\alpha_i\,\Delta t\Gamma^{-1}R^{i-1}$$

$$Q^{n+1} = Q^m$$

Where $\Delta Q^i \equiv Q^i - Q^n and\ i = 1,2\ldots,m$ is the stage counter for the *m*-stage scheme, α_i is the multi stage. The residual $R^i$is computed from the intermediate solution Q^i and for equation (2.42), is given by

$$R^i = \sum^{N_{faces}}\left(F\left(Q^i\right) - G(Q^i)\right).A - VH \tag{2.42}$$

The time step Δt computed from the CFL (Courant-Friedrich-Lewy) condition

$$\Delta t = \frac{2CFL.V}{\Sigma_f \lambda_{f^{max}} A_f} \tag{2.43}$$

Where *V* is the cell volume, A_f is the face area, and $\lambda_{f^{max}}$ is the maximum of local eigenvalues. For study state solution, convergence acceleration of the explicit formulation canachieved with the use of local time stepping, residual smoothing, and full approximation storage

multigrid. Local time stepping is a method by which the solution at each control volume advanced in time on the cell time step, defined by the local stability limits the time to step scheme. Residual smoothing, on the other hand, increases the bound of confidence limits of the time-stepping scheme and hence allows for the use of a large CFL value to achieve fast convergence. The convergence rate of the particular planned can accelerate through use the of the full approximation storage (FAS) multigrid method. By default, ANSYS FLUENT uses a 3-stage Runge-Kutta scheme based on the work by Lynn [81] for steady state flow that use the density based explicit solver.

Implicit residual smoothing, the maximum time step can further increase by increasing the support of the scheme through inherent averaging of the remaining with their neighbors. The residual filtered through a Laplacian smoothing operator:

$$\bar{R}_i = R_i + \epsilon \sum(\bar{R}_j - \bar{R}_i) \tag{2.44}$$

This equation can solve with the following Jacobi iteration

$$\bar{R}_i = \frac{R_i + \epsilon \sum \bar{R}_j^{m-1}}{1 + \epsilon \sum 1} \tag{2.45}$$

Two Jacobi iterations are usually sufficient to allow doubling the time step with a value of $\epsilon = 0$

Implicit formulation, in the implicit scheme, a Euler implicit discretization in time of the governing equations (2.41) is combined with a Newton-type linearization of the fluxes to produce the following linearized system I delta form. [82]

$$\left[D + \sum_j^{n_{faces}} S_{j,k}\right] \Delta Q^{n+1} = -R^n \tag{2.46}$$

The center and off-diagonal coefficient matrices, D and $S_{j,k}$ are given by

$$D = \frac{V}{\Delta t}\Gamma + \sum_j^{N_{faces}} S_{j,k} \tag{2.47}$$

$$S_{j,k} = \left(\frac{\partial F_j}{\partial Q_k} - \frac{\partial G_i}{\partial Q_k}\right) A_j \tag{2.48}$$

In addition, the residual vector Rn and time step Δt defined as in equation (2.42) and equation (2.43) respectively. Equations (2.46) solve using either Incomplete Lower Upper (ILU) factorization by default or symmetric point Gauss-Seidel algorithm. In conjunction with algebraic multigrid (AMG), method will adapt for coupled sets of equations.

Explicit relaxation can improve the convergence to a steady state of the implicit formulation. The exact relaxation enables for the implicit solver and uses a factor of 0.75. You can specify an element αto control the amount that the solution vector Q changes between iterations after the end of the algebraic multigrid (AMG) cycle:

$$Q_{new} = Q_{old} + \alpha \Delta Q \tag{2.49}$$

By specifying a value, less than the default value of one forα, the variables in the solution vector will be under-relaxed, and the convergence history can improve.

2.2.3.3 Transient Solver

The explicit time stepping approach is available only for the exact scheme described above. The time step was control by the CFL condition. The accuracy of the solution time, the time explicitly uses the same time step of each domain cell (this is also known as global time step) (this also known as global time step), and with preconditioning disabled. By default, ANSYS FLUENT uses a stage Runge-Kutta scheme for transient flows.

The Implicit-time stepping method (also known as dual-time formulation) is available in the density–based explicit and implicit formulation. When performing transient simulations with implicit time stepping (dual-time stepping), ANSYS FLUENT is using a low Mach number time-derivative transient preconditioned to provide accurate result both for the simple convective process. (e.g., simulating transient

turbulence) and for acoustic methods (e.g., simulating wave propagation). [83][84]

Here we introduce a preconditioned pseudo-time –derivative term into equation

$$\frac{\partial}{\partial t}\int_V WdV + \oint[F-G].dA = \int_V HdV \qquad (2.50)$$

As follows:

$$\frac{\partial}{\partial t}\int_V WdV + \Gamma\frac{\partial}{\partial \tau}\int_V QdV + \oint[F-G].dA = \int_V HdV \qquad (2.51)$$

Where *t* denotes physical-time and τ is a pseudo-time used in the time-marching procedure. Note, that as $\tau\to\infty$, the second term on the left side of equation (2.51) vanishes and equations (2.50).

The time-dependent term in equation (2.52), discretize in an implicit fashion by means of either a first or second-order accurate, backward difference in time.

The dual-time formulation written in semi-discrete form as follows:

$$\left[\frac{\Gamma}{\Delta\tau}+\frac{\epsilon_0}{\Delta t}\frac{\partial W}{\partial Q}\right]\Delta Q^{k+1} + \frac{1}{V}\oint[F-G].dA = H - \frac{1}{\Delta t}(\epsilon_0 W^k - \epsilon_1 W^n + \epsilon_2 W^{n-1} \qquad (2.52)$$

Where $\{\epsilon_0 = \epsilon_1 = ½,\ \epsilon_2 = 0\}$ gives first-order time accuracy, and $\{\epsilon_0 = 3/2,\ \epsilon_1 = 2,\ \epsilon_2 = 1/2\}$ gives second-order. k is the inner iteration counter and n represent any given physical-time level. The pseudo-time-derivative is drive to zero at each physical time level by a series of inner iterations using either the implicit or the explicit time-marching algorithm. Throughout the (inner) iteration is pseudo-time, W^n and W^{n-1} are held constant and W_k is computed fromO^k. As $\tau\to\infty$, the solution at the next physical time level$W_n + 1$ is given by $W(O^k)$.

Note that the physical time steps Δt limited only by the level temporal accuracy. The pseudo-time-step $\Delta\tau$ is determine by the CFL condition of the (implicit or explicit) time-marching scheme.

2.2.3.4 Incompressible Ideal Gas Law

In ANSYS Fluent, if you choose to define the density using the ideal gas law for incompressible flow the solver will compute the density as

$$\rho = \frac{p_{oP}}{\frac{R}{M_w}T} \tag{2.53}$$

Where,

R = the universal gas constant

M_w = the molecular weight of the gas

poP = Operating pressure

2.2.3.5 Energy Equation

Equation solved in fluent

$$\frac{\partial(\rho h)}{\partial t} = \nabla.(k\nabla T) + S_h \tag{2.54}$$

The dependent variable h is the enthalpy. S_h Includes the heat of chemical reaction, and any other volumetric heat sources you have defined

$$h = \int_0^T C_p \, dT \tag{2.55}$$

Anisotropic thermal conductivity is only available for solid material. By default, the thermal conductivity considered isotropic. For anisotropic material, the thermal conductivity is a matrix

$$q_i = -k_{ij}\frac{\partial T}{\partial x_j} \tag{2.56}$$

Thermal conductivity matrix can defined using one of five different methods:

- Orthotropic
- Cylindrical orthotropic
- General anisotropic
- Biaxial (shell conduction only)
- Anisotropic thermal conductivity (UDF)

Anisotropic thermal conductivity for the solid zone:

- Defining parameters may depend on temperature
- UDF or constant/polynomial definition is also possible

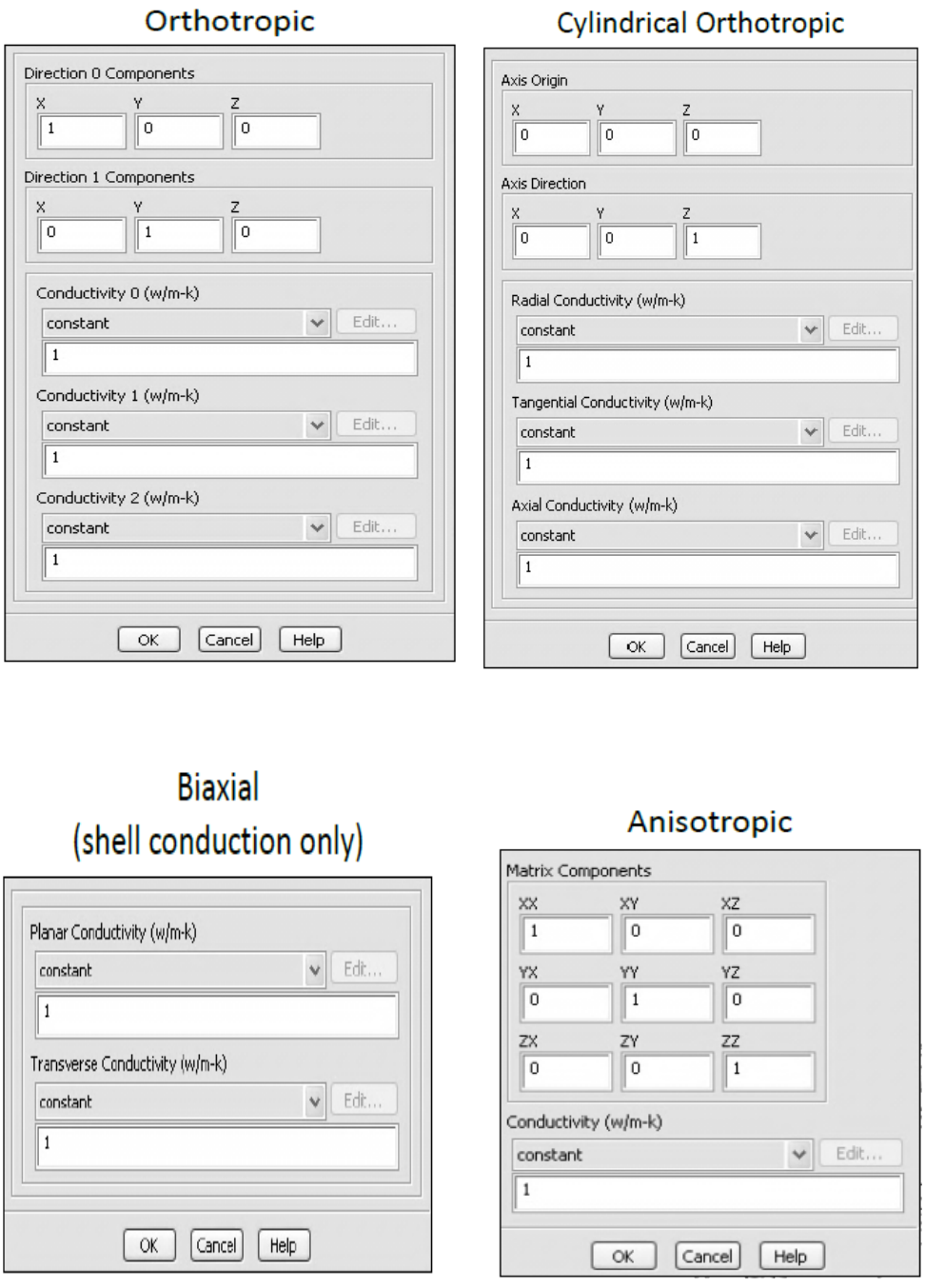

Fig.18. Anisotropic thermal conductivity for solid zone

2.2.3.6 Thermal Wall Boundary Condition

a) Temperature Boundary Condition

When temperature boundary condition applied at the wall, the heat flux to the wall form a fluid cell computed as

$$q = h_f(T_w - T_f) + q_{rad} \tag{2.57}$$

WhereH_f is fluid-side local heat transfer coefficient, T_w is wall surface temperature, T_f is local fluid temperature, q_{rad} is radiative heat flux.

Note that fluid-side heat transfer coefficient computed based on the local flow-field conditions. Heat transfer to the wall boundary from a solid cell computed as

$$q = \frac{k_s}{\Delta n}(T_w - T_s) + q_{rad} \tag{2.58}$$

K_s thermal conductivity of the solid $T_s$is local solid temperature, the Δn distance between the wall surface and the solid cell center.

b) Heat flux boundary conditions

When you define a heat flux boundary condition at a wall, you specify the heat flux at wall surface. Fluent uses equation (2.58) and your input of heat flux to determine the wall surface temperature adjacent to fluid cell as

$$T_w = \frac{q - q_{rad}}{h_f} + T_f \tag{2.59}$$

Where, as noted above, the fluid-side heat transfer coefficient computed based on the local flow field conditions. When the wall borders is a solid region. The wall surface temperature computed as

$$T_w = \frac{(q - q_{rad})\Delta n}{k_s} + T_s \tag{2.60}$$

c) Convective Heat Transfer Boundary Conditions

When you specify a convective heat transfer coefficient in boundary condition at a wall, FLUENT uses your inputs of the external heat sink temperature to compute the heat flux to the wall as

$$q = h_f(T_w - T_f) + q_{rad}$$
$$= h_{ext}(T_{ext} - T_w) \quad (2.61)$$

Whereh_{ext} is external heat transfer coefficient defined by you, T_{ext} is external heat sink defined by you; q_{rad} is radiative heat flux.

d) When the external radiation boundary condition is used FLUENT, the heat flux to the wall is computed as

$$q = h_f(T_w - T_f) + q_{rad}$$
$$= \epsilon_{ext}\sigma(T_\infty^4 - T_w^4) \quad (2.62)$$

Where

$\in_{ext}$ is emissivity of the external wall surface defined by you, σ is Stefan-Boltzmann Constant, T_w is surface temperature of the wall, T_∞ is the temperature of the radiation source or sink on the exterior of the domain, defined by you, q_{rad} is radiative heat flux to the wall from within the domain. Equation (57) assumes a wall zero thickness.

e) Combined external convection and radiation boundary condition

When you choose the combined external heat transfer condition, the heat flux to the wall computed as

$$q = h_f(T_w - T_f) + q_{rad}$$
$$= h_{ext}(T_{ext} - T_w) + (\epsilon_{ext}\sigma(T_\infty^4 - T_w^4) \quad (2.63)$$

Where the variables are as defined above. Equation (2.63) assumes a wall of zero thickness.

f) Calculation of Fluid-Side heat transfer coefficient

In laminar flow, the fluid side in heat transfers at walls computed using Fourier´s law applied to the walls. Fluent use its discrete form:

$$q = k_f \left(\frac{\partial T}{\partial n}\right)_{wall} \quad (2.64)$$

Where n is the local coordinate normal to the wall. For turbulent flow, FLUENT uses the law-of-the-wall for temperature derived using the analogy between heat and momentum transfer. [85]

2.2.3.7 Turbulent flow (*k*-ε model)

Turbulence is the three-dimensional unsteady random motion observed in fluids at moderate to high Reynolds numbers [86] as technical flows typically based on fluids of low viscosity, almost all technical flows are turbulent. Many quantities of technical interest depend on turbulence, such as: Mixing of momentum, energy, and species

- Heat transfer
- Pressure losses and efficiency
- Forces on aerodynamic bodies

While turbulence is, in principle, described by the Navier-Stokes equations, it is not feasible in most situations to resolve the broad range of scales in time and space by Direct Numerical Simulation (DNS) as the CPU requirements would by far exceed the available computing power for any near future. For this reason, averaging procedures have to apply to the Navier-Stokes equations to filter out all, or at least, parts of the turbulent spectrum. The most widely used averaging method is Reynolds averaging (which, for all practical purposes is time averaging) of the equations, resulting in the Reynolds-Averaged Navier-Stokes (RANS) equations.

By this process, all turbulent structures eliminated from the flow and a smooth variation of the averaged velocity and pressure fields can obtain. However, the averaging process introduces additional unknown terms into the transport equations (Reynolds Stresses and Fluxes), which need to provide by suitable turbulence models (turbulence closures). The quality of the simulation can depend crucially on the selected turbulence model, and it is important to make the proper design choice as well as to provide a suitable numerical grid for the chosen model.

An alternative to RANS is Scale-Resolving Simulation (SRS) models. With SRS methods, at least a portion of the turbulent spectrum resolved in at least a part of the flow domain. The most well know such method is Large Eddy Simulation (LES), but many new hybrids (models between RANS and LES) are appearing. As all SRS methods require time-resolved simulations with relatively minor steps, it is important to understand that these methods are substantially more computationally expensive tan RANS simulations.

The *k*-epsilon model is one of the most common turbulence models, although it just [87] does not perform well in cases of large adverse pressure gradients [88]. It is a two-equation model that means it includes two extra transport equations to represent the turbulent properties of the flow. This allows a two-equation model to account for history effects like convection and diffusion of turbulent energy.

The first transported variable is turbulent kinetic energy. The second transported variable, in this case, is the turbulent dissipation $\in$. It is the variable that determines the scale of the turbulence, whereas the first variable, *k* determines the energy in the turbulence.

There are two major formulations of *k*-epsilon models. [89] [90] That of Launder and Sharma is typically called the "Standard" *k*-epsilon Model. The original impetus for the *k*-epsilon model was to improve the mixing-length model; as well as to find an alternative to algebraically prescribing turbulent length scales in moderate to high complexity flows.

As described in [91], the *k*-epsilon model has been shown to be useful for free-shear layer flows with relatively small pressure gradients. Similarly, for wall-bounded and internal flows, the model gives good results only in cases where mean pressure gradients are small; accuracy has shown experimentally to reduce for flows containing large adverse pressure gradients. One might infer then, that

the *k*-epsilon model would be an inappropriate choice for problems such as inlets and compressors.

In this case, is using RNG k-ε model. The RNG *k*-ε model has a similar form the standard k-ε model:

$$\frac{\partial}{\partial t}(\rho k) + \frac{\partial}{\partial x_i}(\rho k u_i) = \frac{\partial}{\partial x_j}\left(\alpha_\varepsilon \mu_{eff} \frac{\partial k}{\partial x_j}\right) + G_k + G_b - \rho\varepsilon - Y_M + S_k \quad (2.65)$$

And

$$\frac{\partial}{\partial t}(\rho \varepsilon) + \frac{\partial}{\partial x_i}(\rho \varepsilon u_i) = \frac{\partial}{\partial x_j}\left(\alpha_\varepsilon \mu_{eff} \frac{\partial \varepsilon}{\partial x_j}\right) + C_{1\varepsilon}\frac{\varepsilon}{k}(G_k + C_{3\varepsilon}G_b) - C_2\rho\frac{\varepsilon^2}{k} - R_\varepsilon + S_\varepsilon \quad (2.66)$$

In these equations, G_k represents the generation of turbulence kinetic energy due to the mean velocity gradients. G_h, is the generation of turbulence kinetic energy due to buoyancy Y_M represent the contribution of the fluctuating dilatation incompressible turbulence to the overall dissipation rate. The quantities αk and αε are inverse effective Prandtl numbers for *k* and*ε,* respectively, S_k and S_ε are user-defined source term.

2.2.3.8 Discrete Ordinates (DO) Radiation Model Theory

The discrete ordinate (DO) radiation model solves the radiation transfer equation (RTE) for a finite number of discrete solid angles, each associated with a vector direction $\vec{S}$ fixed in the global Cartesian system (x, y, and z).

The DO model consider the radiative equation (DTE) in the direction $\vec{s}$ as a field equation is written as

$$\nabla.(I(\vec{r},\vec{s})\vec{s}) + (a+\sigma_s)I(\vec{r},\vec{s}) = an^2\frac{\sigma T^4}{\pi} + \frac{\sigma_s}{4\pi}\int_0^{4\pi} I(\vec{r},\vec{s}')\Phi(\vec{s},\vec{s}')d\Omega' \quad (2.67)$$

In addition, ANSYS FLUENT allows the modeling of non-gray radiation using a gray-band model. The RTE of the spectral intensity $I_\lambda(\vec{r}.\vec{s})$can write as

$$\nabla.(I_\lambda(\vec{r},\vec{s})\vec{s}) + (a_\lambda+\sigma_s)I_\lambda(\vec{r},\vec{s}) = a_\lambda n^2 I_{b\lambda} + \frac{\sigma_s}{4\pi}\int_0^{4\pi} I_\lambda(\vec{r},\vec{s}')\Phi(\vec{s},\vec{s}')d\Omega' \quad (2.68)$$

Here λ is the wavelength $a_{\lambda,}$ is the spectral absorption coefficient, and I_α is the black body intensity given by the plank

function. The scattering coefficient, the phase function, and the refractive index *n* assume independent of wavelength.

The non-gray DO implementation divides the radiation spectrum into N wavelength bands, which need not be contiguous or equal extent. The wavelength intervals are supplied by you and correspond to value in a vacuum (n=1). The RTE is the integrated over each wavelength interval, resulting in transport equations for the quantity$I_\lambda \Delta\lambda$, the radiant energy contained in the wavelength band $\Delta\lambda$. The behavior in each band assumed gray. The black body emission in the wavelength band per unit solid angle written as

$$[F(0 \to n\lambda_2 T) - F(0 \to n\lambda_1 T]n^2 \frac{\sigma T^4}{\pi} \tag{2.69}$$

Where $F(0 \to n\lambda_2 T)$ is the fraction of radiant energy emitted by a black body in the wavelength interval from zero to λ at the temperature T in a medium of refractive index *n*. λ_2 and λ_1 are the wavelength boundaries of the band. The total intensity $I(\vec{r}, \vec{s})$ in each direction $\vec{s}$ at position $\vec{r}$ computed using

$$I(\vec{r}, \vec{s}) = \sum_k I_{\lambda_k}(\vec{r}, \vec{s})\Delta\lambda_k \tag{2.70}$$

Where, the summation is over the wavelength bands.

Boundary conditions for the non-gray DO model applied on a band basis. The treatment within a band is the same as that for the gray DO model.

2.2.3.9 Solution Method SIMPLE

The simple algorithm uses a relationship between velocity and pressure correction to enforce mass conservation and to obtain the pressure field.

If momentum equation is solved with a guessed pressure field ***p****, the resulting face flux, $\boldsymbol{J^*_f}$,

$$J_f^* = \hat{J}_f^* + d_f(p_{c0}^* - p_{c1}^*) \tag{2.71}$$

It does not satisfy the continuity equation. Consequently, a correction J'_f is added to the face flux J^*_f so that the correct face flux, J_f

$$J_f = J_f^* + J_f' \tag{2.72}$$

It satisfies the continuity equation. The SIMPLE algorithm postulates that J'_f written as

$$J_f' = d_f(p_{c0}' - p_{c1}') \tag{2.73}$$

Where, p' is the cell pressure correction.

The SIMPLE algorithm substitutes the flux correction equations (Equations 40 and (2.72) into the discrete continuity equation

$$\sum_f^{N_{faces}} J_f A_f = 0 \tag{2.74}$$

To obtain a discrete equation for the pressure correction P′ in the cell

$$aP\ p' = \sum_{nb} a_{nb} p_{nb}' + b \tag{2.75}$$

Where the source term b is the net flow rate into the cell:

$$b = \sum_f^{N_{faces}} J_f^* A_f \tag{2.76}$$

The pressure-correction equation (42) may solve using the algebraic multigrid (AMG) method. Once a solution obtained, the cell pressure and the face flux corrected using.

$$p = p^* + \alpha_p p' \tag{2.77}$$

$$J_f = J_f^* + d_f(p_{c0}' - p_{c1}') \tag{2.78}$$

Here α_p is the under-relaxation factor for pressure. The corrected face flux, J_f, satisfies the discrete continuity equation identically during iteration.

CHAPTER 3. METHODOLOGY

3.1 Geometry

3.1.1 2-Dimensional Axisymmetric simulation of one vertical coil

The coil was assumed to be located vertically in a spacious room measuring 4.5 m x 4.5 m. Conduction, natural convection and radiation process were considered for the 2D axisymmetric case. The number of cells used was 10,000. Mesh elements were quad and type paved. In the present study, the geometry was performed using Gambit 2.4.6 FLUENT Inc. USA and CFD package ANSYS FLUENT.

Figure 19 shows a vertical cross section of the coil were x axis is the symmetry axis of the coil and the position of steel coil is vertical (only half of the section is shown).

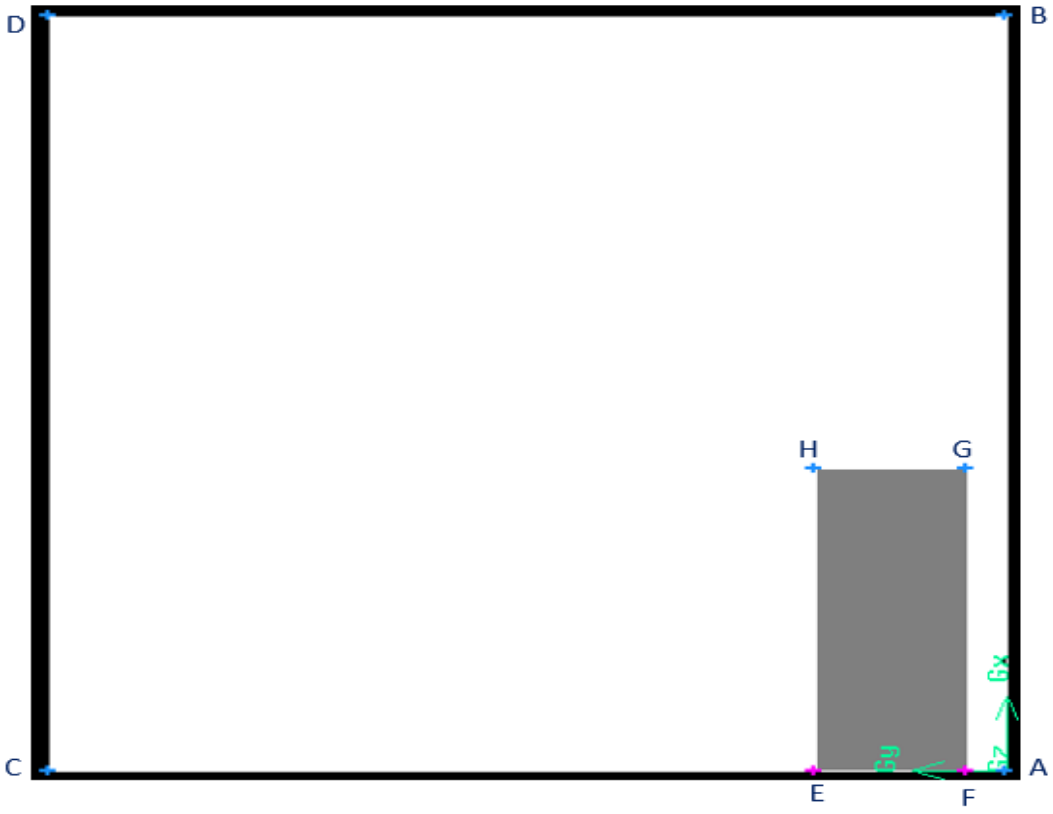

Fig.19. 2-Dimensional axisymmetric (vertical coil)

Gambit 2.4.6 was used to create the geometry before it was exported to ANSYS FLUENT. The coordinates for creating 2-Dimensional axisymmetric geometry were as follows:

Table 1. Coordinates for 2-Dimensional axisymmetric case

Point	***x***	***y***
A	0	0
B	4.5	0
C	0	4.5
D	4.5	4.5
E	0	0.9
F	0	0.18
G	1.8	0.1800
H	1.8	0.9

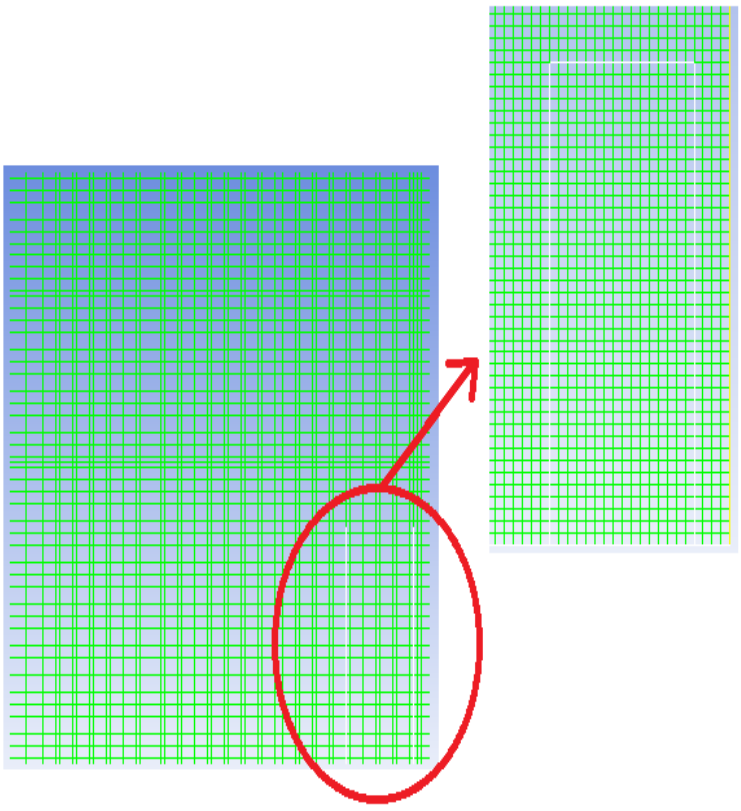

Fig.20. 2-Dimensional axisymmetric mesh (10,000 cells)

The characteristics used for the 2D axisymmetric case were:

a) Solver

Solver	**Settings**
Type	Pressure based
Time	Transient
Velocity Formulation	Absolute
Gravity (x coordinate)	-9.8 m/s^2

b) Models

Models	**Settings**
Energy	On
Space	2D axisymmetric
Viscous	RNG k-epsilon Turbulence model
Heat transfer	Enabled
Radiation	Discrete Ordinate Model

c) Material properties

Steel (Solid)			
Property	**Units**	**Method**	**Value(s)**
Density	kg/m^3	constant	8030
Cp (Specific Heat)	J/kg-K	constant	504.48001
Thermal Conductivity	W/m-k	constant	45
Absorption Coefficient	1/m	constant	0
Scattering Coefficient	1/m	constant	0
Scattering Phase Function		isotropic	
Refractive Index		constant	1
Calcium carbonate (Solid)			
Density	kg/m^3	constant	2800
Cp (Specific Heat)	J/kg-K	constant	856
Thermal Conductivity	W/m-k	constant	2.25
Absorption Coefficient	1/m	constant	0
Scattering Coefficient	1/m	constant	0
Scattering Phase Function		isotropic	
Refractive Index		constant	1
Air (Fluid)			
Density	kg/m^3	Incompressible-ideal gas	
Cp (Specific Heat)	J/kg-K	constant	1006.43
Thermal Conductivity	W/m-k	constant	0.0242
Viscosity	kg/m-s	constant	1.7894001e-05
Molecular Weight	kg/kgmol	constant	28.966
Absorption Coefficient	1/m	constant	0
Scattering Coefficient	1/m	isotropic	0
Scattering Phase Function		constant	0
Thermal Expansion Coefficient	1/k	constant	1
Refractive Index	m/s	none	

d) Cell zone conditions

Name	**Type**	**Material**
scoils	Solid	Steel
sair	Fluid	Air

e) Boundary conditions

Zones	Type
bottom1	wall
coils	wall
coils:012	wall
coils:012-shadow	wall
default interior	interior
default interior:013	interior
lefttside	wall
Interior	interior
upper	pressure inlet

f) Convergence parameters

Residual	Monitor check
Continuity	1e-06
X velocity	1e-06
Y velocity	1e-06
Energy	1e-06
k	1e-06
epsilon	1e-06
do intensity	1e-06

3.1.2 2-Dimensional Planar simulation of one horizontal coil

The coil was assumed to be located horizontally in a spacious room measuring 6 m x 6 m. Conduction, natural convection and radiation processes were considered for the 2-Dimensional planar case. The number of cells was 110,202. Mesh elements were quad and type paved. In the present study, the geometry is performed by using Gambit 2.4.6 FLUENT Inc. USA and CFD package ANSYS FLUENT.

Figure 21 shows a vertical cross section of the horizontal coil were the symmetry axis of the coil is perpendicular to the drawing x (only half of the section is shown).

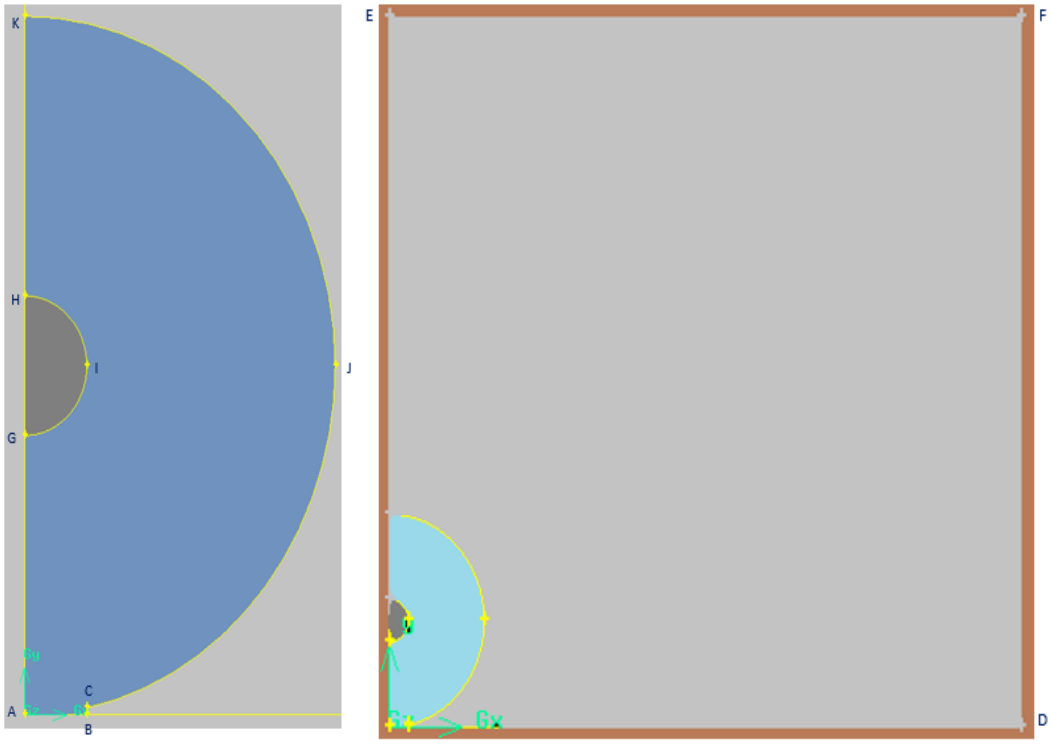

Fig.21. 2-Dimensional planar

Gambit 2.4.6 was used to define the geometry before exported to ANSYS FLUENT. The coordinates for creating the 2-Dimensional planar geometry were as follows:

Table 2. Coordinates for 2-Dimensional planar case

Point	***x***	***y***
A	0	0.000
B	0.18	0.000
C	0.180	0.018184
D	6	0
E	0	6
F	6	6
G	0	0.72
H	0	1.08
I	0.18	0.9
J	0.9	0.9
K	0	1.8

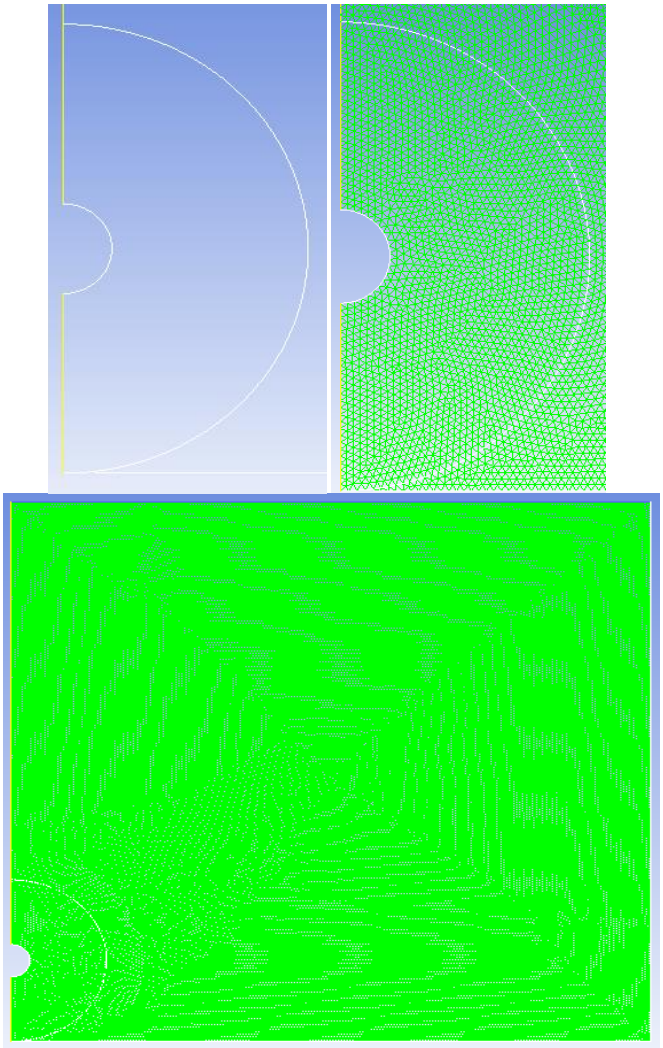

Fig.22. 2-Dimensional planar mesh (110,202 cells)

The characteristics used for the 2D planar case were as follows:

a) Solver

Solver	**Settings**
Type	Pressure based
Time	Transient
Velocity Formulation	Absolute
Gravity (y coordinate)	-9.8 m/s^2

b) Models

Models	**Settings**
Energy	On
Space	2D planar
Viscous	RNG k-epsilon Turbulence model
Heat transfer	Enabled
Radiation	Discrete Ordinate Model

c) Material properties

Steel (Solid)			
Property	**Units**	**Method**	**Value(s)**
Density	kg/m^3	constant	8030
Cp (Specific Heat)	J/kg-K	constant	504.48001
Thermal Conductivity	W/m-k	constant	45
Absorption Coefficient	1/m	constant	0
Scattering Coefficient	1/m	constant	0
Scattering Phase Function		isotropic	
Refractive Index		constant	1
Calcium carbonate (Solid)			
Density	kg/m^3	constant	2800
Cp (Specific Heat)	J/kg-K	constant	856
Thermal Conductivity	W/m-k	constant	2.25
Absorption Coefficient	1/m	constant	0
Scattering Coefficient	1/m	constant	0
Scattering Phase Function		isotropic	
Refractive Index		constant	1
Air (Fluid)			
Density	kg/m^3	Incompressible-ideal gas	
Cp (Specific Heat)	J/kg-K	constant	1006.43
Thermal Conductivity	W/m-k	constant	0.0242
Viscosity	kg/m-s	constant	1.7894001e-05
Molecular Weight	kg/kg.mol	constant	28.966
Absorption Coefficient	1/m	constant	0
Scattering Coefficient	1/m	isotropic	0
Scattering Phase Function		constant	0
Thermal Expansion Coefficient	1/k	constant	1
Refractive Index	m/s	none	

d) Cell zone conditions

Name	Type	Material
scoils	Solid	Steel
sair	Fluid	Air

e) Boundary conditions

Zones	Type
bottom	wall
coil	wall
coil:012	axis
coils:012-shadow	wall
default-interior	interior
default-interior:013	interior
left_side	wall
line_symmetry	symmetry
Line_symmetry:019	symmetry
upper	pressure inlet
wall	wall

f) Convergence parameters

Residual	Monitor check
Continuity	1e-06
X velocity	1e-06
Y velocity	1e-06
Energy	1e-06
k	1e-06
epsilon	1e-06
do intensity	1e-06

3.1.3 3-Dimensional simulation of one horizontal coil

The coil was assumed to be located horizontally in a spacious room measuring 12 m x 12 m x 12 m. Conduction, natural convection and radiation processes were considered for the 3-Dimensional cooling simulation. The number of cells used was 386,340. Elements were quad and type paved. In the present study, the geometry is performed by using Gambit 2.4.6 FLUENT Inc. USA and CFD package ANSYS FLUENT.

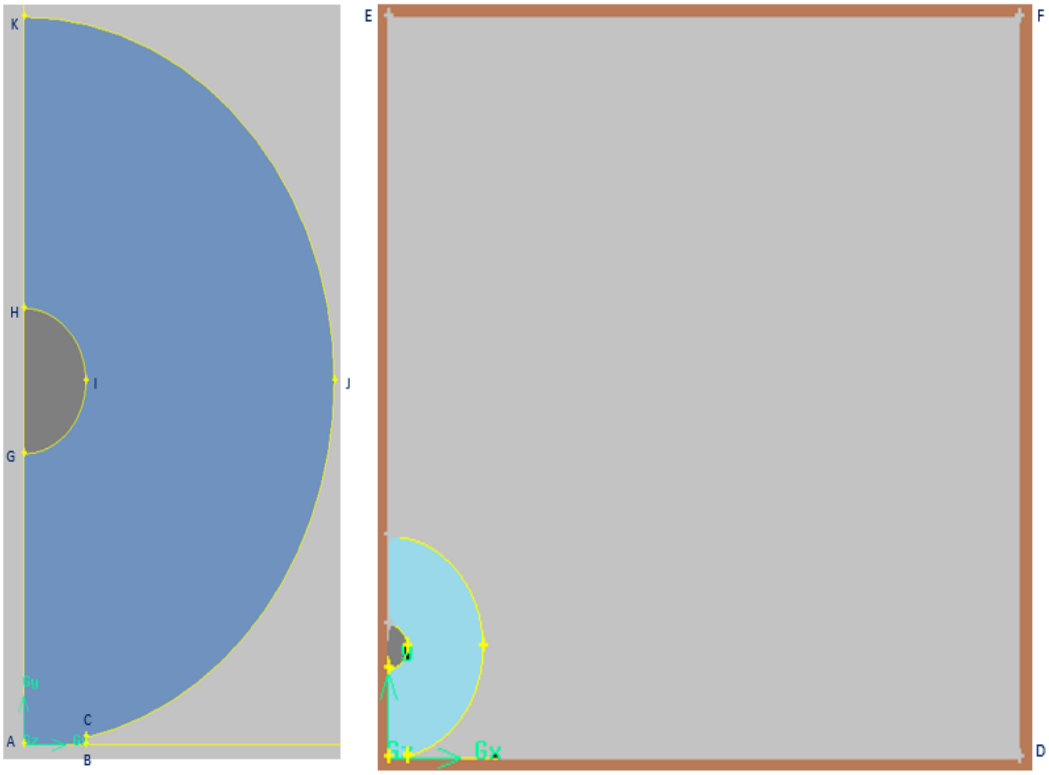

Fig.23. 3-Dimensional one coil

Gambit 2.4.6 was used to define the geometry before exported to ANSYS FLUENT. The coordinates for creating the 3-dimensional geometry of one coil were as follows:

Table 3. Coordinates for 3-Dimensional one coil case

Point	***x***	***y***
A	0	0.000
B	0.18	0.000
C	0.180	0.018184
D	6	0
E	0	6
F	6	6
G	0	0.72
H	0	1.08
I	0.18	0.9
J	0.9	0.9
K	0	1.8

The first step of testing simulations was using steady flow (Time-steady), which aims to obtain a constant temperature (673.15 K) in the coil and the direction of the air velocity during the coil cooling. Once completed the steady flow, its solution was used as the initial conditions for the transient solver.

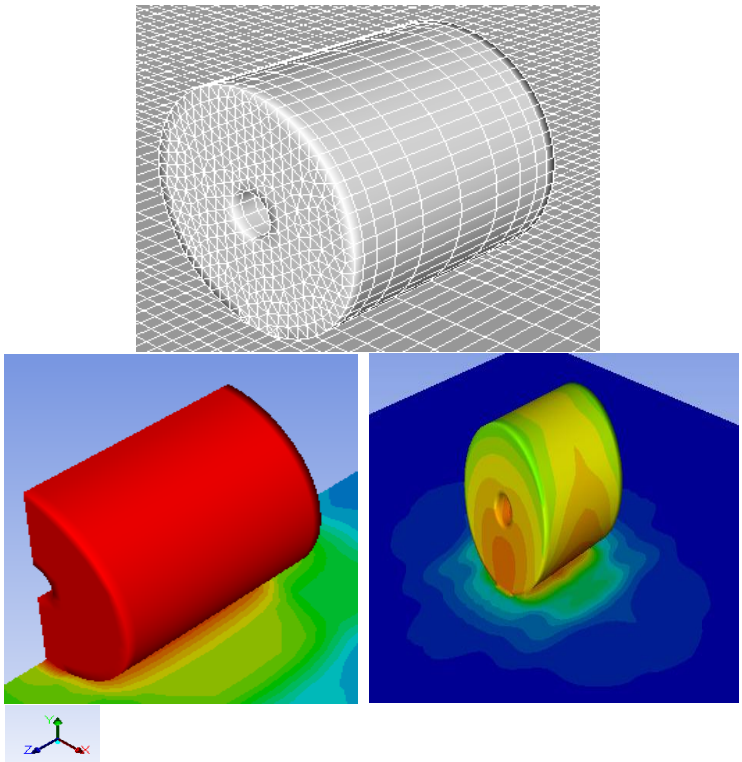

Fig.24. 3-Dimensional one-coil model (386,340 cells)

The Characteristics used for the 3-dimensional three coils were as follows:

a) Solver

Solver	**Settings**
Type	Pressure based
Time	Transient
Velocity Formulation	Absolute
Gravity (y coordinate)	-9.8 m/s^2

b) Models

Models	**Settings**
Energy	On
Space	3D one coil
Viscous	RNG k-epsilon Turbulence model
Heat transfer	Enabled
Radiation	Discrete Ordinate Model

c) Material properties

Steel (Solid)			
Property	**Units**	**Method**	**Value(s)**
Density	kg/m^3	constant	8030
Cp (Specific Heat)	J/kg-K	constant	504.48001
Thermal Conductivity	W/m-k	constant	45
Absorption Coefficient	1/m	constant	0
Scattering Coefficient	1/m	constant	0
Scattering Phase Function		isotropic	
Refractive Index		constant	1
Calcium carbonate (Solid)			
Density	kg/m^3	constant	2800
Cp (Specific Heat)	J/kg-K	constant	856
Thermal Conductivity	W/m-k	constant	2.25
Absorption Coefficient	1/m	constant	0
Scattering Coefficient	1/m	constant	0
Scattering Phase Function		isotropic	
Refractive Index		constant	1
Air (Fluid)			
Density	kg/m^3	Incompressible-ideal gas	
Cp (Specific Heat)	J/kg-K	constant	1006.43
Thermal Conductivity	W/m-k	constant	0.0242
Viscosity	kg/m-s	constant	1.7894001e-05
Molecular Weight	kg/kg.mol	constant	28.966
Absorption Coefficient	1/m	constant	0
Scattering Coefficient	1/m	isotropic	0
Scattering Phase Function		constant	0
Thermal Expansion Coefficient	1/k	constant	1
Refractive Index	m/s	none	

d) Cell zone conditions

Name	**Type**	**Material**
scoils	Solid	Steel
sair	Fluid	Air

e) Boundary conditions

Zones	Type
cbelow	wall
cbelow:014	wall
ccoils	wall
coils-shadow	wall
cfrontside	wall
cmidsymmetry	symmetry
cmidsymmetry:011	symmetry
crightside	wall
csymmetry	symmetry
csymmetry:013	symmetry
cupper	pressure inlet
default-interior	interior
default-interior:015	interior

f) Convergence parameters

Residual	Monitor check
Continuity	1e-06
X velocity	1e-06
Y velocity	1e-06
Energy	1e-06
k	1e-06
epsilon	1e-06
do intensity	1e-06

3.1.4 3-Dimensional simulation of three horizontal coils

For the simulation of a 3-dimensional geometry of the three coils, 488,100 cells were used. The size of the room was 12 m x 12 m x 12 m. The results of the steady flow (Time-steady) were used to obtain the initial conditions for the transient solver, analogously to the previous case.

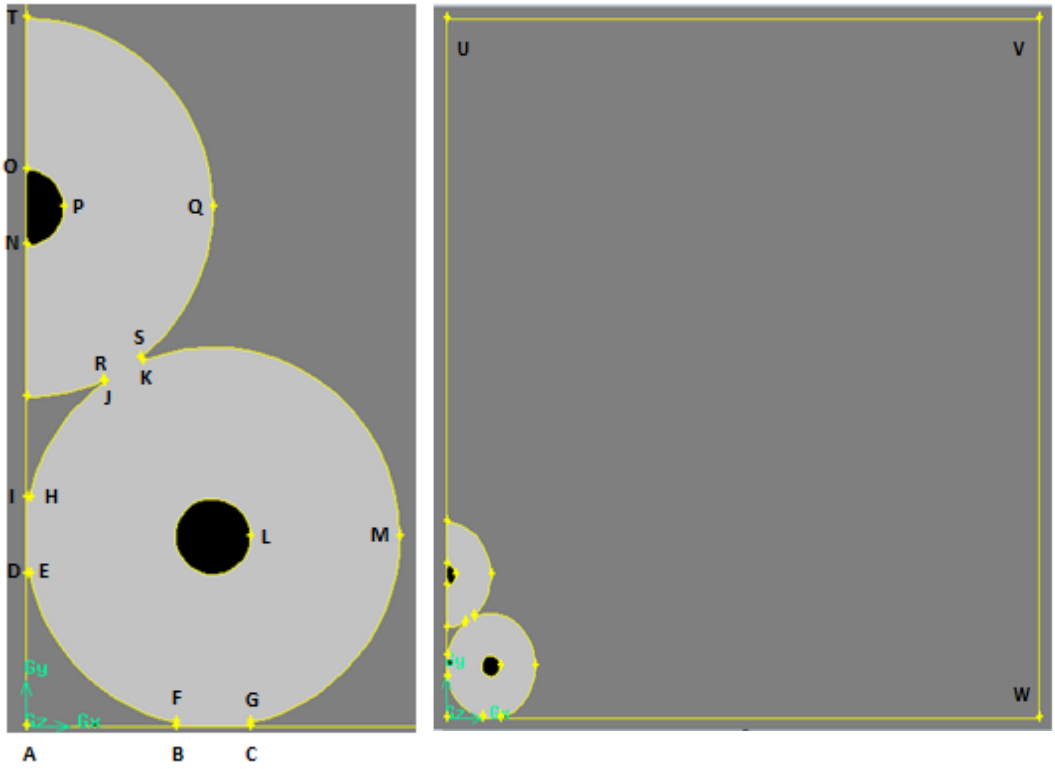

Fig.25. 3-dimensional three coils

We use Gambit 2.4.6 for geometry before export to ANSYS FLUENT. The coordinate for creating 3-dimensional three coils geometry are as follows:

Table 4. Coordinates for 3-Dimensional three coils case

Point	***x***	***y***
A	0.0	0.0
B	0.72	0.0
C	1.08	0.0
D	0.0	0.72
E	0.018184	0.72
F	0.72	0.018184
G	1.08	0.018184
H	0.0	1.08
I	0.018184	1.08
J	0.374811	1.630874
K	0.559485	1.733096
L	1.08	0.9
M	1.8	0.9
N	0.0	2.280937
O	0.0	2.640938
P	0.18	2.460938
Q	0.9	2.460938
R	0.369409	1.640244
S	0.551019	1.749335
T	0.0	3.360937
U	0.0	12
V	12	12
W	12	0

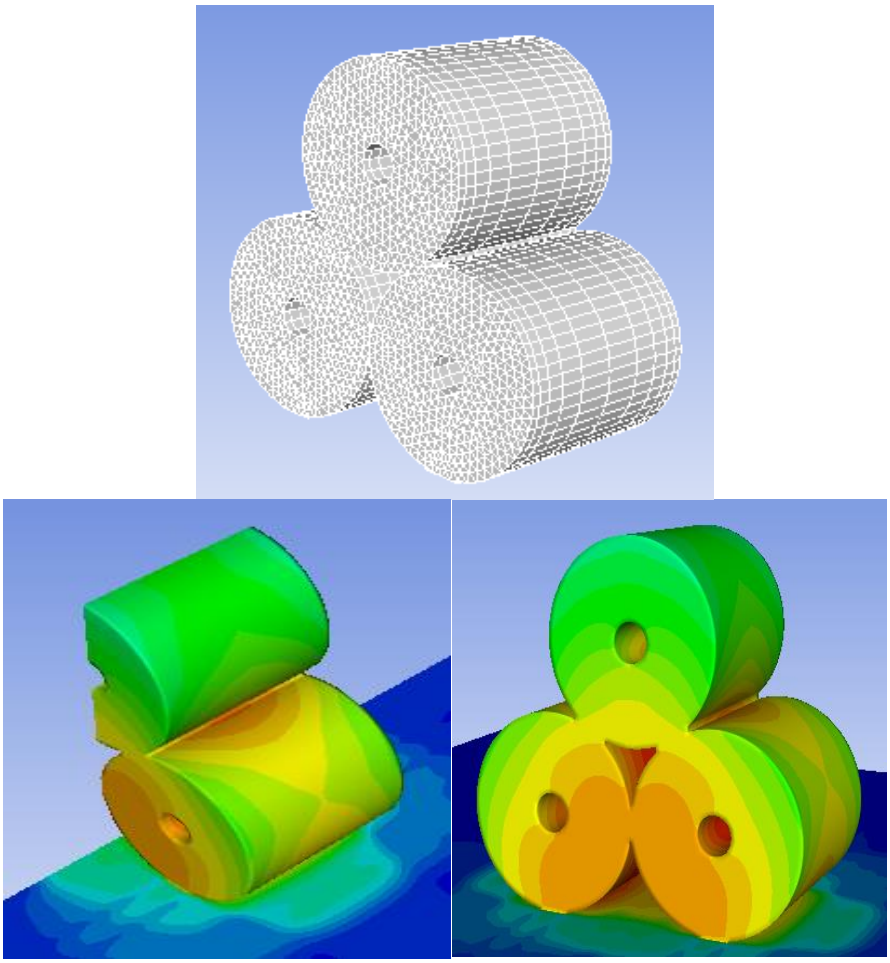

Fig.26. 3D model of three coils

The data used for the 3-dimensional three coils were as follows:

a) Solver

Solver	**Settings**
Type	Pressure based
Time	Transient
Velocity Formulation	Absolute
Gravity (y coordinate)	-9.8 m/s^2

b) Models

Models	**Settings**
Energy	On
Space	3D three coils
Viscous	RNG k-epsilon Turbulence model
Heat transfer	Enabled
Radiation	Discrete Ordinate Model

c) Material properties

Steel (Solid)			
Property	**Units**	**Method**	**Value(s)**
Density	kg/m^3	constant	8030
Cp (Specific Heat)	J/kg-K	constant	504.48001
Thermal Conductivity	W/m-k	constant	45
Absorption Coefficient	1/m	constant	0
Scattering Coefficient	1/m	constant	0
Scattering Phase Function		isotropic	
Refractive Index		constant	1
Calcium carbonate (Solid)			
Density	kg/m^3	constant	2800
Cp (Specific Heat)	J/kg-K	constant	856
Thermal Conductivity	W/m-k	constant	2.25
Absorption Coefficient	1/m	constant	0
Scattering Coefficient	1/m	constant	0
Scattering Phase Function		isotropic	
Refractive Index		constant	1
Air (Fluid)			
Density	kg/m^3	Incompressible-ideal gas	
Cp (Specific Heat)	J/kg-K	constant	1006.43
Thermal Conductivity	W/m-k	constant	0.0242
Viscosity	kg/m-s	constant	1.7894001e-05
Molecular Weight	kg/kg.mol	constant	28.966
Absorption Coefficient	1/m	constant	0
Scattering Coefficient	1/m	isotropic	0
Scattering Phase Function		constant	0
Thermal Expansion Coefficient	1/k	constant	1
Refractive Index	m/s	none	

d) Cell zone conditions

Name	Type	Material
scoils	Solid	Steel
sair	Fluid	Air

e) Boundary conditions

Zones	Type
cbelow	wall
cbelow:014	wall
ccoils	wall
coils-shadow	wall
cfrontside	wall
cmidsymmetry	symmetry
cmidsymmetry:011	symmetry
crightside	wall
csymmetry	symmetry
csymmetry:013	symmetry
cupper	pressure inlet
default-interior	interior
default-interior:015	interior

f) Convergence parameters

Residual	Monitor check
Continuity	1e-06
X velocity	1e-06
Y velocity	1e-06
Energy	1e-06
k	1e-06
epsilon	1e-06
do intensity	1e-06

3.2 Specific heat and thermal conductivity varying with temperature and the interlayer pressure

Coils are formed by different strips and depending on the interlayer pressure and temperature of the different points inside the coils, thermal conductivity and specific heat vary. Simulations with both specific heat and thermal conductivity constant will be compared to the simulations performed with radial variation of the thermal conductivity (cyl-orthotropic thermal conductivity varying with the interlayer pressure and constant temperature). Also, Simulations with the later conditions will be compared to cyl-orthotropic thermal conductivity with four points at different temperatures.

Figure 27 shows the directions (radial, axial and tangential) in which specific heat and thermal conductivity may vary.

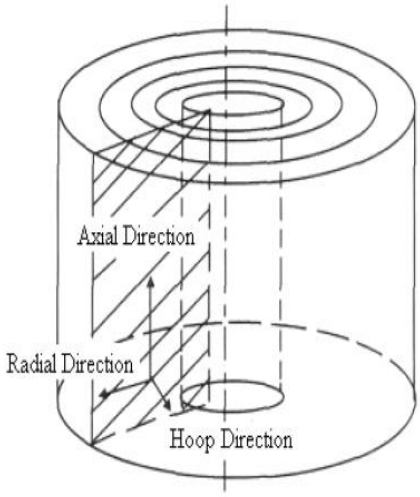

Fig.27. Different directions in the geometry of strip coils

Saboonchi and Hassanpour [65] obtained the values of the specific heat and the thermal conductivity for the mentioned cases. They are shown on tables 5, 6 and 7.

Table.5. Specific heat and thermal conductivity with constant value

Specific Heat (c) (J/Kg-K)	Constant	502.48
Thermal Conductivity (Ks) (W/m-k)	Constant	45

Table.6. Constant specific heat and cyl-orthotropic thermal conductivity at different interlayer pressures and one point (673.15 K)

		Interlayer pressure (MPa)			
		0	2	5	10
Specific Heat (c) (J/Kg-K)	Constant	502.48	502.48	502.48	502.48
Thermal conductivity (K) (W/m-K) *cyl-orthotropic*	Radial Conductivity	5.31	17.00	25.225	32
	Tangencial Conductivity	45	45	45	45
	Axial Conductivity	45	45	45	45

Table.7. Variable specific heat and cyl-orthotropic thermal conductivity at different interlayer pressures and with four points (temperatures).

		Points	**Temperature (K)**	**Interlayer Pressure (MPa)**			
				0	2	5	10
Specific Heat (c) (J/Kg-K)	piecewise-linear	1	373.15	490.5	490.5	490.5	490.5
		2	473.15	527.5	527.5	527.5	527.5
		3	573.15	563.5	563.5	563.5	563.5
		4	673.15	611.8	611.8	611.8	611.8
Thermal Conductivity (K) (W/m-K) *cyorthotropic*	Radial Conductivity	1	373.15	3.48	15.89	24.64	31.51
		2	473.15	4.16	16.27	24.85	31.66
		3	573.15	4.75	16.63	25.01	31.76
		4	673.15	5.31	17.00	25.225	32.00
	Tangential Conductivity	1	373.15	53	53	53	53
		2	473.15	50	50	50	50
		3	573.15	45	45	45	45
		4	673.15	43	43	43	43
	Axial Conductivity	1	373.15	53	53	53	53
		2	473.15	50	50	50	50
		3	573.15	45	45	45	45
		4	673.15	43	43	43	43

3.3 Cooling law: Equation of the temperature decrease

The total heat transfer from the coil to the ambient may be considered as a combination of convection and radiation effects. The equations that describe these two phenomena are the following:

Convection

$$\frac{dT}{dt} = -k_1(T - T_0) \tag{3.1}$$

Radiation

$$\frac{dT}{dt} = -k_2(T^4 - T_0^4) \tag{3.2}$$

Radiative cooling is described by the Stefan-Boltzmann law which states that rate of heat loss per unit surface area of a body at temperature T is proportional to $T^4–T_0^4$, where T_0 is the mean temperature of the surrounding radiation sources. Thus the combined rate of heat energy loss from a body of surface area A due to both convection and radiation is:

$$hS(T - T_0) + \varepsilon\sigma A(T^4 - T_0^4) \tag{3.3}$$

where the constant h is the heat transfer coefficient for pure convection and depends on the cooling conditions. ε is the emissivity of the surface and σ is the Stefan-Boltzmann constant. Thus the rate of change of temperature of the body is given by

$$-\frac{dT}{dt} = \frac{hS}{C}(T - T_0) + \frac{\varepsilon\sigma S}{C}(T^4 - T_0^4) \tag{3.4}$$

Where $C = \frac{\partial Q}{\partial T}$ is the heat capacity of the body.

Or

$$-m\,C_P\frac{dT}{dt} = \dot{Q}_{Convection} + \dot{Q}_{Radiation} \tag{3.5}$$

$$-m\,C_p\frac{dT}{dt} = Ah(T - T_0) + A\varepsilon\sigma(T^4 - T_0^4) \tag{3.6}$$

$$-\frac{dT}{dt} = k_1(T - T_0) + k_2(T^4 - T_0^4) \tag{3.7}$$

$$k_1 = \frac{Ah}{m\,Cp}\ ;\ k_2 = \frac{A\varepsilon\sigma}{m\,Cp}$$

Integrals solution:

$$t = -\int_{T_i}^{T} \frac{dT}{k_1(T-T_0)+k_2(T^4-T_0^4)} \tag{3.8}$$

$$k_1T^4 + k_1T - (k_1T_0 + k_2T_0^4) = 0 \tag{3.9}$$

This equation has 2 real and 2 conjugated complex roots. Therefore, the general solution must be a combination of these two types of roots. However, it is not possible to develop a general analytic solution mathematically. Instead, an equation based on logarithmic (real roots) and arctangent (complex roots) terms, which describe convection and radiations effects, has been proposed and verified.

Therefore, considering the boundary restrictions of the problem, the equation suggested was:

$$t\ = a \cdot \ln\left(\frac{T_i-T_0}{(T+c)-T_0}\right) + b \cdot \text{arctg}\left(\frac{T_i-(T+c)}{T_i-T_0}\right) \tag{3.10}$$

With T_i *= 673.15 K ;* T_0*=300 K ;* been the initial and ambient temperatures: the initial and final states.

Finally, for each of the studied cases, the values for *a,b* and *c* are determined to fit the numerical results, as described in the following sections:

$$t = a \cdot \ln\left(\frac{(673.15-300)}{(T+c)-300}\right) + b \cdot arctg\left(\frac{673.15-(T+c)}{(673.15-300)}\right) \tag{3.11}$$

CHAPTER 4. RESULT AND ANALYSIS

4.1 2-Dimensional axisymmetric analysis of coil cooling

Figure 28 shows the average temperature versus time during the cooling for the 2-Dimensional axisymmetric simulation. The initial temperature of the coil of was 673.15 K. It decreased to 492.666 K after 12 hours. It then further decreased to 420.75 K after 24 hours. The temperature undergoes a very significant decrease between the first 12 hours and the second 12 hours. In the first 12 hours, the temperature decreased by 180.484 K, and in the second 12 hours, it decreased by 71.916 K.

The coil temperature at the end of the second, third, fourth, and fifth day was 358.118 K, 331.764 K, 318.563 K, and 311.226 K successively. This means that the temperature decreased by 26.353 K on the third day, by 13.536 K on the fourth day, and 7.27 K on the fifth day.

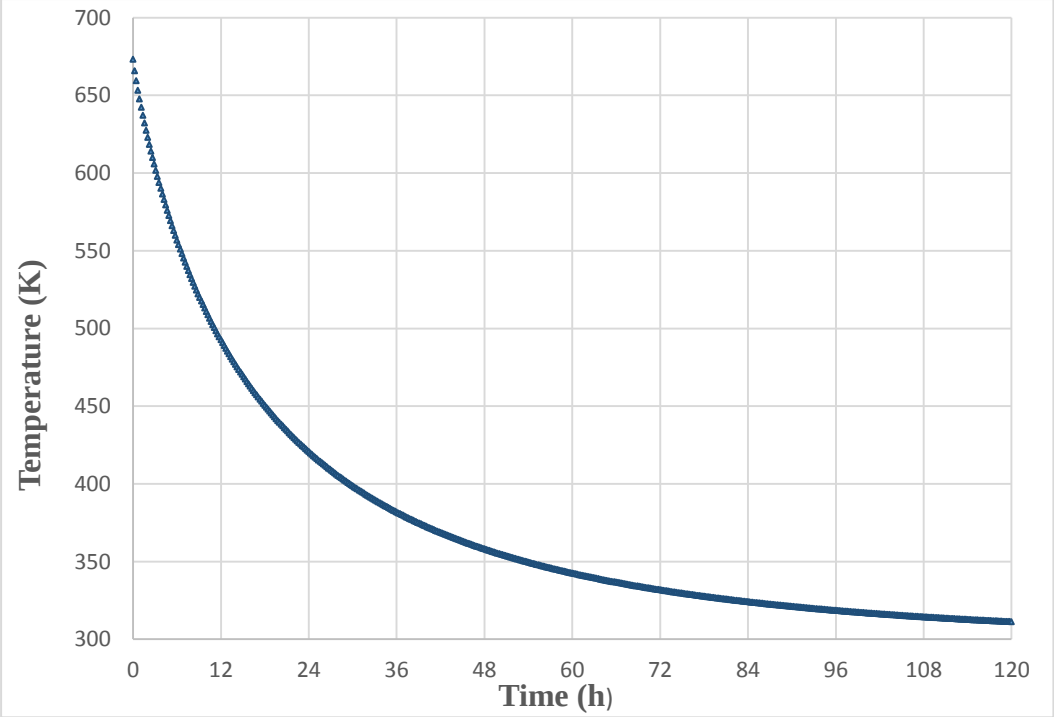

Fig.28. Average temperature during cooling of coil 2D axisymmetric model

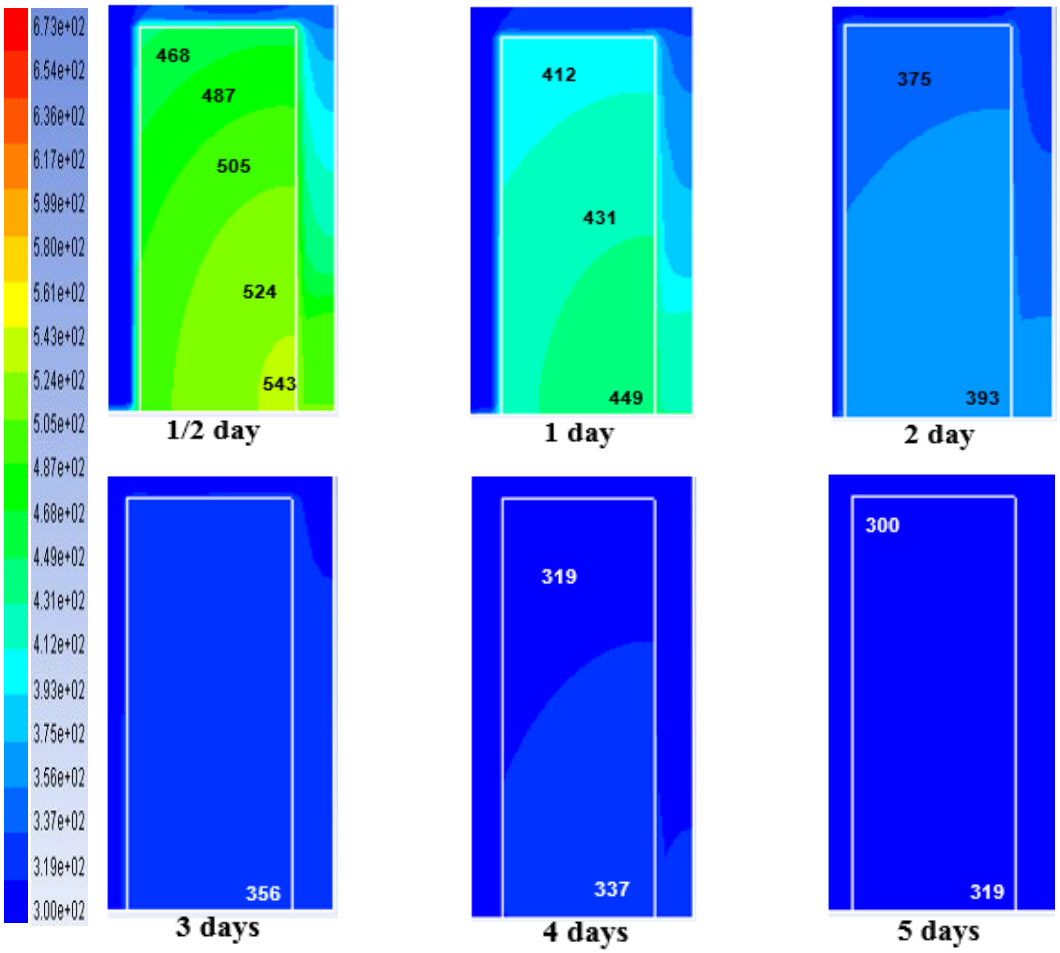

Fig.29. Temperature distribution (K) during the coil cooling
2D axisymmetric model

According to the figure 29, the initial temperature was 673.15 K, and the temperature distribution measured radial direction in the outer and inner surface of the coil. After half a day, the highest temperature was 526 K at inner coil surface, and the lowest temperature was 447 K at the outer coil surface. On the first day, the highest temperature was 440 K at the inner coil surface, and the lowest temperature was 391 K at the outer coil surface. The second day, the highest temperature was 365 K at the inner coil surface, and the lowest temperature was 346 K at the outer surface coil. The third day, the highest temperature was 335 K at the inner coil surface and the lowest

temperature was 328 K at the outer coil surface. The fourth day, the highest temperature was 320 K at the inner coil surface, and the lowest temperature was 315 K at the outer coil surface, the fifth day, the highest temperature was 312 K at the inner coil surface and the lowest temperature 308K at the outer coil surface.

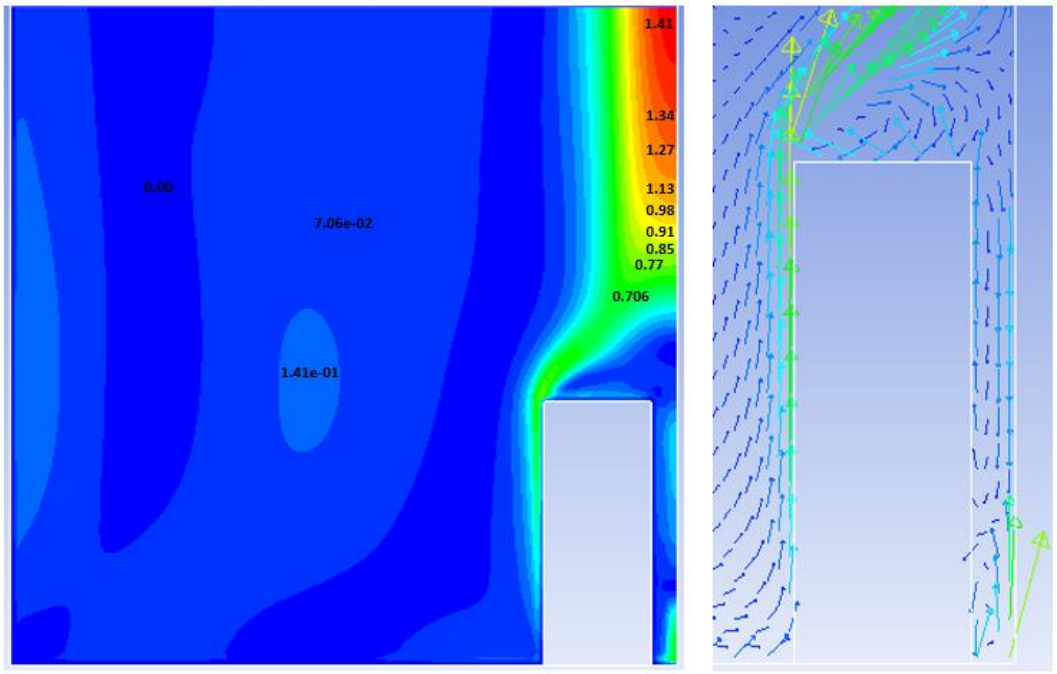

Fig.30. Velocity distributions 2D axisymmetric

The flow air velocity around the coil at the end of the cooling is shown in Figure 30. The main flow outside the coil is going up according natural convection because there is a remaining part of the coil at higher temperature than the atmospheric one. During the cooling process, velocity distributions have similar distributions but different values. The closest are the initial conditions, the highest the velocity magnitudes. In the first 12 hours, the cooling process occurs very rapidly because the air density differences between the different parts are very great due to great temperature differences (buoyancy effect). In the following hours and days, the flow velocity is slower due to the fact that the coil temperatures are much lower.

4.2 2-Dimensonal planar analysis of the coil cooling

Figure 31 shows the average temperature versus time during the cooling for the 2-Dimensional planar simulation. The initial temperature of the coil of was 673.15 K. It decreased to 542.114 K after 12 hours. It then further decreased to 470.402 K after 24 hours. The temperature undergoes a very significant decrease between the first 12 hours and the second 12 hours. In the first 12 hours, the temperature decreased by 131.036 K, and in the second 12 hours, it decreased by 71.712 K.

The coil temperature at the end of the second, third, fourth, and fifth day was 391.231 K, 351.551 K, 329.935 K, and 317.607 K successively. It means that the temperature decreased by 39.680 K on the third day, by 21.616 K on the fourth day, and 12.328 K on the fifth day.

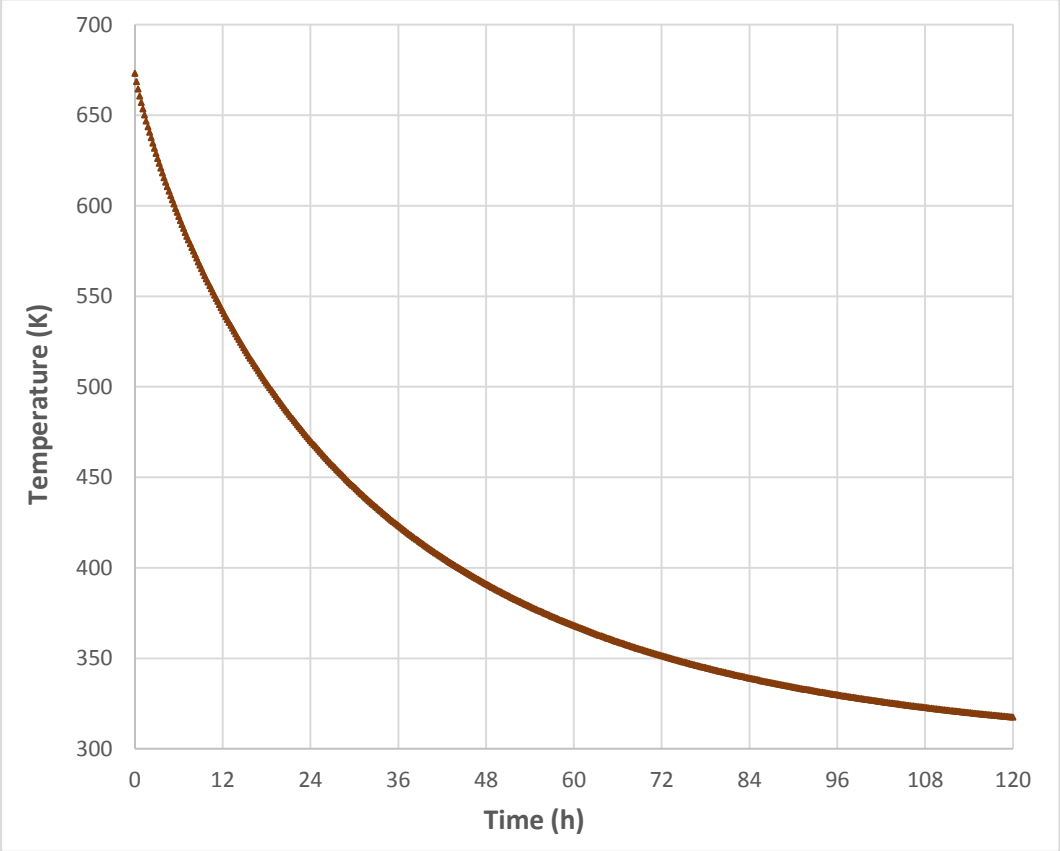

Fig.31. Average temperature during coil cooling 2D planar model

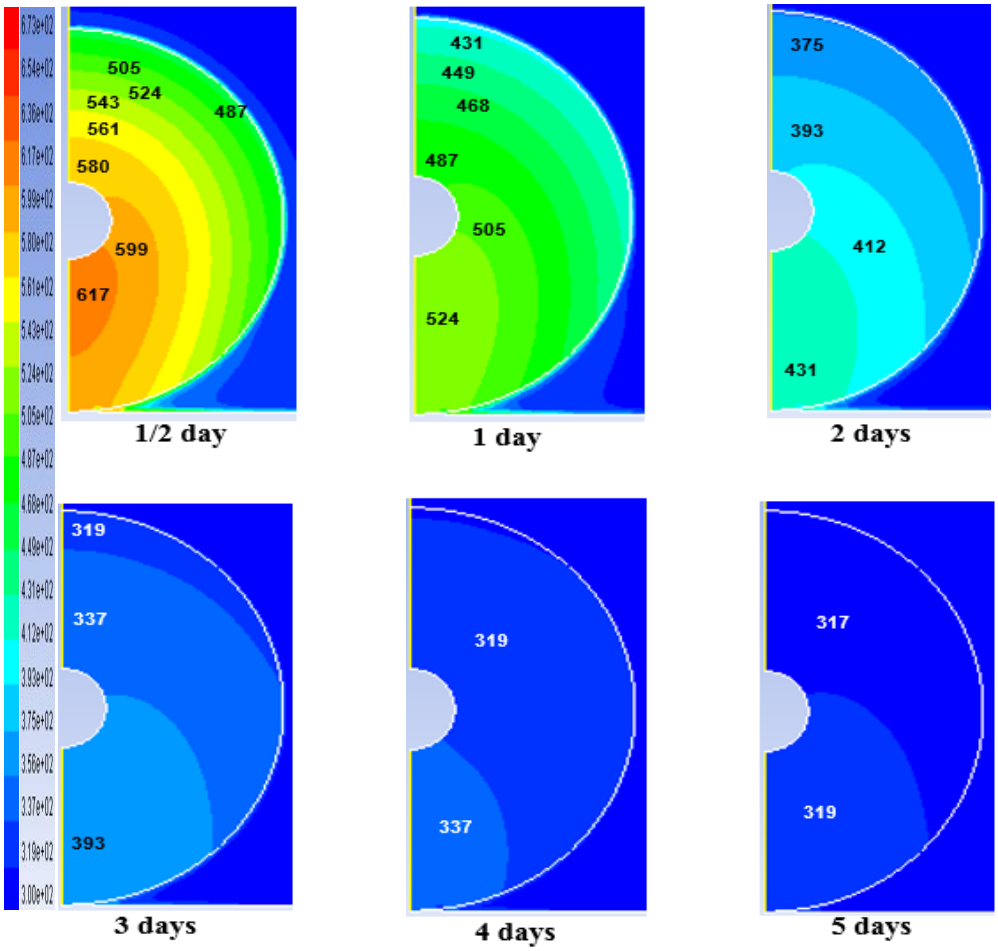

Fig.32. Temperature distribution cooling of one coil and 2D planar model

The initial temperature was 673.15 K. In figure 32, the temperature distribution during the cooling of one coil is presented.

After half a day, the highest temperature was 617 K at the inner surface of the coil, and the lowest temperature was 487 K at the outer coil surface. After the first day, the highest temperature was 524 K at inner coil surface, and the lowest temperature was 431 K at the outer coil surface.

The second day, the highest temperature was 431 K at the inner coil surface, and the lowest temperature was 375 K at the outer coil surface. The third day, the highest temperature was 393 K at inner coil surface, and the lowest temperature was 319 K at the outer coil surface.

The fourth day, the highest temperature was 337 K inner coil surface, and the lowest temperature was 319 K at the outer coil surface.

The fifth day, the highest temperature was 319 K at inner coil surface and the lowest temperature 317 K at the outer coil surface.

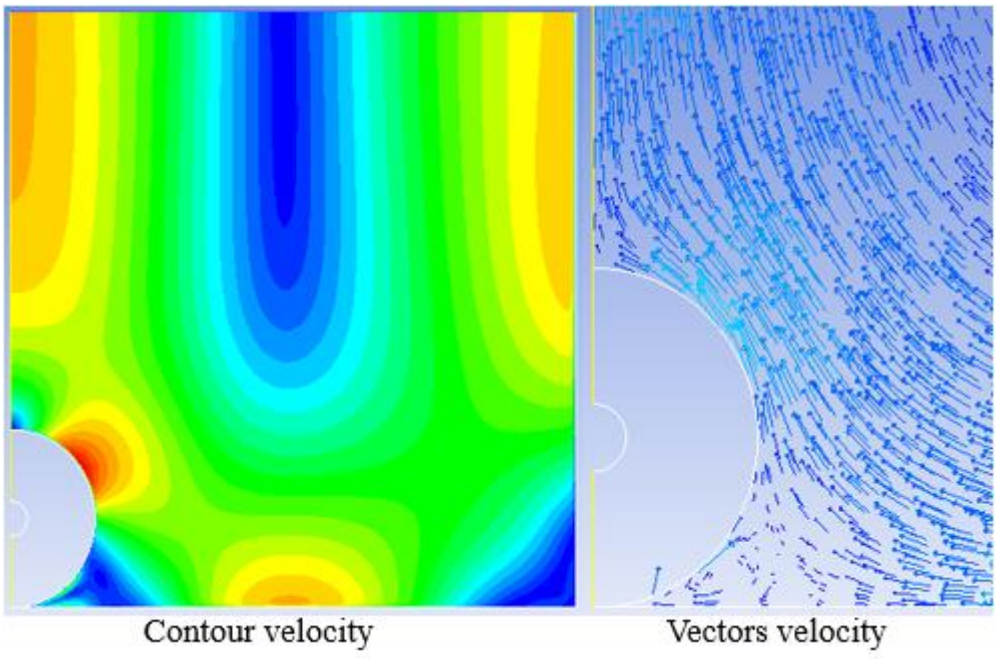

Fig.33. Velocity distributions 2D planar model

The velocity flow air for cooling around hollow the coil varied shown in Figure 33. The cooling process was natural so that there was velocity difference of cooling flow around the coil every day. In the first 12 hours, the cooling process occurs so that the flow velocity will around hollow the coil very rapidly because of the air pressure of the heat flow exit around the coil. In the following days, the flow velocity was slower due to the influence of the coil of temperature which the lower.

The flow air velocity around the horizontal coil during the cooling is shown in Figure 30. Analogously to the vertical arrangement, the main flow outside the coil is going up according natural convection. The closest is the initial conditions, the highest the velocity magnitudes. In the first 12 hours, the cooling process occurs very rapidly (buoyancy effect) and in the following hours and days, the flow velocity is slower due to the fact that the coil temperatures are much lower.

Comparison between vertical and horizontal arrangements of the coils, according to the 2D simulations the better way to cool the coils is to locate them vertically as shown in figure 34.

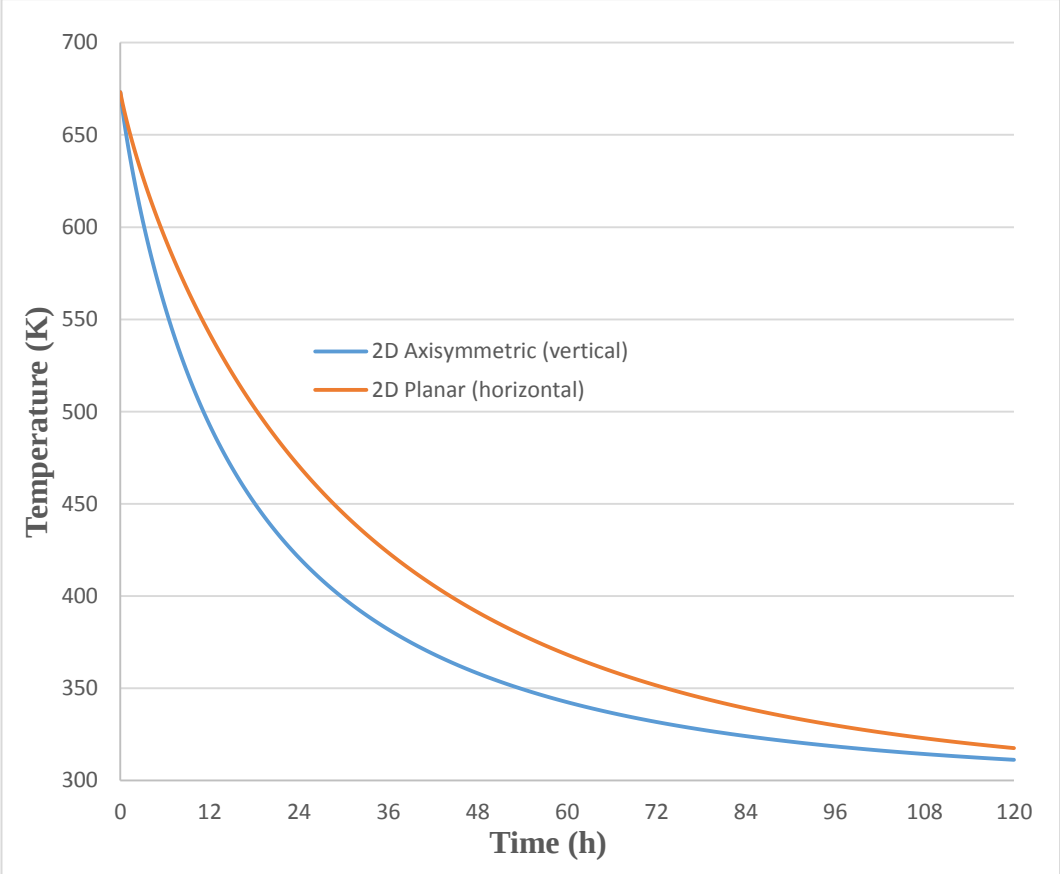

Fig.34. Comparison between the average temperature for vertical and horizontal coils

Initially, the cooling rate is greater for the vertical coil than for the horizontal one. This is coherent with the natural convection that is stronger for the vertical arrangement. The temperature differences are greater in the vertical dimension because the planar model considers only 1 m length (instead of 1.8 m) and it does not take into account the edge effects that increase the heat transfer released to the ambient. Nonetheless, after 5 days the average temperature is quite the same.

It is more realistic to compare the vertical coil simulated with the 2D axisymmetric model with the horizontal 3D simulation of one coil because both simulations consider the real length of 1.8 m and the edge effects.

4.3 3- Dimensional simulations of one coil cooling

To complete the study a 3-Dimensional model was used in order to obtain results that are more accurate.

First, the vertical coil simulated with the 2D axisymmetric model is compared with the horizontal 3D simulation of one coil. Figure 35 show that the average temperature follows a very similar evolution through time in both cases.

Due to space limitations, coils are placed in rows in the warehouse. To locate the coils vertically is more difficult and dangerous than to locate them horizontally. It is easy to transport and locate the horizontal coils by taking them by the hollow. Also, to lock the coils horizontally is easier using the hollows.

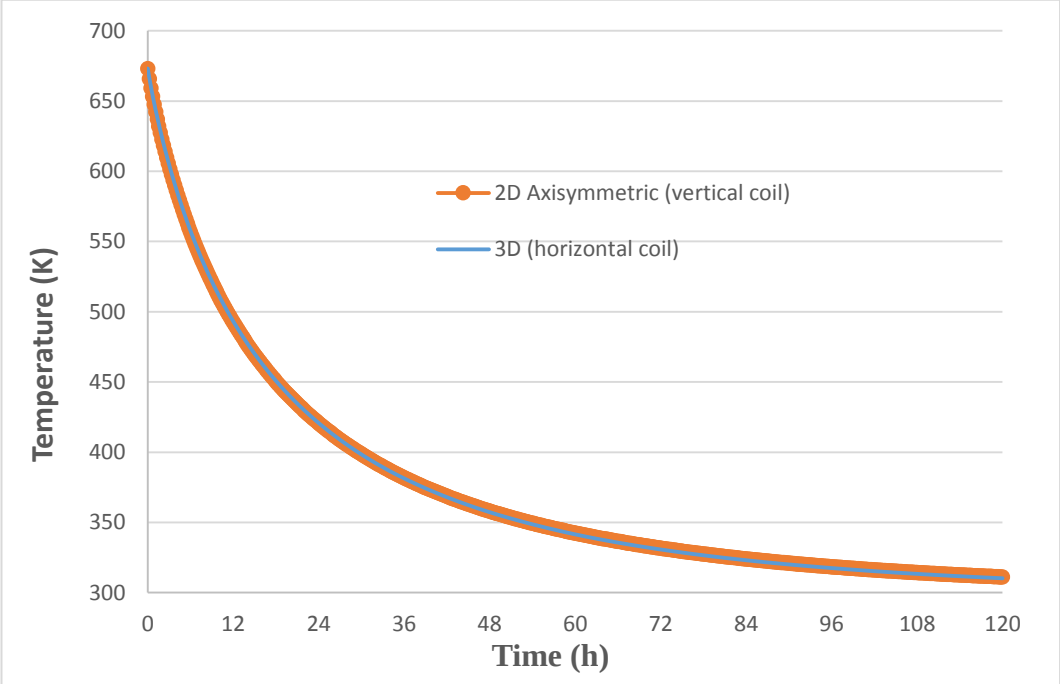

Fig.35. Comparison of the average temperature between 2D Axisymmetric (vertical coil) and 3D (horizontal coils) models

Figure 36 shows average temperature versus time for one horizontal coil simulated with the 2D planar model compared with the 3D simulation. Initially, the cooling rate is greater for the 3D than for 2D planar model. After 5 days, the average temperature is almost the same.

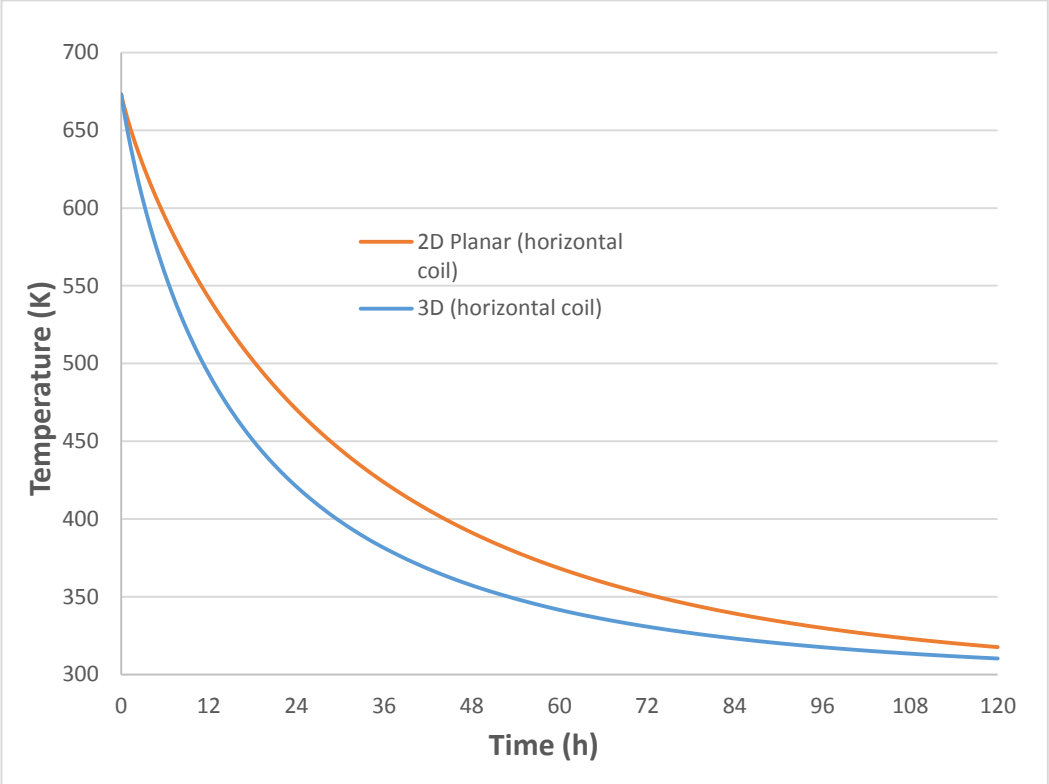

Fig.36. Comparison between the average temperature for 2D Planar and 3D horizontal coils

For the 3D simulation of one horizontal coil, the initial temperature of the coil was also 673.15 K. It decreased to 493.209 K after 12 hours. It then further decreased to 420.779 K after 24 hours. Similar results to the ones obtained with the 2D axisymmetric simulation for horizontal coils were obtained, but the cooling rate of the 3D simulation is greater for the first 2 days and after them, they are quite similar (Figure 35). The parts of the coils closest to the surfaces are cooled before than the internal parts and the temperature is a bit greater near the hollow.

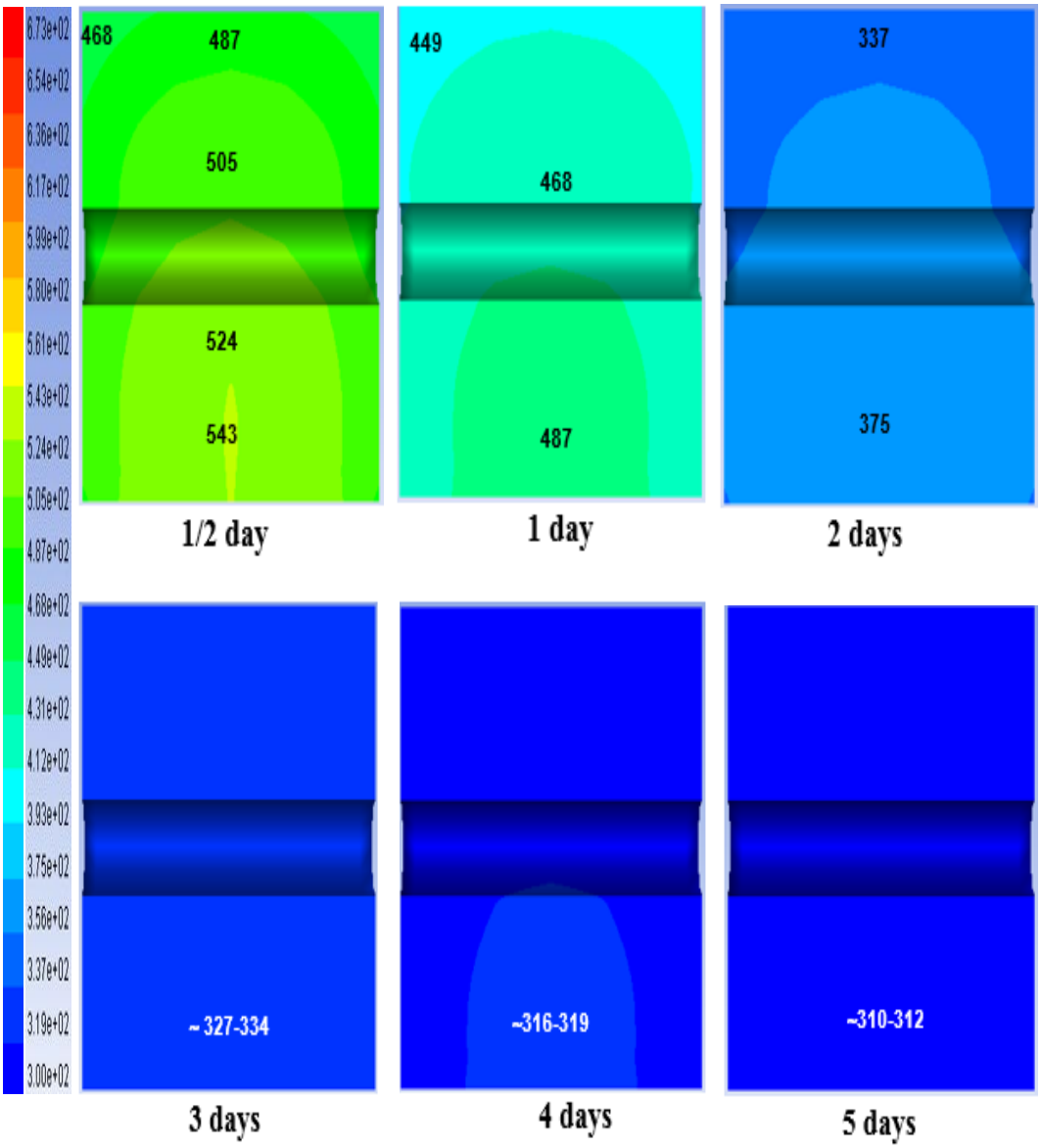

Fig.37. Temperature distribution on the middle plane of the coil obtained with the 3D model during the cooling process

The coil of temperature was 673.15 K, in figure 37 and temperature distribution during the cooling of one coil is presented.

After half a day, the highest temperature was 543 K at the inner surface of the coil, and the lowest temperature was 468 K at the outer coil surface. After first day, the highest temperature was 487 K at the inner coil surface, and the lowest temperature was 449 K at the outer coil surface.

The second day, the highest temperature was 375 K at inner coil surface, and the lowest temperature was 337 K in the outer coil surface. The third day, the

highest temperature was 334 K at the inner coil surface, and the lowest temperature was 327 K at the outer coil surface.

The fourth day, the highest temperature was 319 K at inner coil surface, and the lowest temperature was 316 K at the outer coil surface.

The fifth day, the highest temperature was 312 K at inner coil surface and the lowest temperature 309 K at the outer coil surface.

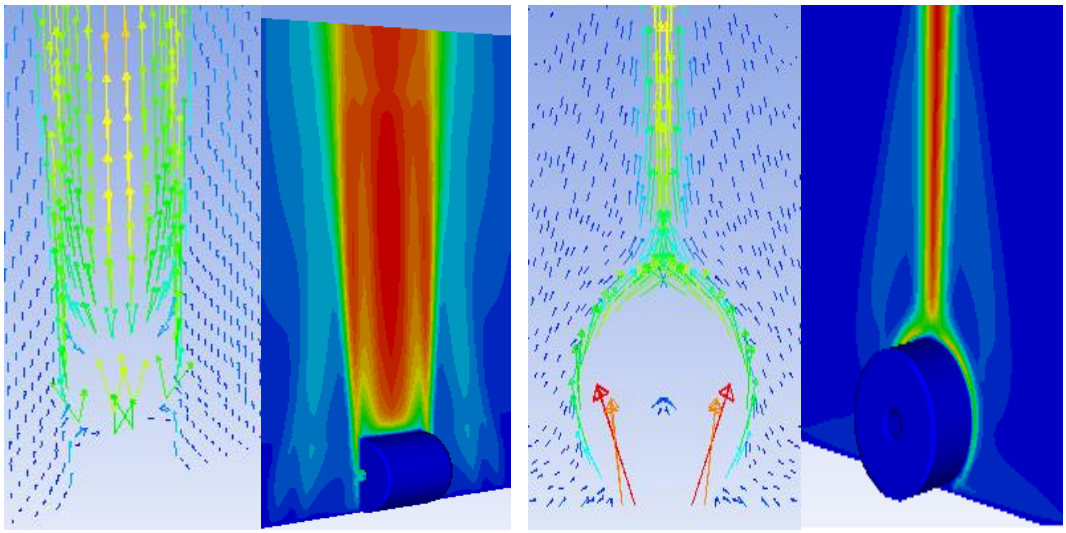

Fig.38. Velocity distributions on a vertical plane containing the symmetry axis of the coil and on a vertical plane perpendicular to the symmetry axis of the coil 3D model for one-coil

Figure 38 presents the velocity distributions on a vertical plane containing the symmetry axis of the coil and on a vertical plane perpendicular to the symmetry axis of the coil. It can be seen that the maximum airflow is concentrated in a vertical thin layer going up above the coil all along the length because it is maintained close to the rounded surface until it reaches the higher part of the coil. The vertical mas of fluid going up from the coil are due to big gradients of temperature.

4.4 3-Dimensional simulation of three coils in two rows

Similar results to the ones obtained with the 3D simulation for one horizontal coil were obtained for three horizontal coils placed in two rows. The cooling rate is greater for the 3D simulation of one coil than the rate obtained for three coils, all along the time (Figure 39). After five days, the difference is very small, but obviously, the remaining temperature for three coils is a little bit greater.

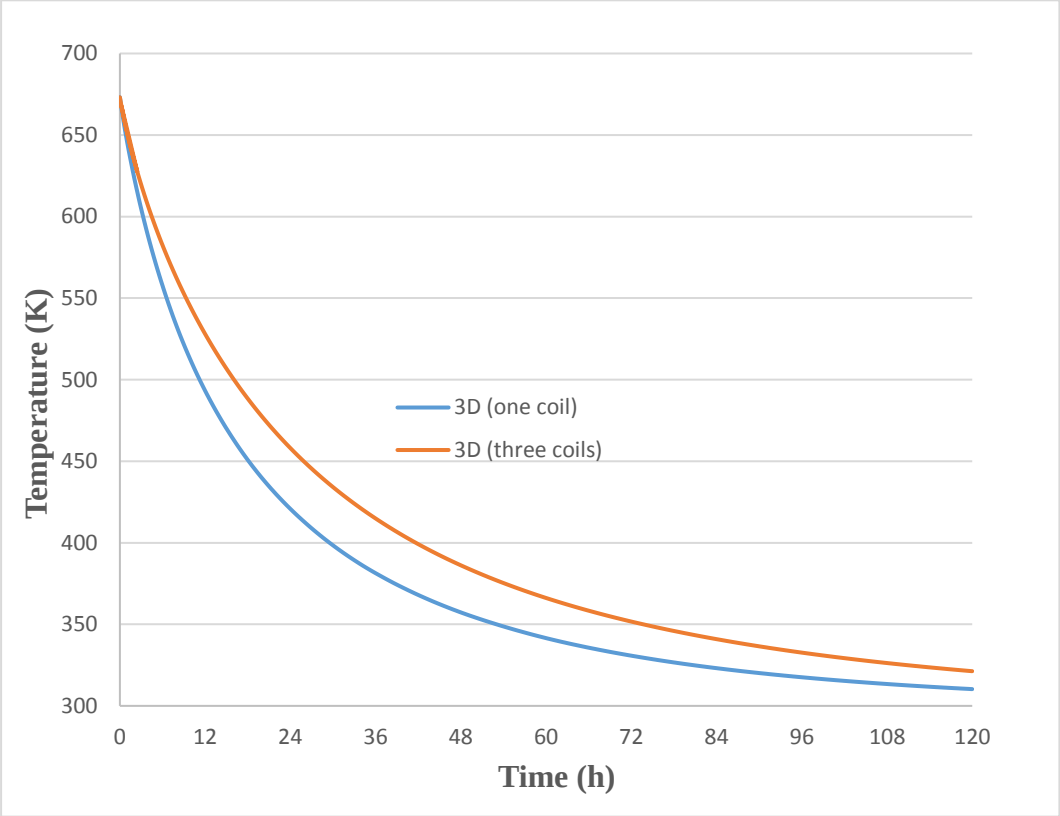

Fig.39. Comparison between the average temperature for 3D models of one and three coils (horizontally oriented).

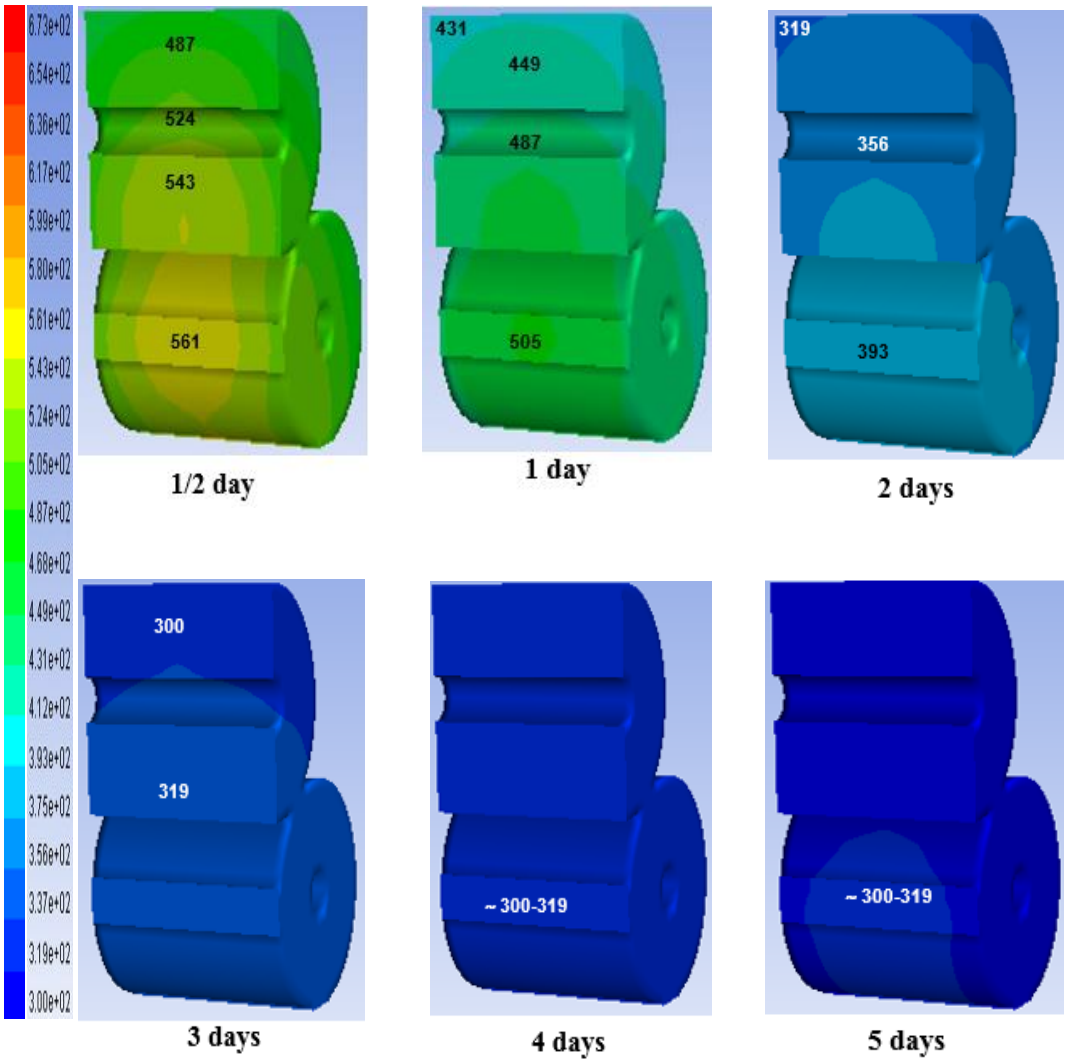

Fig.40. Temperature distribution on the middle plane obtained with the 3D model for three coils during the cooling process.

From figure 40 it can be deduced that in the case of three coils the temperature differences in the vertical direction are similar to the ones obtained in the case of one coil (figure 37), but the distances are greater and therefore, the temperature gradient is lower.

The coil of temperature was 673.15 K, in figure 40 and temperature distribution during the cooling of one coil is presented.

After half a day, the highest temperature was 558 K at the inner coil surface and the lowest temperature was 416 K at the outer coil surface. After first

day, the highest temperature was 470 K at the inner coil surface and the lowest temperature was 385 K at the outer coil surface.

The second day, the highest temperature was 387 K at inner coil surface and the lowest temperature was 348 K at the outer coil surface. The third day, the highest temperature was 350 K at inner coil surface and the lowest temperature was 320 K at the outer coil surface.

The fourth day, the highest temperature was 331 K at inner coil surface and the lowest temperature was 315 K at the outer coil surface.

The fifth day, the highest temperature was 320 K at inner surface coil and the lowest temperature 308 K at the outer surface coil.

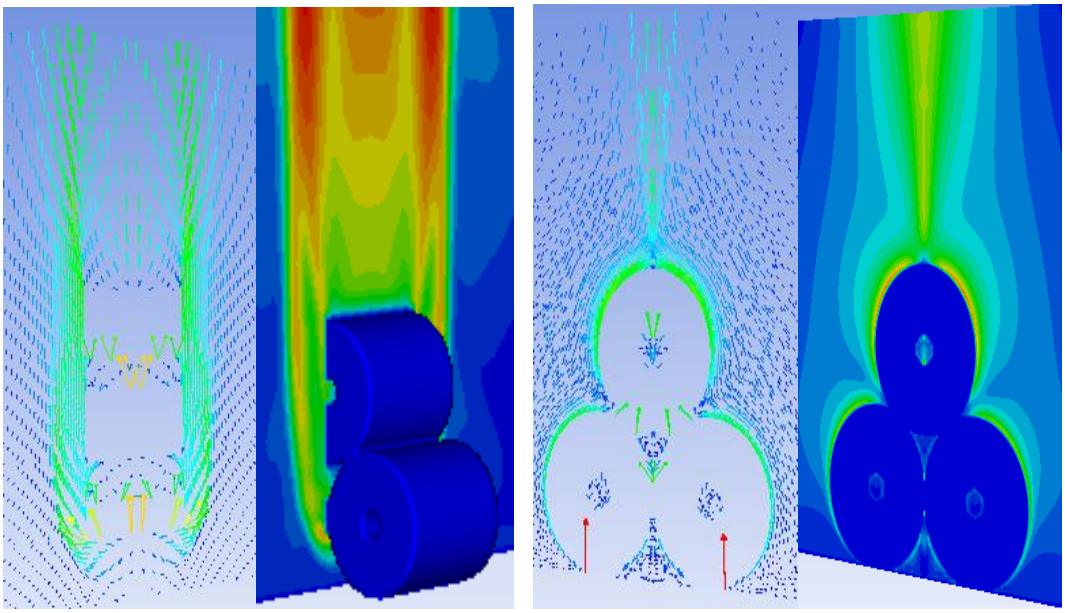

Fig.41. Velocity distributions 3D simulation of three coils

Figure 41 shows the velocity distributions on a middle plane parallel to the symmetry axes of the coils and on a vertical plane perpendicular to the mentioned axes. It is similar to the velocity field for one coil (figure 38) and the maximum airflow is concentrated in a vertical thin layer above the coils all along their length but farther from the coils than in the case of one coil. This is coherent with the lower gradient of temperature explained before.

4.5 Effect of variable specific heat and Cyl-orthotropic thermal conductivity with different interlayer pressures

Analogously to the previous cases, the effect of variable specific heat and thermal conductivity was study for the cases defined on tables 5, 6 and 7. Simulations were performed for these new cases to obtain the cooling graphics (average temperature versus time).

Figures 42 and 43 show that the greater the interlayer pressure, the greater the cooling rate. This is because the interlayer pressure has a great influence in thermal conductivity. The cooling rate for constant specific heat and isotropic thermal conductivity is the greatest (the greatest thermal conductivity).

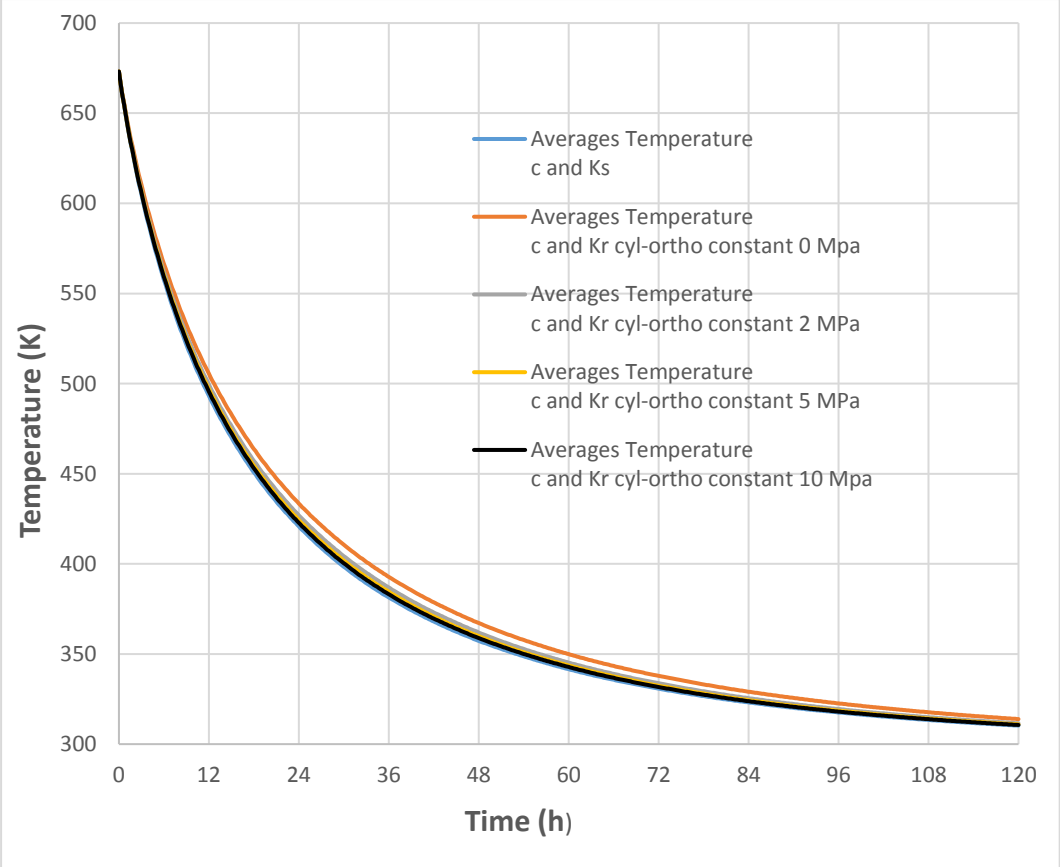

Fig. 42. Average temperature versus time for constant specific heat and thermal conductivity compared to one point thermal conductivity with different interlayer pressures.

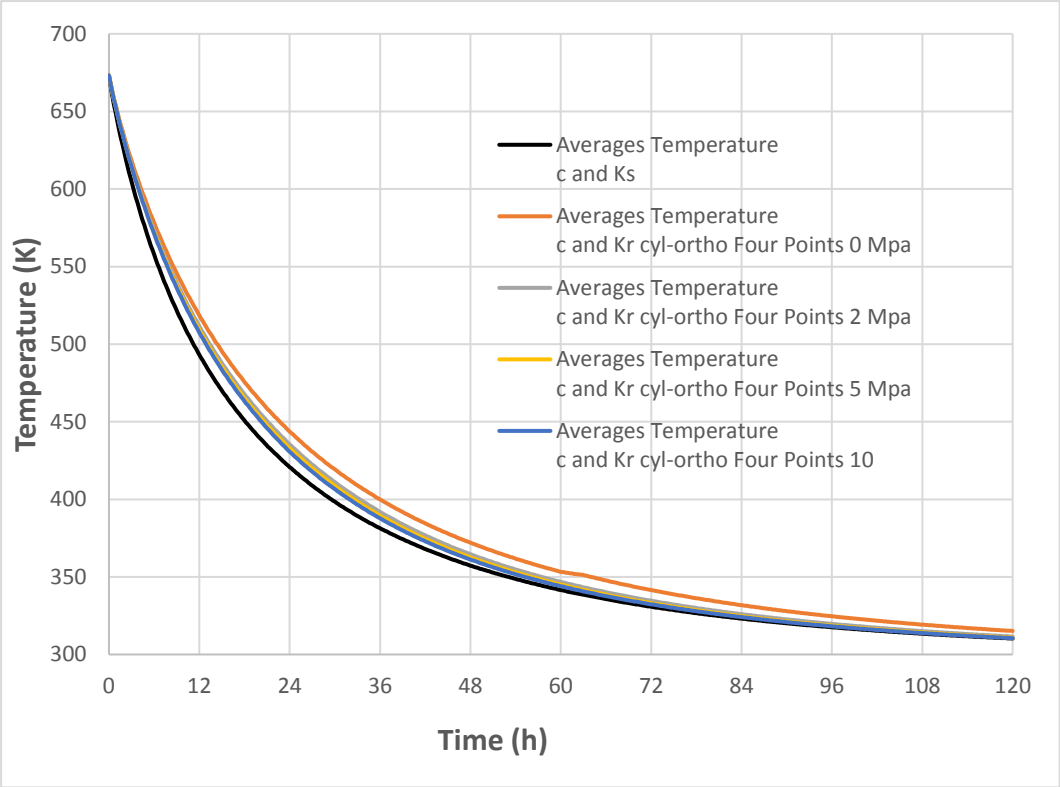

Fig. 43. Average temperature for constant specific heat and thermal conductivity compared to four point specific heat and thermal conductivity with different interlayer pressures.

Figures 44, 45, 46, and 47 compare the cooling law for the same interlayer pressure but different number of points.

The thermal conductivity in the radial direction is the most important for the conduction through a cylinder. That the main reason why heat transfer conduction is stronger for the cases with the greater radial thermal conductivity (cyl-orthotropic and one point). Consequently, the cooling rate is greater for the cases with one point.

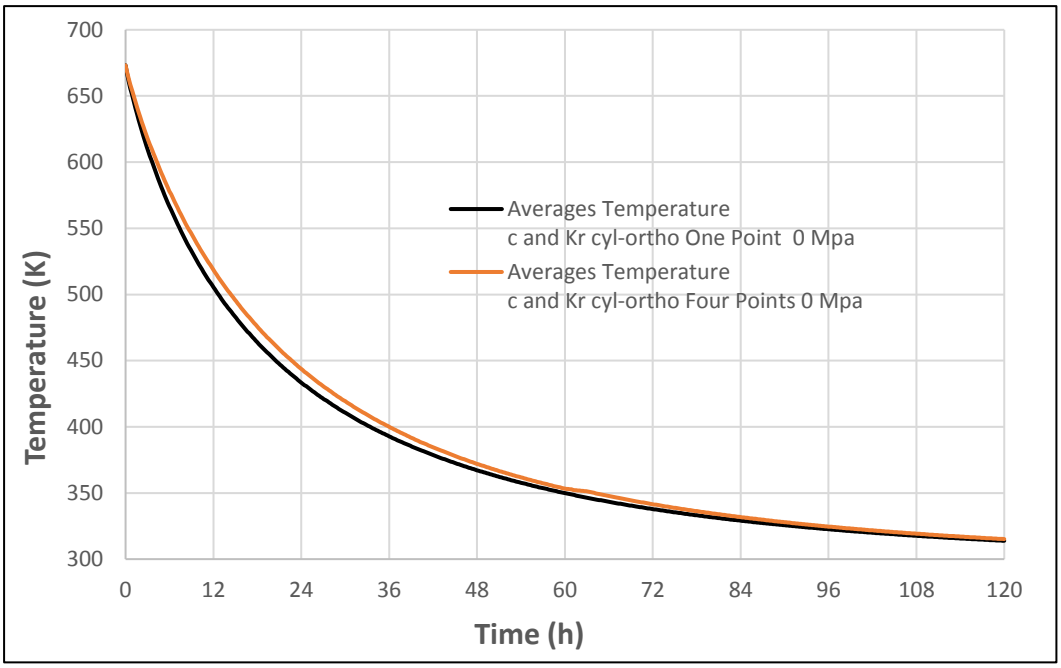

Fig. 44. Comparison of the average temperature versus time at 0 MPa interlayer pressure for one point and four points.

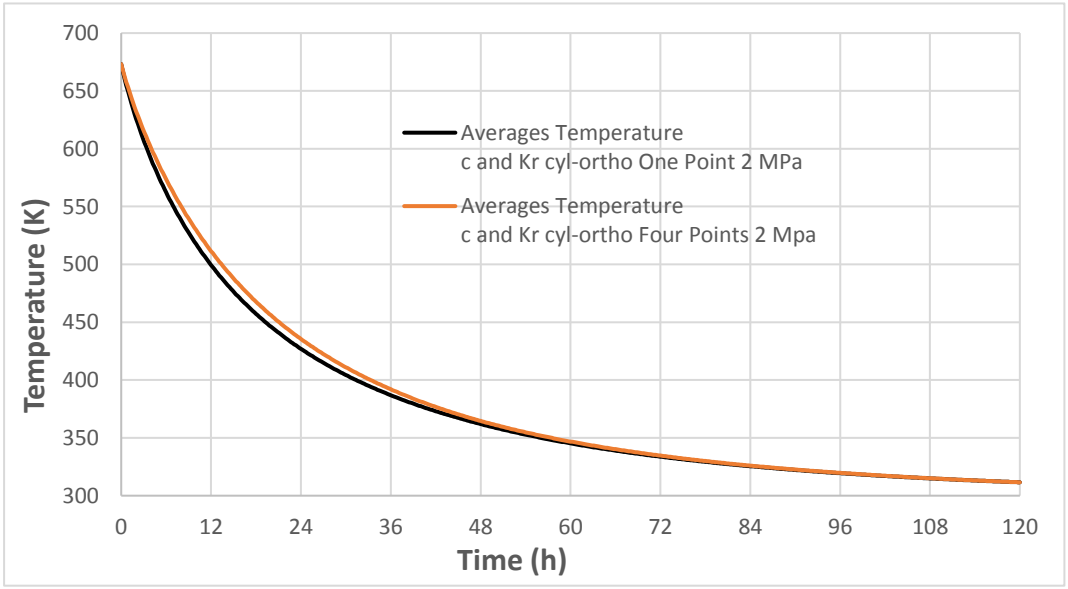

Fig. 45. Comparison of the average temperature versus time at 2 MPa interlayer pressure for one point and four points.

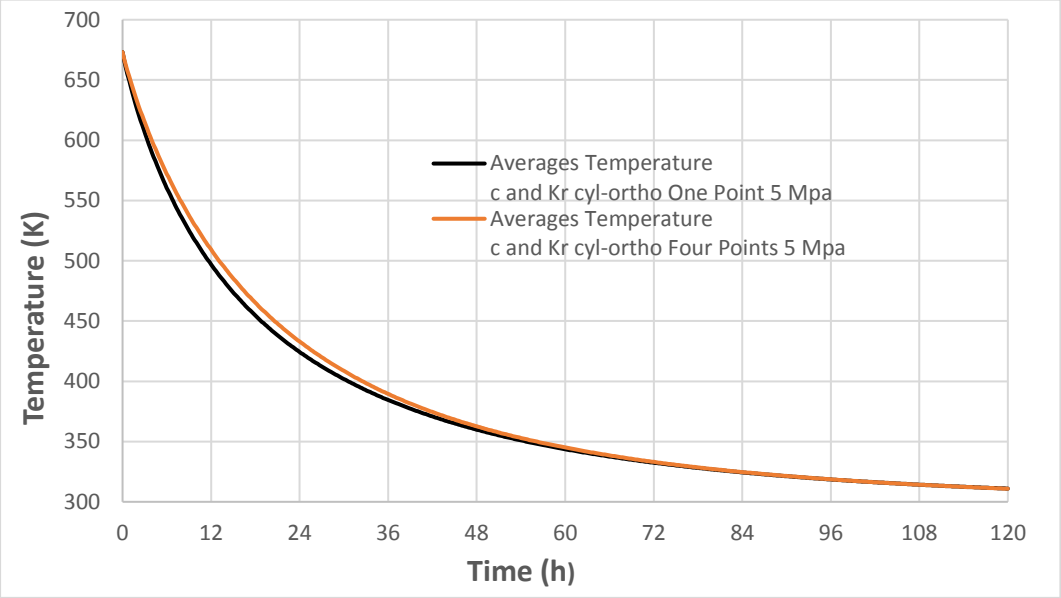

Fig. 46. Comparison of the average temperature versus time at 5 MPa interlayer pressure for one point and four points.

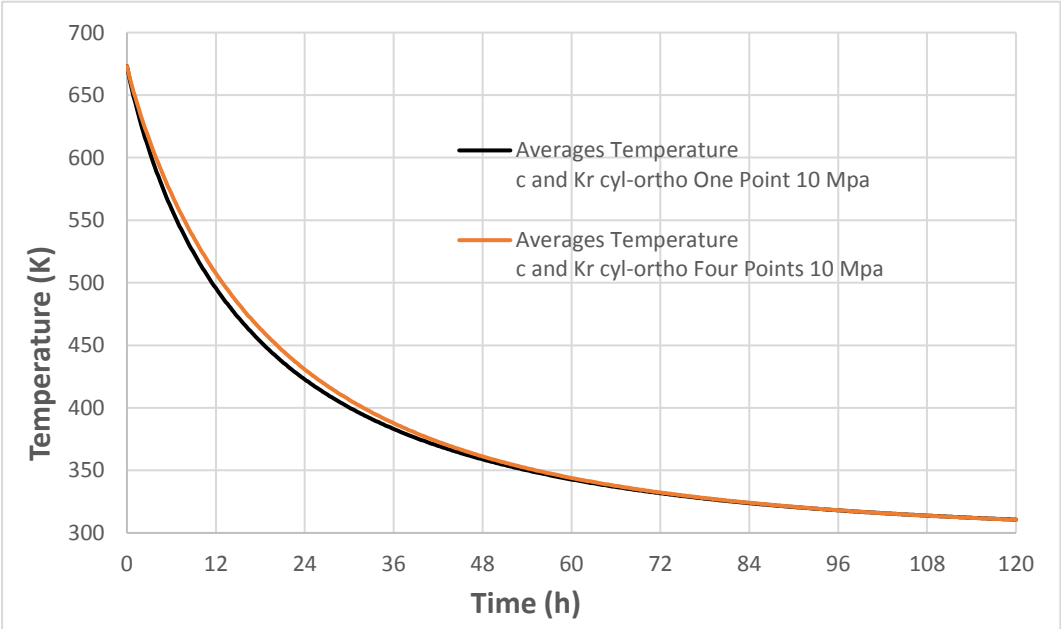

Fig. 47. Comparison of the average temperature versus time at 10 MPa interlayer pressure for one point and four points.

4.6 Cooling law equation parameters

The parameter values of the equation 3.11 for the different cases were obtained by the method of least squares and the goodness-of-fit was measured by the coefficient of determination (R^2). Those values are shown in tables 8, 9 and 10.

Table.8. Equation parameters for the basis models

	a (x 10^{-5})	**b (x 10^{-5})**	**c**	**R^2**
2D Axisymmetric	1.296	-1.074	-4.539	0.9997
2D planar	1.552	-0.744	-1.691	0.9999
3D one coil	1.393	-1.021	-3.425	0.9999
3D three coils	1.595	-1.087	-6.771	0.9998

Table.9. Equation parameters for model with constant specific heat and cyl-orthotropic thermal conductivity at different interlayer pressures and one point (673.15 K)

Interlayer pressure (MPa)	**a (x 10^{-5})**	**b (x 10^{-5})**	**c**	**R^2**
0	1.391	-1.054	-4.959	0.9998
2	1.332	-1.039	-3.841	0.9998
5	1.321	-1.040	-3.691	0.9997
10	1.299	-1.036	-3.658	0.9997

Table.10. Equation parameters for model with variable specific heat and cyl-orthotropic thermal conductivity at different interlayer pressures and four points (temperatures).

Interlayer pressure (MPa)	**a (x 10^{-5})**	**b (x 10^{-5})**	**c**	**R^2**
0	1.417	-0.9783	-5.059	0.9997
2	1.291	-0.852	-3.941	0.9998
5	1.263	-0.834	-3.804	0.9998
10	1.256	-0.850	-3.716	0.9997

Parameter "a" is the coefficient affecting the natural logarithm that comes from the both mechanism: convection and radiation. This parameter has of the same order of magnitude as $\frac{m\,Cp}{Ah}$, which is $1/k_1$, which is coherent with the mathematical development.

Parameter "b" multiplies the function arctangent, which is a correction of the main term (natural logarithm) due to radiation. It takes into account that the heat transfer by radiation depends on the deference of the fourth powers of the absolute temperatures (according to Boltzmann's law), and it decreases along the time of cooling. Therefore, parameter "b" is negative.

Parameter "c" accounts for the conduction inside the coil. T represents the average temperature and $T + c$, the temperature at the surface of the coil. Therefore, parameter "c" measures the difference between the surficial and the average temperatures. During the cooling process, parameter "c" is negative.

According to table 8, the results are coherent with the previous ones. 2D axisymmetric parameters are quite similar to the ones of the 3D simulation for one coil. For three coils, the absolute values of the parameters are greater than for one coil. Parameter "c" is greater in absolute value for three coils than for one coil, meaning that the difference between the average and the surface temperatures is

greater. The cooling rate is greater when the absolute values of the parameters are lower.

Tables 9 and 10 shown that the higher the interlayers pressure the lower the absolute value of the parameters, and the cooling rate increases when the absolute value of the parameters decreases.

The difference between the cases 3D one coil (table 8) and cyl-orthotropic thermal conductivity at different interlayer pressures on table 9 is that they have constant specific heats but they are calculated at different temperatures and also different radial thermal conductivities. Therefore, it should affect the convection and the conduction. It is reflected in parameters "a" and "c". Parameter "c" is greater in absolute value (ΔT) when the radial thermal conductivity is lower. Thus, absolute value of c is greater for the cyl-orthotropic than for the isotropic cases.

Parameter "a" is greater for the cases with variable specific heat and cyl-orthotropic thermal conductivity at different interlayer pressures and four points than those of one point because the thermal properties decrease strongly the heat transfer conduction. But the absolute values of "b" are lower for the cases with four points because the radiation effects are greater (higher temperature of the surfaces).

Figure 48 and 49 are comparison result from simulation (ANSYS FLUENT), and equation coil cooling was showed quite similar and states that the mathematical equations obtained appropriate with the simulation results.

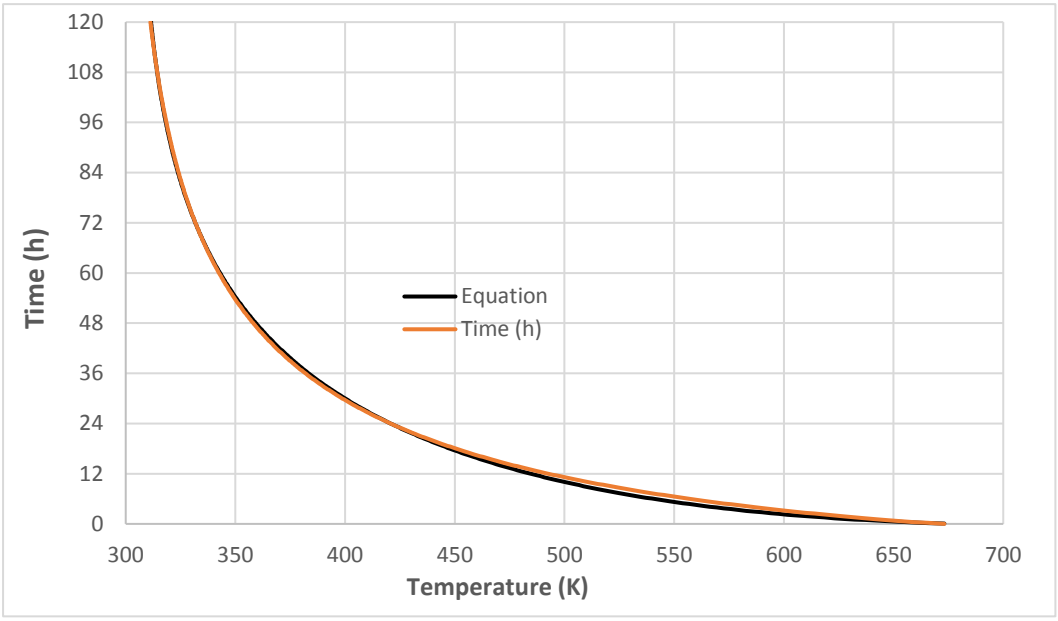

Fig. 48. Graph of calculation between the simulation and the equation for 2D Axisymmetric

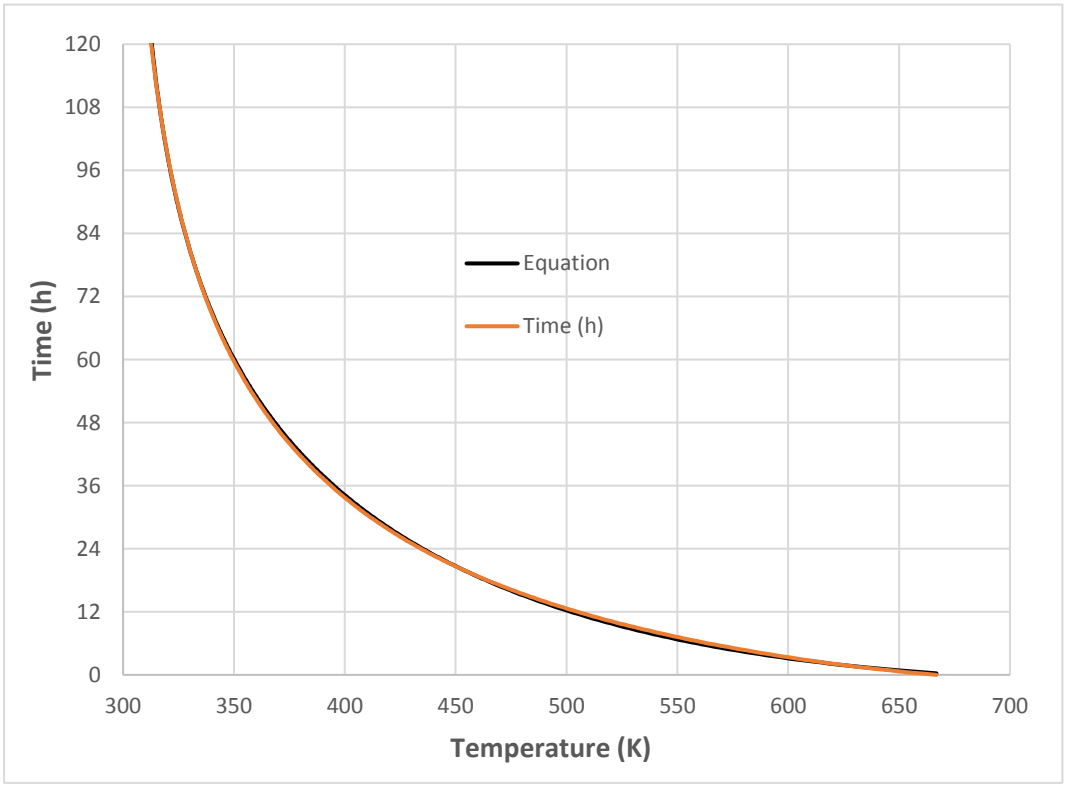

Fig.49.Graph of calculation between the simulation and the equation for one coil

CHAPTER 5. CONCLUSION

5.1 Conclusion

Steel coils must be cooled from temperatures of about 400ºC to ambient temperature to be handle and transported for sale. Coils cooling takes between four and six days depending on weather conditions. It produces unwanted stocks. The coil geometries are cylindrical and usually stored in stacks of two or three levels.

A methodology to calculate the cooling law of a coil and three coils placed in two rows is presented in this paper. The cooling law is expressed by a mathematical equation depending only on 3 parameters. The parameters have been obtained by numerical analysis with the software ANSYS – FLUENT. 2D and 3D models were used to study the heat transfer mechanisms involved in the cooling of coils and also, to characterize the temperature distributions inside the coil, as well as the temperature and velocity distributions around the coils.

The cooling law for one coil placed vertically and horizontally is almost identical but, due to space limitations, coils are placed in rows in the warehouse. It is easy to handle, transport and lock the coils horizontally. Also, the cooling rate was calculated for one coil and three coils. The cooling rate is greater for the one coil than the rate obtained for three coils.

The effect of variable specific heat and Cyl-orthotropic thermal conductivity with different interlayer pressures is also studied. The greater the interlayer pressure, the greater the cooling rate. The cooling rate is greater for the cases with one point than for cases with four points mainly because the radial thermal conductivity is bigger. The cooling rate for constant specific heat and isotropic thermal conductivity is the greatest of all the studied cases for the same reason.

The values of the three parameters defined by the equation of the cooling law obtained are very good because the coefficient of determination is very close to 1. Also, the values are coherent with the physical concepts of heat transfer mechanisms.

The methodology allows quantifying temperatures, times, cooling rates by means of the cooling law for the cases studied. It could be interesting to study the influence of geometrical dimensions, number of coils and rows; by following the defined methodology for a larger number of cases, in order to be able to extrapolate the results to different cases and avoiding the simulations. Experimental measurements would be very useful to contrast the numerical models.

REFERENCES

[1] The EU steel industry-Growth-European Commission. (2016, August 06). Retrieved May & June, 2016, from https://ec.europa.eu/growth/sector/raw-materials/industries/metals/steel_en

[2] Europe Economic and Steel Market Outlook, 2012

[3] OECD DSTI/SU/SC(2012) 12 The future of the steel industry: selected trends and policy issues (December 2012)

[4] Prospective scenarios on energy efficiency and CO2 emissions in the Iron & Steel industry (2012) – JRC

[5]Estimates of Emissions Reduction Potential for the 2015 Report

[6] Directive 2012/27/EU

[7] COM (2013) 180 final

[8] (n.d.). Retrieved May 31, 2016, Eric Solsten and Sandra W. Meditz, editors. *Spain: A Country Study*. Washington: GPO for the Library of Congress, 1988. from http://countrystudies.us/spain/64.htm

[9] https://www.ceicdata.com/en/indicator/spain/crude-steel-production

[10] (n.d.). Retrieved May 31, 2016, from http://countrystudies.us/spain/64.htm

[11](n.d). Retrieved June , 2016, from http://gas-electricity-2012.blogspot.com.es/

[12] Helle,H.(2014). Towards sustainable Iron-and steelmaking with economic optimization.

[13] Huitu K, Helle H, Helle M, Kekkonen M, Saxén H. (2014). Optimization of steelmaking using fastmet direct reduced iron in the blast furnace. *ISIJ Int*;53:2038–46.

[14] Dhunna, R., Khanna, R., Mansuri, I., & Sahajwalla, V. (2014). Recycling waste bakelite as an alternative carbon resource for ironmaking applications. *ISIJ international*, *54*(3), 613-619.

[15] IEA. Energy technology perspectives (2010) – scenarios and strategies to 2050. Paris, France;. p. 650.

[16] Pal P, Gupta H, Kapur D (2014). Carbon mitigation potential of Indian steel industry. *Mitig Adapt Strateg Glob Change*;19:1–12.

[17] Wårell L. (2014). Trends and developments in long-term steel demand—the intensity-of-use hypothesis revisited. *Resourc Policy*;39:134–43.

[18] Bellevrat, E., & Menanteau, P. (2009). Introducing carbon constraint in the steel sector: ULCOS scenarios and economic modeling. *Revue de Métallurgie*, *106*(09), 318-324

[19] Association WS. World steel in figures (2013). World Steel Association ⟨http://www.worldsteelorg/dms/internetDocumentList/bookshop/WSIF_2011/docu ment/World⟩; 2

[20] Pauliuk S, Milford RL, Müller DB, Allwood JM. (2013). The steel scrap age. *Environment Science Technology* ;47:3448–54.

[21] Pardo, N., & Moya, J. A. (2013). Prospective scenarios on energy efficiency and CO 2 emissions in the European iron & steel industry. *Energy*, *54*, 113-128

[22] Milford RL, Pauliuk S, Allwood JM, Müller DB. (2013). The roles of energy and material efficiency in meeting steel industry CO2 targets. . *Environment Science Technology*; 47:3455–62

[23] Fu J-x, Tang G-h, Zhao R-j, Hwang W-s. (2014). Carbon reduction programs and key technologies in global steel industry. *J Iron Steel Res*, Int;21:275–81

[24] Johansson, M. T., & Söderström, M. (2014). Electricity generation from low-temperature industrial excess heat—an opportunity for the steel industry.*Energy efficiency*, *7*(2), 203-215

[25] Moya, J. A., Pardo, N., & Mercier, A. (2011). The potential for improvements in energy efficiency and CO 2 emissions in the EU27 cement industry and the relationship with the capital budgeting decision criteria. *Journal of Cleaner Production*, *19*(11), 1207-1215

[26] Kirschen, M., Risonarta, V., & Pfeifer, H. (2009). Energy efficiency and the influence of gas burners to the energy related carbon dioxide emissions of electric arc furnaces in steel industry. *Energy*, *34*(9), 1065-1072

[27] Villar, A., Arribas, J. J., & Parrondo, J. (2012). Waste-to-energy technologies in continuous process industries. *Clean Technologies and Environmental Policy*,*14*(1), 29-39.

[28] Zhang, H., Wang, H., Zhu, X., Qiu, Y. J., Li, K., Chen, R., & Liao, Q. (2013). A review of waste heat recovery technologies towards molten slag in steel industry. *Applied Energy*, *112*, 956-966.

[29] Das, B., Prakash, S., Reddy, P. S. R., & Misra, V. N. (2007). An overview of utilization of slag and sludge from steel industries. *Resources, conservation and recycling*, *50*(1), 40-57.

[30] Alvarez, E. A., Trashorras, A. J. G., Cuesta, J. M. S., & Bernat, J. X. (2012). Steel mill slags energy potential: the case of the steel factory of Arcelor-Mittal in Asturias (Spain). *Clean Technologies and Environmental Policy*, *14*(5), 869-877.

[31] EUROSLAG (2006) Legal status of slag position paper.*The European Slag Association*, Duisburg (Germany).

[32] http://steel-stainless-sheet.com/Structural_steel/2016/0418/44574.html

[33] http://www.abmetals.com/products_flat_hot_rolled_coils.htm

[34] https://en.wikipedia.org/wiki/Rolling_(metalworking)

[35] Degarmo, E, Paul; Black, J T.; Kohser, Ronald A. (2003), *Materials and Processes in Manufacturing (9th ed.), Wiley, ISBN 0-471-65653-4.*

[36]https://sites.google.com/site/nitk1mp/home/primary-metal-working-processes/rolling

[37] Degarmo, E, Paul; Black, J T.; Kohser, Ronald A. (2003), *Materials and Processes in Manufacturing (9th ed.), Wiley, ISBN 0-471-65653-4*, p. 387

[38] http://metalsforasteel.com

[39] http://itcchennai.com/products/

[40] http://docplayer.net/31514739-Steel-making-properties-fabrication-use.html

[41] http://www.eef.org.uk/uksteel/About-the-industry/How-steel-is-made/step-by step/Hot-rolling.htm

[42] Degarmo, E. Paul; Black, J T.; Kohser, Ronald A. (2003), Materials and Processes in Manufacturing (9^{th} ed.), Wiley, ISBN 0-471-65653-4.

[43] Nobari, A. H., & Serajzadeh, S. (2011). Modeling of heat transfer during controlled cooling in hot rod rolling of carbon steels. *Applied thermal engineering*, *31*(4), 487-492.

[44] Phadke, S., Pauskar, P., & Shivpuri, R. (2004). Computational modeling of phase transformations and mechanical properties during the cooling of hot rolled rod. *Journal of materials processing technology*, *150*(1), 107-115.

[45] Yu, W. H., Chen, S. H., Kuang, Y. H., & Cao, K. C. (2009). Development and application of online Stelmor controlled cooling system. *Applied Thermal Engineering*, *29*(14), 2949-2953.

[46] Czaputa, K., & Brenn, G. (2012). The convective drying of liquid films on slender wires. *International Journal of Heat and Mass Transfer*, *55*(1), 19-31.

[47] Le Page, J. F., Chevarin, C., Kondjoyan, A., Daudin, J. D., & Mirade, P. S. (2009). Development of an approximate empirical-CFD model estimating coupled heat and water transfers of stacked food products placed in airflow. *Journal of Food Engineering*, *92*(2), 208-216.

[48] Irawan, D., Garcia, A., Gutiérrez, A. J., Álvarez, E., & Blanco, E. Modeling of Coil Cooling using 2D and 3D Computational Fluid Dynamics (CFD).

[49] Souza, J. L. F., Ziviani, M., &Vitor, J. F. A. (2015). Mathematical modeling of tube cooling in a continuous bed. *Applied Thermal Engineering*, *89*, 80-89.

[50] S.V. Patankar, (1980). Numerical Heat Transfer and Fluid Flow, first ed., Hemisphere Publishing Corporation, Washington.

[51] S.J. Park, B.H. Hong, S.C. Baik, K.H. Oh, Finite element analysis of hot rolled coil cooling, ISIJ International 38 (11) (1998) 1262– 1269.

[52] Karlberg, M. (2011). Modelling of the temperature distribution of coiled hot strip products. *ISIJ international*, *51*(3), 416-422.

[53] Zhang, G. J., Li, K., & Wang, Y. Z. (2011). Numerical Simulation of Hot Rolled Coil Temperature Field in Hot Coil Box.In *Advanced Materials Research* (Vol. 338, pp. 572-575).Trans Tech Publications.

[54] Baik, S. C., Kwon, O., Park, S. J., Hong, B. H., & Oh, K. H. (1999). Analysis of heat transfer in hot rolled coils for optimum condition of forced cooling. *Metals and Materials International*, *5*(4), 369-375.

[55] Bhattacharya, T., Singh, V., Chandra, S., & Kumar, A. M. (2005).Optimization of Cooling Time of Coils in Coil Cooling and Storage Unit of Cold Rolling Mill. *Tata Search*, *2*(2), 413-422.

[56] Cheng, J., Liu, Z., Dong, H., &Gan, Y. (2006). Analysis of the factors affecting thermal evolution of hot rolled steel during coil cooling. *Journal of University of Science and Technology Beijing, Mineral, Metallurgy, Material*, *13*(2), 139-143.

[57]Baskiyar, R. (2004). Finite element method simulation of the cooling of hot-rolled steel rods. *Heat transfer engineering*, *25*(8), 94-98.

[58] Saboonchi, A., &Hassanpour, S. (2007). Heat transfer analysis of hot-rolled coils in multi-stack storing. *Journal of materials processing technology*, *182*(1), 101-106.

[59] Saboonchi, A., &Hassanpour, S. (2008). Simulation of cold rolled steel coil heating during batch annealing process. *Heat Transfer Engineering*, *29*(10), 893-901.

[60] Huin, D.Marlulev, A.V. Mathey, E, (2014). Hot Rolled Coil Property Heterogeneities due to Coil Cooling Impact and Prediction. 10.4028/www.scientific.net/KEM.622-623.919. 919-928.

[61] Wu, W., Yu, F., Zhang, X., &Zuo, Y. (2002). Mathematical model and its application of radial effective thermal conductivity for coil heat transfer in HPH furnace. *Journal of Thermal Science*, *11*(2), 134-137.

[62] Jung, Y. J., Lee, G. T., & Kang, C. G. (2002). Coupled thermal deformation analysis considering strip tension and with/without strip crown in coiling process of cold rolled strip. *Journal of materials processing technology*, *130*, 195-201.

[63] Chen, G., &Gu, M. (2007). Simulation of steel coil heat transfer in a high performance hydrogen furnace. *Heat Transfer Engineering*, *28*(1), 25-30.

[64] Saboonchi, A., Hassanpour, S., &Hajiannezhad, A. (2010).Estimation of Thermal Stresses in Hot-Rolled Steel Coils During Natural Air Cooling. *Journal of Thermal Stresses*, *33*(6), 521-532.

[65] Barry, S. I., &Sweatman, W. L. (2009). Modelling heat transfer in steel coils. *ANZIAM Journal*, *50*, 668-681.

[66] Saboonchi, A., &Hassanpour, S. (2008). Simulation-based prediction of hot-rolled coil forced cooling. *Applied Thermal Engineering*, *28*(13), 1630-1637.

[67] Patankar, S. V., & Spalding, D. B. (1972). A calculation procedure for heat, mass and momentum transfer in three-dimensional parabolic flows. *International journal of heat and mass transfer*, *15*(10), 1787-1806.

[68] Cole, J. D., &Murman, E. M. (1971). Calculation of plane steady transonic flows. *AIAA Journal*, *9*(1), 114-121.

[69] Jameson, A., Schmidt, W., &Turkel, E. (1981).Numerical solutions of the Euler equations by finite volume methods using Runge-Kutta time-stepping schemes.AIAA paper, 1259, 1981.

[70] Roe, P. L. (1981). Approximate Riemann solvers, parameter vectors, and difference schemes. Journal of computational physics, 43(2), 357-372.

[71] Rhie, C. M., & Chow, W. L. (1983). Numerical study of the turbulent flow past an airfoil with trailing edge separation.AIAA journal, 21(11), 1525-1532.

[72] https://paulwmanuel.blogspot.com.es/2013/11/sermon-foremost condescension-phil-26-8.html

[73] M.R Rernandez, B.J Lázaro (2015). Fundamental and Application of Computational Fluid Dynamics. Master's Degree in Numerical Simulation in Engineering with ANSYS, page 2-4.

[74] R.W. Lewis, P. Nithiarasu, K.N.Seetharamu (2004). Fundamentals of the Finite Element Method for Heat and Fluid Flow, John Wiley & Sons, Ltd. page one.

[75] https://quizlet.com/124883329/cnst-251-ch-5-flash-cards/

[76] https://www.coursehero.com/file/p5kunqd/the-side-facing-the-earth-gets-more-sunlight-hence-more-heat-energy-It-also/

[77] https://www.sharcnet.ca/Software/Ansys/17.0/en-us/help/flu_th/flu_th_sec_hxfer_buoy.html

[78] https://www.coursehero.com/file/pogasl/Pool-boiling-at-peak-heat-flux-Film-boiling-3000-35000-300-Condensation-of/

[79] https://www.sharcnet.ca/Software/Ansys/16.2.3/en-us/help/flu_th/flu_th_uns_scheme.html

[80] A. Jameson, W. Schmidt, and E. Turkel (1981). Numerical Solution of the Euler Equations by Finite Volume Methods Using Runge-Kutta Time Stepping Schemes. Technical Report AIAA-81-1259, AIAA 14th Fluid, and Plasma Dynamics Conference, Palo Alto, California, June.

[81] J. F. Lynn (1995). Multigrid Solution of the Euler Equations with Local Preconditioning. PhD thesis, University of Michigan.

[82] J. M. Weiss, J. P. Maruszewski, and W. A. Smith (July 1997). Implicit Solution of the Navier-Stokes Equations on Unstructured Meshes. Technical Report AIAA-97-2103, 13th AIAA CFD Conference, Snowmass, CO.

[83] E. Turkel and V. N. Vatsa (2003). Choice of variables and preconditioning for time dependent problems. Technical Report AIAA-2003-3692, American Institute of Aeronautics and Astronautics, 16th AIAA Computational Fluid Dynamics Conference, Orlando, Florida, June.

[84] S. A. Pandya, S.Venkateswaran, and T. H. Pulliam (2003). Implementation of dual-time procedures in overflow.Technical Report AIAA-2003-0072, American Institute of Aeronautics and Astronautics.

[85] B. E. Launder and D. B. Spalding (1974). The Numerical Computation of Turbulent Flows.Computer Methods in Applied Mechanics and Engineering, 3:269-289.

[86]http://diposit.ub.edu/dspace/bitstream/2445/101672/1/MINELLA%20SIVILL%2c%20GERARD%202015-16%20P.pdf

[87] https://www.cfd-online.com/Wiki/K-epsilon_models

[88] Wilcox, David C (1998). Turbulence Modeling for CFD. Second edition. Anaheim: DCW Industries, 1998. pp. 174

[89] Jones, W. P., and Launder, B. E. (1972), "The Prediction of Laminarization with a Two-Equation Model of Turbulence", International Journal of Heat and Mass Transfer, vol. 15, 1972, pp. 301-314

[90] Launder, B. E., and Sharma, B. I. (1974), "Application of the Energy Dissipation Model of Turbulence to the Calculation of Flow Near a Spinning Disc", Letters in Heat and Mass Transfer, vol. 1, no. 2, pp. 131-138.

[91**]** Bardina, J.E., Huang, P.G., Coakley, T.J. (1997), "Turbulence Modeling Validation, Testing, and Development", NASA Technical Memorandum 110446

Articles derived of the thesis:

Title: A new methodology to calculate the cooling law of steel mills lamination coils

Authors: Doddy Irawan, Antonio J. Gutiérrez-Trashorras, Eduardo Alvarez-Alvarez, Eduardo Blanco-Marigorta

Journal: Advanced Manufacturing Technology

JCR impact factor: 2.209

Under review

Title: Modeling of Coil Cooling using 2D and 3D Computational Fluid Dynamics (CFD)

Authors: D. Irawan, A. García, A.J. Gutiérrez, E. Álvarez, E. Blanco

International Congress on Water, Waste and Energy Management. Rome, 18-20 July 2015

Published

The International Journal of Advanced Manufacturing Technology

A new methodology to calculate the cooling law of steel mills lamination coils

--Manuscript Draft--

Manuscript Number:	
Full Title:	A new methodology to calculate the cooling law of steel mills lamination coils
Article Type:	Original Research
Keywords:	Computational Fluid Dynamics; analytical cooling law; numerical models; heat transfer mechanisms; velocity distributions
Corresponding Author:	Antonio J. Gutiérrez-Trashorras Universidad de Oviedo Gijón, SPAIN
Corresponding Author Secondary Information:	
Corresponding Author's Institution:	Universidad de Oviedo
Corresponding Author's Secondary Institution:	
First Author:	Doddy Irawan
First Author Secondary Information:	
Order of Authors:	Doddy Irawan
	Antonio J. Gutiérrez-Trashorras
	Eduardo Alvarez-Alvarez, Ph.D.
	Eduardo Blanco-Marigorta, Ph.D.
Order of Authors Secondary Information:	
Funding Information:	Erasmus Mundus Swap&Transfer (2013-2537 001-001 EMA2) — Mr. Doddy Irawan
Abstract:	The hot-rolled steel production processes controlled cooling after finishing rolling plays an important role on the final microstructure and mechanical properties of the product. Steel coil produced at a steel mill after the lamination must be cooled from a high temperature to the ambient temperature, to be transported and sold. Coil cooling takes between four and six days depending on weather conditions. Usually, the coil will be stored in a warehouse until it reaches the ambient temperature. In this work, a new methodology to obtain the coils cooling law has been developed. Numerical models were used to simulate and study the rate of the coil cooling and to calculate the values of the parameters involved in the cooling law. The geometry of the coil is a cylinder with a height between 1.6 m and 1.8 m and an outer diameter of 0.9 m. The coils also have a coaxial hollow of small diameter. The simulations of the coil cooling process were performed by using CFD techniques with ANSYS FLUENT software in transient conditions for 2D (two-dimensional) and 3D (three-dimensional) geometries to obtain the optimal rate of temperature decrease. Different geometries corresponding to a single coil in horizontal and vertical positions and their combinations in groups of various height levels were simulated. Specifically, 2D axisymmetric and 3D simulation models were used to study the steel coils natural cooling. Both models are consistent and the results obtained are quite similar. It takes five days for a steel coil become cooled from 673.15 K to ambient temperature, and the relationship between average coils temperature and time is nearly equal. Besides, an equation (cooling law) based on logarithmic and arctangent terms was obtained. This equation describes conduction, convection and radiations effects and has been proposed and verified, considering the boundary restrictions of the problem.
Suggested Reviewers:	José María Sala Lizárraga, Proffesor Universidad del Pais Vasco josemariapedro.sala@ehu.es

	He is an expert in thermal engineering
	Luis M. López-Gonzalez, Proffesor Universidad de la Rioja luis-maria.lopez@dim.unirioja.es He is an expert in Thermal Engineering
	Frank Rosillo-Calle, Proffesor Imperial College London f.rosillo-calle@imperial.ac.uk He is an expert in Thermal Engineering

Departamento
de Energía
Universidad de Oviedo

ASTURIAS
CAMPUS DE EXCELENCIA
INTERNACIONAL
AD FUTURUM

Advanced Manufacturing Technology

I am going to send you a paper titled “A new methodology to calculate the cooling law of steel mills lamination coils”.

It presents a new methodology to obtain the coils cooling law. Numerical models were used to simulate and study the heat transfer mechanisms and the rate of the coil cooling and to calculate the values of the parameters involved in the cooling law.

This paper has not been published previously, it is not under consideration for publication elsewhere, and if accepted it will not be published elsewhere in substantially the same form, in English or in any other language, without the written consent of the Publisher.

I wish the paper were of your interest and suitable of being published in the *Advanced Manufacturing Technology.*

Waiting your answer I send you my best regards.

Antonio J. Gutiérrez-Trashorras
Energy Department. Escuela Politécnica de Ingeniería.
Edificio de Energía. Universidad de Oviedo.
33204 Campus de Viesques. Gijón (Asturias) Spain.
Tel.: +34985 18 2369.
E-mail address: gutierrezantonio@uniovi.es

A new methodology to calculate the cooling law of steel mills lamination coils

Doddy Irawan, Antonio J. Gutiérrez-Trashorras*, Eduardo Álvarez-Álvarez , Eduardo Blanco-Marigorta

Energy Department. Escuela Politécnica de Ingeniería. Edificio de Energía. Universidad de Oviedo. 33203 Campus de Viesques. Gijón (Asturias) Spain

Abstract

The hot-rolled steel production processes controlled cooling after finishing rolling plays an important role on the final microstructure and mechanical properties of the product. Steel coil produced at a steel mill after the lamination must be cooled from a high temperature to the ambient temperature, to be transported and sold. Coil cooling takes between four and six days depending on weather conditions. Usually, the coil will be stored in a warehouse until it reaches the ambient temperature. In this work, a new methodology to obtain the coils cooling law has been developed. Numerical models were used to simulate and study the rate of the coil cooling and to calculate the values of the parameters involved in the cooling law. The geometry of the coil is a cylinder with a height between 1.6 m and 1.8 m and an outer diameter of 0.9 m. The coils also have a coaxial hollow of small diameter. The simulations of the coil cooling process were performed by using CFD techniques with ANSYS FLUENT software in transient conditions for 2D (two-dimensional) and 3D (three-dimensional) geometries to obtain the optimal rate of temperature decrease.
Different geometries corresponding to a single coil in horizontal and vertical positions and their combinations in groups of various height levels were simulated. Specifically, 2D axisymmetric and 3D simulation models were used to study the steel coils natural cooling. Both models are consistent and the results obtained are quite similar. It takes five days for a steel coil become cooled from 673.15 K to ambient temperature, and the relationship between average coils temperature and time is nearly equal. Besides, an equation (cooling law) based on logarithmic and arctangent terms was obtained. This equation describes conduction, convection and radiations effects and has been proposed and verified, considering the boundary restrictions of the problem.

Keywords: Computational Fluid Dynamics; analytical cooling law; numerical models; heat transfer mechanisms; velocity distributions

1. Introduction

Steel is an essential material in construction and manufacturing. However, some trends in steelmaking technology and steel use could affect the steel demand. Design and innovation can be expected to be the key drivers for such trends.

The improvement of competitiveness must increase the value-added steel products as a differentiator from competitors. Studies of the Organization for Economic Co-operation

*Corresponding author. Energy Department. Escuela Politécnica de Ingeniería. Edificio de Energía. Universidad de Oviedo. 33203 Campus de Viesques. Gijón (Asturias) Spain. Tel.: +34985 18 23 69.
E-mail address: gutierrezantonio@uniovi.es.

and Development (OECD) show that the value added of steel products is still limited to the share of steel demand due to intense competition. Regularly steel production costs are very high and require substantial investments in research and development (R&D) [1].

According to the study of Pardo et al. [2], energy prices fluctuate significantly influencing energy prices in the future, and this is a challenge for policy makers. A second study by the global commission on the economy and climate shows the efficient cost recovery in 2030 and the payback period is two years, with a margin increase in CO_2 emissions of approximately 20%. Meanwhile, in 2030, for a payback period of six years, the margin improvement in CO_2 emissions is the range between 50% and 65% [3].

Reduce input costs, due to the high investment required energy efficiency and policies must take into account the impact on competitiveness. EU Commission will monitor the consequences or impact caused by carbon leakage to contribute Directive on Energy Efficiency to be sustainable development. [4].

The success of technology in reducing CO_2 emissions is crucial. The challenge is the high cost and public awareness and acceptance that has been presented at on the Commission's Communication on the Future of Carbon Capture and Storage in Europe [5].

The intensive energy in iron and steel industry often conducts production processes at high temperatures. The steel industry has experienced significant advances in the development of new technique for the emissions reduction and the energy efficiency. One of the possible events is the energy recovery from coils process. The goal was to analyze an innovative heat recovery solution to accomplish energy efficiency opportunities and to increase the sustainability [6]. The iron and steel industry faced with a broad range of environmental concern that fundamentally related to high-energy requirements, material usage, and the by-products associated with generating enormous quantities of steel. Steel produced after several processing steps, including iron making, steelmaking, casting, and hot rolling. These processes followed by various fabrication processes: cold rolling, forming, forging, joining, machining, coating, and heat treatment. Steel industry produces steel from raw materials (e.g. iron ore, coal, and limestone) or recycling steel scrap. Molten slag, as a kind of by-product during the steelmaking process, exhausted in extremely high temperature and thus, it carries a great deal of high-grade heat accounting for 10% of waste energy in the steel industry and 35% of high-temperature waste heat. Unfortunately, this amount of heat is one of the few high-temperature waste heat resources that have not well recycled in the entire steelmaking industry due to immature heat recovery technologies [7].

In metalworking, rolling is a metal forming process in which metal stock is passed through one or more pairs of rolls to reduce the thickness and to make the thickness uniform. The concept is similar to the rolling of dough. Rolling is classified according to the temperature of the metal rolled.

If the temperature of the metal is above its recrystallization temperature, then the process is known as hot rolling. If the temperature of the metal is below its recrystallization temperature, the process is known as cold rolling. In terms of usage, hot rolling processes more tonnage than any other manufacturing process, and cold rolling processes the most tonnage out of all cold working processes. Plants and users of this type of steel normally

call hot-rolled as ‘black steel’ to differentiate it from the cold-rolled commonly known as ‘white steel’.

Hot-rolled in the form of coils and plates are steel products produced from the hot rolling process. After the grains deform during processing, they recrystallize, which maintains an equiaxed microstructure and prevents the metal from work hardening. The starting materials are usually large pieces of metal, like semi-finished casting products, such as slabs, blooms, and billets. If these products came from a continuous casting operation, the products usually fed directly into the rolling mills at the proper temperature.
In the hot-rolled steel production processes the control of the cooling after finishing rolling plays an important role on the final microstructure and mechanical properties of the product. Mainly the speed at which the rolled product is cooled will affect the mechanical properties of the steel. The cooling rate is usually controlled by spraying water on the steel as it passes through and leaves the mill, although occasionally the rolled steel is air-cooled by using fans.

Considerable researches have been devoted to research the thermal and microstructural behaviors of steels in controlled cooling process. For example, Nobari&Serajzadeh [8] developed a mathematical model to predict temperature variations and austenite phase transformation in steel during controlled cooling. Shivpuri et al. [9] presented a computational approach to grain size evolution and mechanical properties of hot rolled rod. Yu et al. [10] developed an online Stelmor controlled cooling system for the stabilization of process operation. These numerical models have been successfully applied to controlled cooling process for realizing stable operation and improving product quality. Thus, in industrial practice, with more and more manipulated variables under control, the fact that the product quality varies with season and climate is more and more outstanding.

Up to now, it is no available in the literature to describe the quantitative analysis on the impacts of ambient temperature and humidity upon the cooling process of hot rolled steel. Some investigations in the similar treatment were reported. For instance, Czaputa& Brenn [11] discussed the effects of ambient conditions on the drying process of liquid coatings on round metal wires. Page et al. [12] reported a model to analyze the effects of ambient conditions during air treatment operations of food. These research results provide base for the study of the effects of ambient conditions on the controlled cooling of hot-rolled wire rod of steel.

Thermal conductivity of the steel is a very important parameter to take into account when there is heat transfer by conduction. It depends on the temperature and therefore, it does not take a uniform value inside the coil. The equivalent thermal conductivity can be given as a function of material properties, strip thickness, surface characteristic of pieces, average compressive stress and temperature. For this reason, numerical analysis for cooling of hot-rolled coil were carried out by Park et al. [13] under various cooling conditions by using the equivalent thermal conductivity in the radial direction. The results has been compared with data calculated using isotropic thermal conductivity and with experimental data. The cooling curves calculated using the equivalent thermal conductivity as the radial thermal conductivity showed reasonable effects of radial thermal stress and are in good agreement with experimental data.

Karlberg studied the temperature distribution of the products throughout the hot strip rolling process including the last coiling operation. That coil cooling process is crucial to decide the heat flux from the coil for an accurate description of the boundary condition to predict the cooling rate [14].

Steel coils produced in steel plants after lamination must be cooled from temperatures of about 400ºC to ambient temperature, to be transported for sale. Its geometry is cylindrical with heights between 1.6 m and 1.8 m. The outside diameter of the coil is about 0.9 m. They have a central hollow coaxial of several diameters (approximately of 0.18 m). Coils cooling takes between four and six days depending on weather conditions, because usually they are let cool in a workshop virtually weatherproof. It produces unwanted stocks and thus represents a "bottleneck" in the marketing process. The cooling by liquids is not allowed because it could change the mechanical properties of the coils.

The study of coils cooling encloses several difficulties such as the fact that the geometries are not simple and usually stored in stacks of two or three levels; it is an unsteady phenomenon, with long cooling times, involving the main heat transfer mechanisms. The knowledge of the coil cooling law by conduction, natural convection and radiation has not been deeply study in the literature and it is fundamental to widen the understanding of the cooling mechanisms to be able to control the cooling process.

The main objective of this thesis is to obtain a methodology to calculate the cooling law of a coil. This cooling law will be expressed by a mathematical equation depending on a few number of parameters. The parameters can be obtained either by simulations or experimentally, allowing to obtain the general cooling law that can be extrapolated for other cases with different geometries and conditions; and avoiding to simulate o perform the experimental studies which are complex and depend on a large number of parameters.

2. Methodology

Numerical analysis with the software ANSYS - FLUENT was performed to simulate the coils cooling process. The geometry and mesh were defined by using Gambit 2.4.6. 2D and 3D models were used to study of the heat transfer mechanisms involved in the cooling of coils and also, to characterize the temperature distributions inside the coil, as well as the temperature and velocity distributions around the coils.

Depending on the orientation of the coils and the number of coils different models were used to obtain the more appropriate one for each arrangement. For the simulation of one coil, 2D axisymmetric and planar model were used, as well as a 3D model. The simulation of three coils was done by using a 3D model. These models allow to characterize the heat transfer mechanisms taking place in the coils cooling and to obtain the temperature decrease along time during the cooling process. Consequently, the analytical equations of temperature inside the coil versus time, under different configurations: one vertical coil, one horizontal coil, rows of coils, etc., can be obtain (cooling law).

2.1. 2-Dimensional Axisymmetric model of one vertical coil

The coil was assumed to be located vertically in a spacious room measuring 4.5 m x 4.5 m. Conduction, natural convection and radiation process were considered for the 2D

axisymmetric case. The number of cells used was 10,000. Mesh elements were quad and type paved.

Figure 1 shows a vertical cross section of the mesh were x axis is the symmetry axis of a vertical steel coil (only half of the section is shown).

Pressure inlet was used on the top of the mesh as boundary condition to simulate the natural convection. The employed model was 2D axisymmetric. The RNG k-epsilon Turbulence model (viscous) and Discrete Ordinate Model (radiation) were selected. Heat transfer was enabled and the energy equation activated. Also, the standard properties of steel and air (as an ideal gas) were selected.

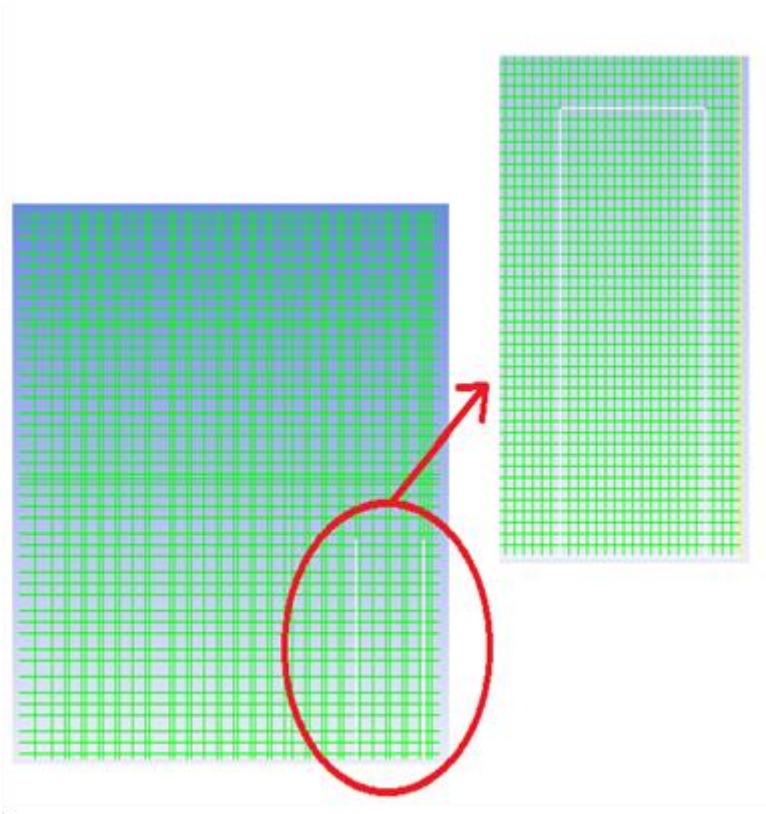

Fig. 1. 2-Dimensional axisymmetric mesh

2.2. 2-Dimensional Planar model of one horizontal coil

The coil was assumed to be located horizontally in a spacious room measuring 6 m x 6 m. Conduction, natural convection and radiation processes were considered for the 2-Dimensional planar case. The number of cells was 110,202. Mesh elements were quad and type paved.
Figure 2 shows a vertical cross section of the horizontal coil were the symmetry axis of the coil is perpendicular to the drawing x (only half of the section is shown).

Pressure inlet was used on the top of the mesh as boundary condition and symmetry for the left hand side axis. The employed model was 2D planar and the rest of the model parameters and material properties were the same as those defined for the 2D axisymmetric model.

2.3. 3-Dimensional model of one horizontal coil

The coil was assumed to be located horizontally in a spacious room measuring 12 m x 12 m x 12 m. Conduction, natural convection and radiation processes were considered for the 3-Dimensional cooling simulation. The number of cells used was 386,340. Elements were quad and type paved. The employed model was 3D and the rest of the model parameters and material properties were the same as those defined for previous models (Figure 3).

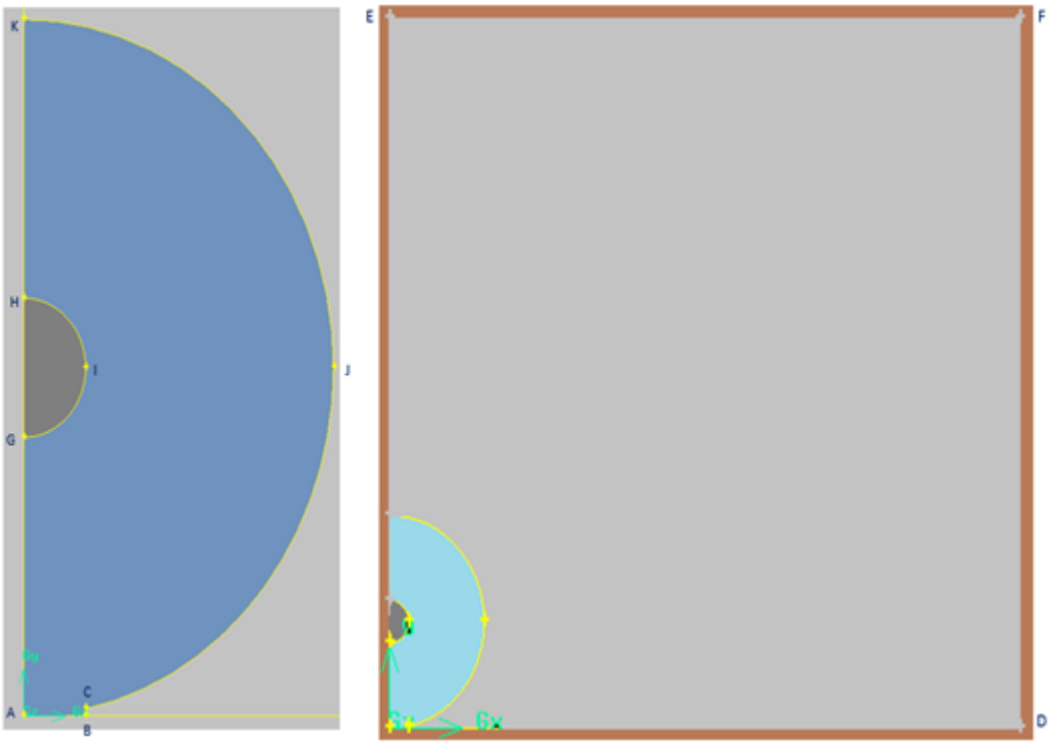

Fig. 2. Geometry of the 2-Dimensional planar model

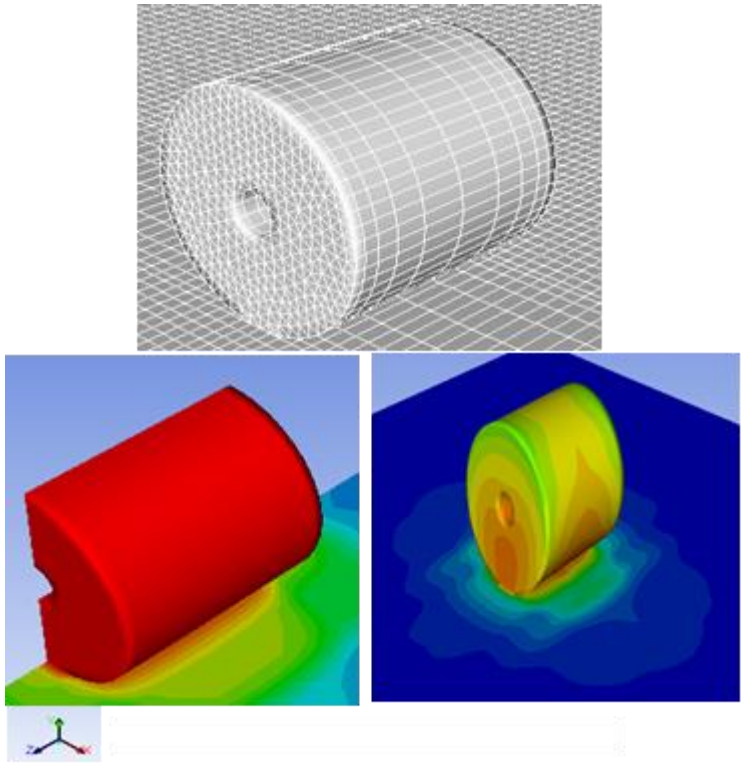

Fig. 3. 3D model of one coil

The first step of testing simulations was using steady flow (Time-steady), which aims to obtain a constant temperature (673.15 K) in the coil and the direction of the air velocity during the coil cooling. Once completed the steady flow, its solution was used as the initial conditions for the transient solver.

2.4. 3-Dimensional model of three horizontal coils

For the simulation of a 3-dimensional geometry of the three coils, 488,100 cells were used. The size of the room was 12 m x 12 m x 12 m. The results of the steady flow (Time-steady) were used to obtain the initial conditions for the transient solver, analogously to the previous case (Figure 4). The rest of the model parameters and material properties were the same as those defined for previous models

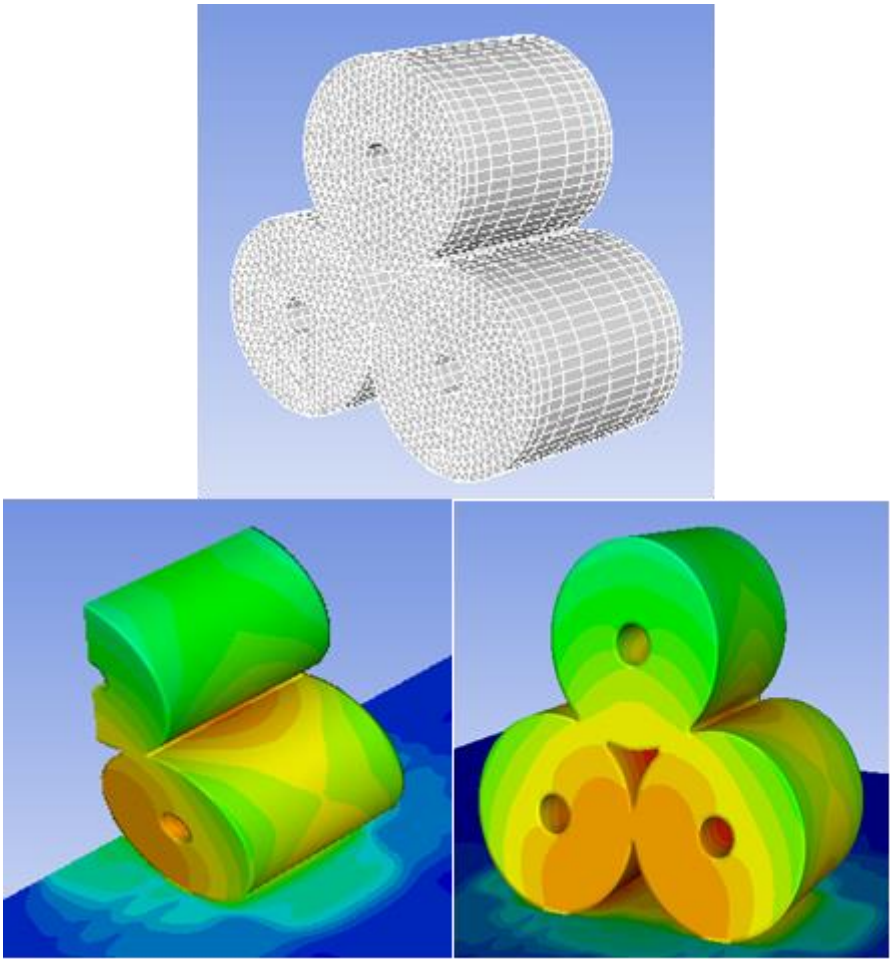

Fig. 4. 3D model of three coils

2.5. Cooling law: Equation of the temperature decrease

The total heat transfer from the coil to the ambient may be considered as a combination of convection and radiation effects. Radiative cooling is described by the Stefan-Boltzmann law which states that rate of heat loss per unit surface area of a body at temperature T is proportional to $T^4 – T_0^4$, where T_0 is the mean temperature of the surroundings. Thus the combined rate of heat energy loss from a body of surface area A due to both convection and radiation is:

$$hS(T - T_0) + \varepsilon\sigma A(T^4 - T_0^4) \quad (1)$$

where h is the convection heat transfer coefficient for pure convection and depends on the cooling conditions. ε is the emissivity of the surface and σ is the Stefan-Boltzmann constant.
The energy balance of the coil can be expressed analytically:

$$-m\, C_P \frac{dT}{dt} = \dot{Q}_{Convection} + \dot{Q}_{Radiation} \quad (2)$$

where $C_p = \partial Q/\partial T$ is the specific heat capacity of the body.

$$-m\, C_p \frac{dT}{dt} = Ah(T - T_0) + A\varepsilon\sigma(T^4 - T_0^4) \quad (3)$$

Thus the rate of change of temperature (cooling rate) of the coil is given by:

$$-\frac{dT}{dt} = k_1(T - T_0) + k_2(T^4 - T_0^4) \quad (4)$$

with:

$$k_1 = \frac{Ah}{m\,Cp}\ ;\ k_2 = \frac{A\varepsilon\sigma}{m\,Cp} \quad (5)$$

Integrating and considering the boundary restrictions of the problem, the equation suggested was:

$$t\ = a \cdot \ln\left(\frac{T_i - T_0}{(T+c) - T_0}\right) + b \cdot \text{arctg}\left(\frac{T_i - (T+c)}{T_i - T_0}\right) \quad (6)$$

With T_i = *673.15 K ;* T_0*=300 K ;* been the initial temperature of the coil and the ambient temperature recpectively.

Finally, for each of the studied cases, the values for *a,b* and *c* are to be determined to fit the numerical results, as described in the following sections:

$$t = a \cdot ln\left(\frac{(673.15 - 300)}{(T+c) - 300}\right) + b \cdot arctg\left(\frac{673.15 - (T+c)}{(673.15 - 300)}\right) \quad (7)$$

3. Results and discussion

3.1. Cooling simulation of one vertical coil. 2-Dimensional Axisymmetric model

The flow air velocity around the coil at the end of the cooling is shown in Figure 5. The main flow outside the coil is going up according natural convection because there is a remaining part of the coil at higher temperature than the atmospheric one. During the cooling process, velocity distributions have similar distributions but different values. The closest the initial conditions, the highest the velocity magnitudes. In the first 12 hours, the cooling process occurs very rapidly because the air density differences between the different parts are very great due to great temperature differences (buoyancy effect). In the following hours and days, the flow velocity is slower due to the fact that the coil temperatures are much lower (Figure 6).

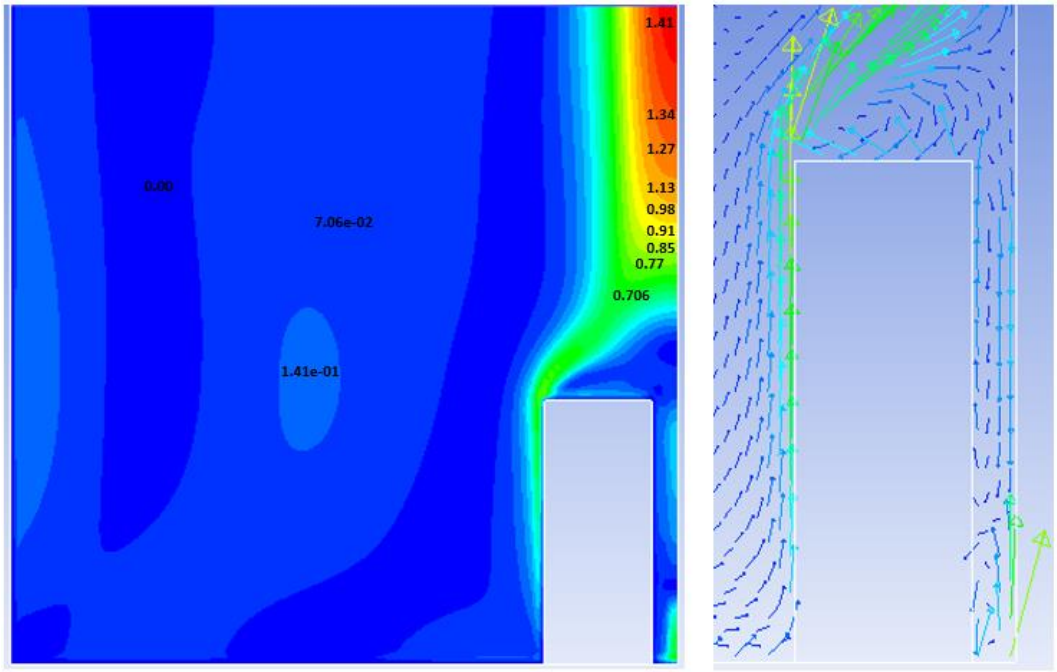

Fig. 5. Velocity distributions. 2D axisymmetric model

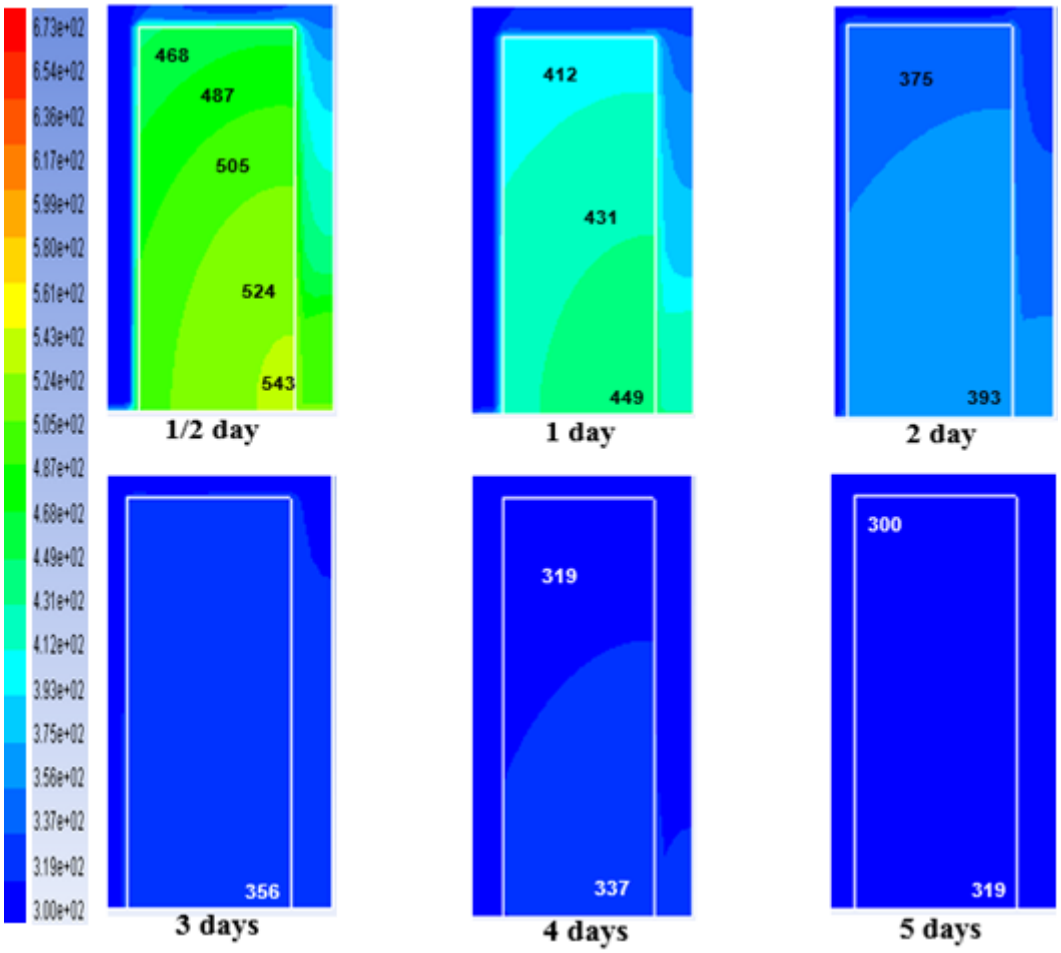

Fig. 6. Temperature distribution (K) during the coil cooling. 2D axisymmetric model.

The evolution of the average temperature of the coil is presented in the figure 7.
Initial cooling rates are greater than the final ones according to the lower effect of the heat transfer mechanisms throughout time.

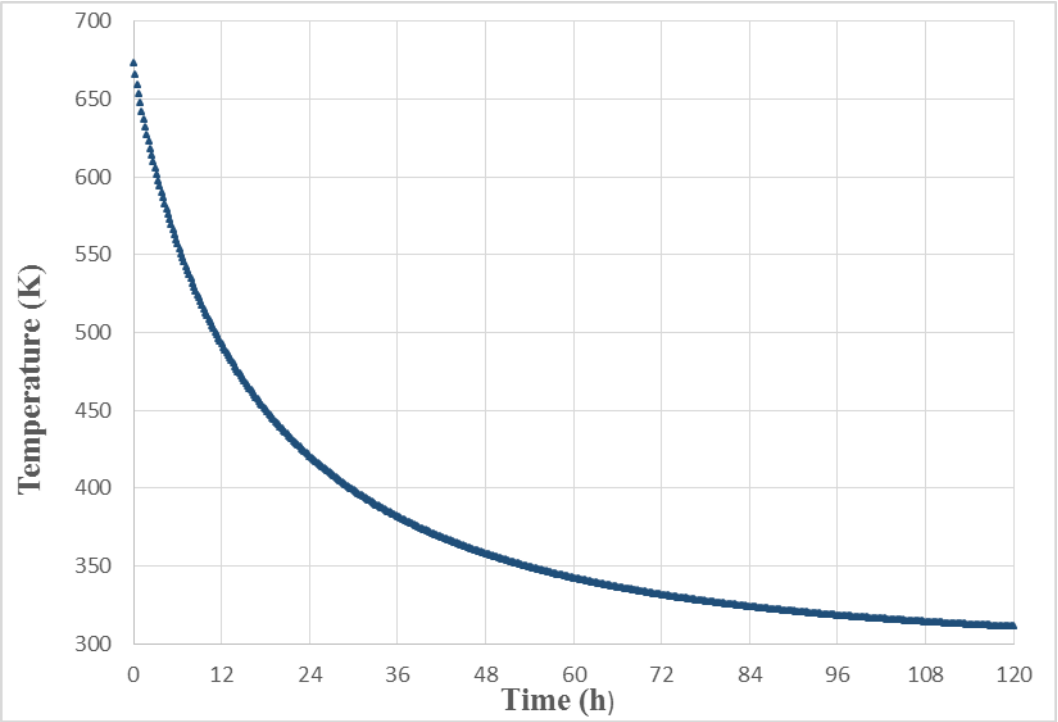

Fig.7. Average temperature during cooling of a vertical coil. 2D axisymmetric model

3.2. Cooling simulation of one horizontal coil. 2-Dimensional planar model

The air velocity around the horizontal coil during the cooling is shown in Figure 8. Analogously to the vertical arrangement, the main flow outside the coil is going up according natural convection. The closest the initial conditions, the highest the velocity magnitudes. Figure 9 shows the temperature distributions during the cooling.

Comparison between vertical and horizontal arrangements of the coils

According to the 2D simulations the better way to cool the coils is to locate them vertically as shown in figure 10. Initially, the cooling rate is greater for the vertical coil than for the horizontal one. This is coherent with the natural convection that is stronger for the vertical arrangement. The temperature differences are greater in the vertical dimension because the planar model considers only 1 m length (instead of 1.8 m) and it does not take into account the edge effects that increase the heat transfer released to the ambient. Nonetheless, after 5 days the average temperature is quite the same.
It is more realistic to compare the vertical coil simulated with the 2D axisymmetric model with the horizontal 3D simulation of one coil because both simulations consider the real length of 1.8 m and the edge effects.

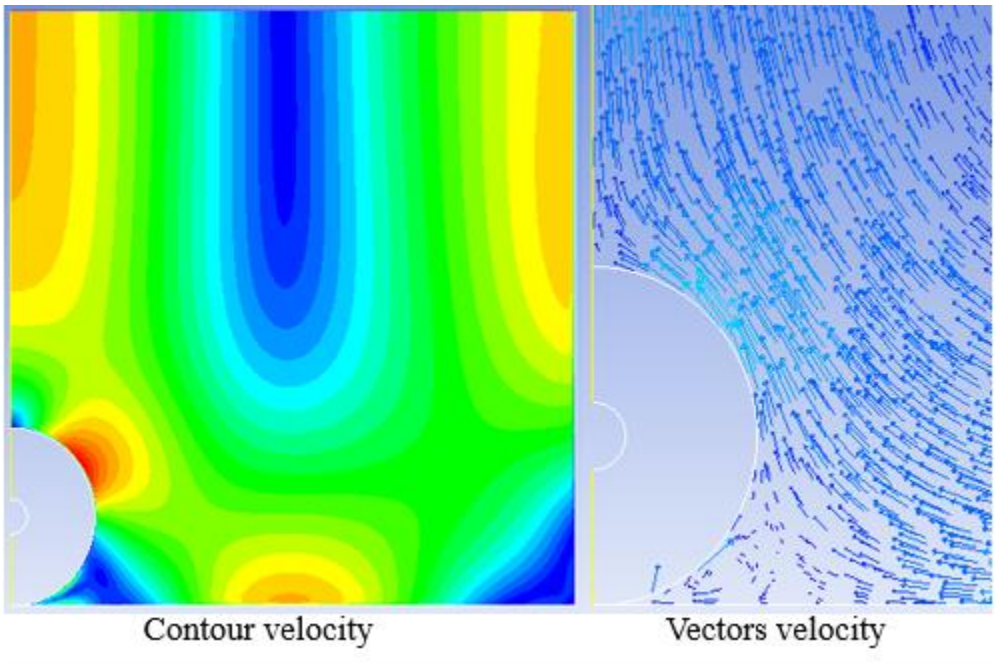

Fig. 8. Velocity distributions. 2D planar model

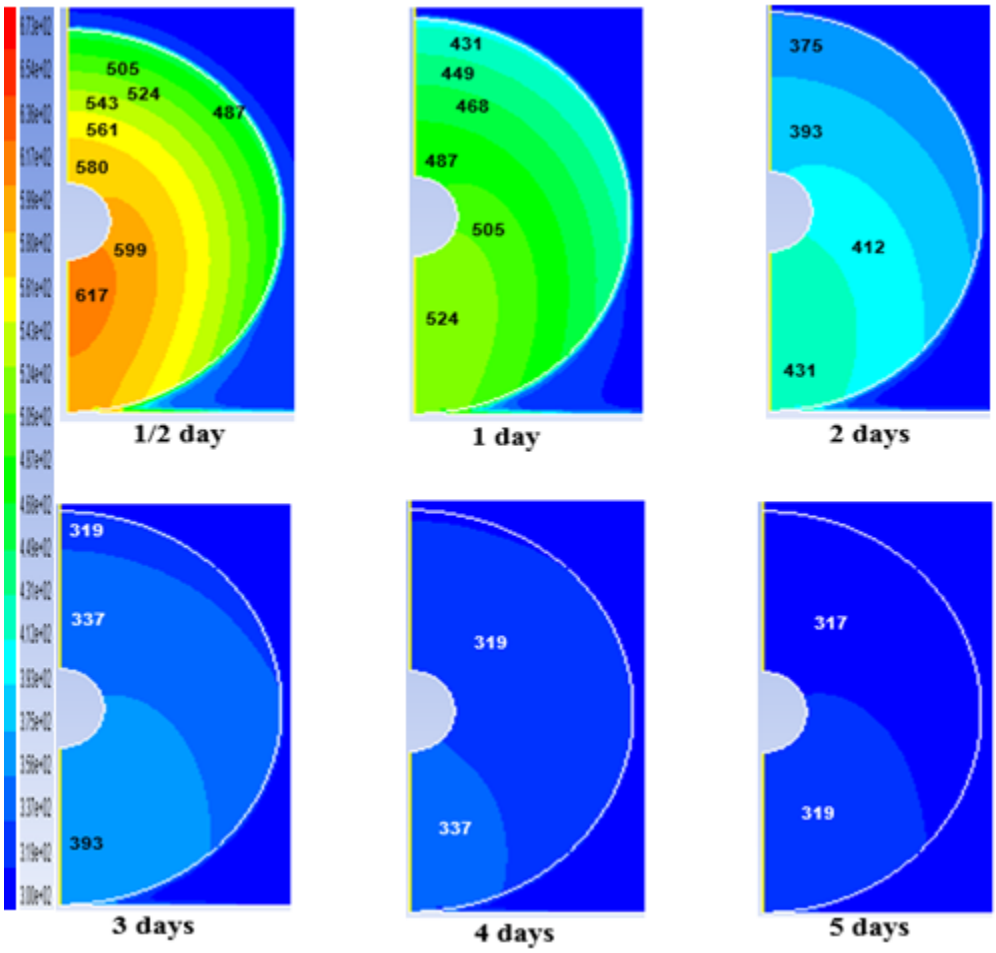

Fig. 9. Temperature distributions. Cooling of one coil and 2D planar model

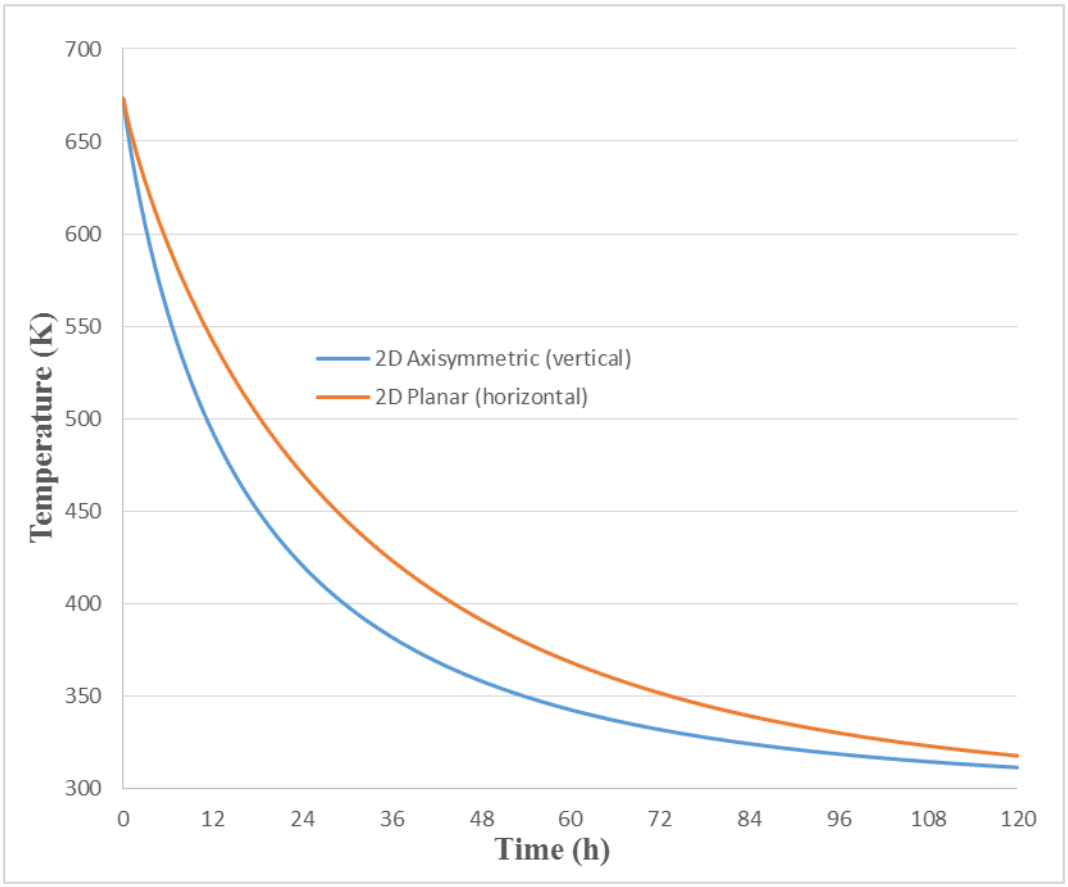

Fig. 10. Comparison between the average temperature for vertical and horizontal coils

3.3. Cooling simulation of one horizontal coil. 3-Dimensional model

To complete the study a 3-Dimensional model was used in order to obtain more accurate results. Figure 11 presents the velocity distributions on a vertical plane containing the symmetry axis of the coil and on a vertical plane perpendicular to the symmetry axis of the coil. It can be seen that the maximum air flow is concentrated in a vertical thin layer going up above the coil all along the length because it is maintained close to the rounded surface until it reaches the higher part of the coil. The vertical mas of fluid going up from the coil is due to big gradients of temperature.

First, the vertical coil simulated with the 2D axisymmetric model is compared with the horizontal 3D simulation of one coil. Figure 12 shows that the average temperature follows a very similar evolution through time in both cases. Due to space limitations, coils are placed in rows in the warehouse. To locate the coils vertically is more difficult and dangerous than to locate them horizontally. It is easy to transport and locate the horizontal coils by taking them by the hollow. Also, to lock the coils horizontally is easier using the hollows.

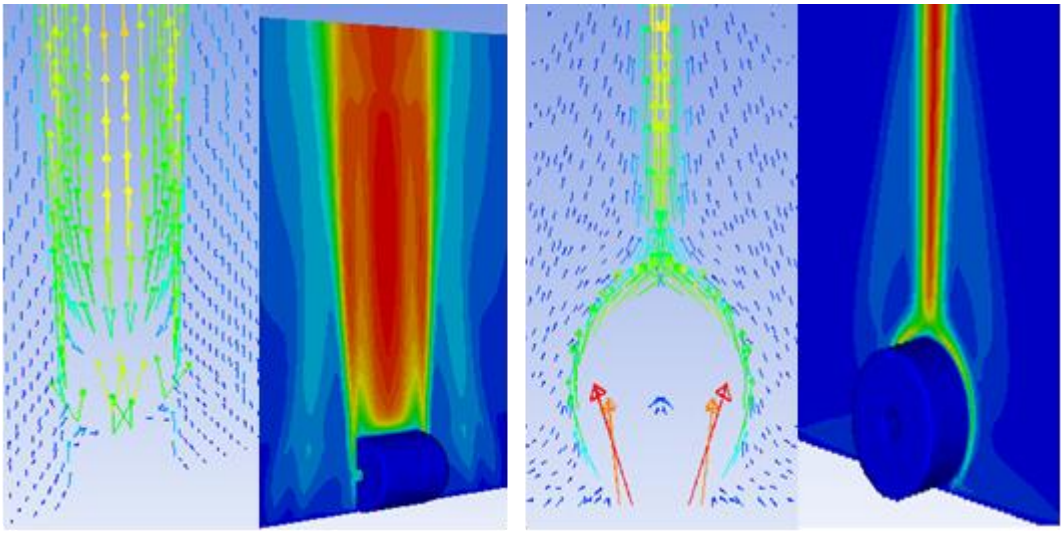

Fig.11. Velocity distributions on a vertical plane containing the symmetry axis of the coil and on a vertical plane perpendicular to the symmetry axis of the coil. 3D model for one-coil

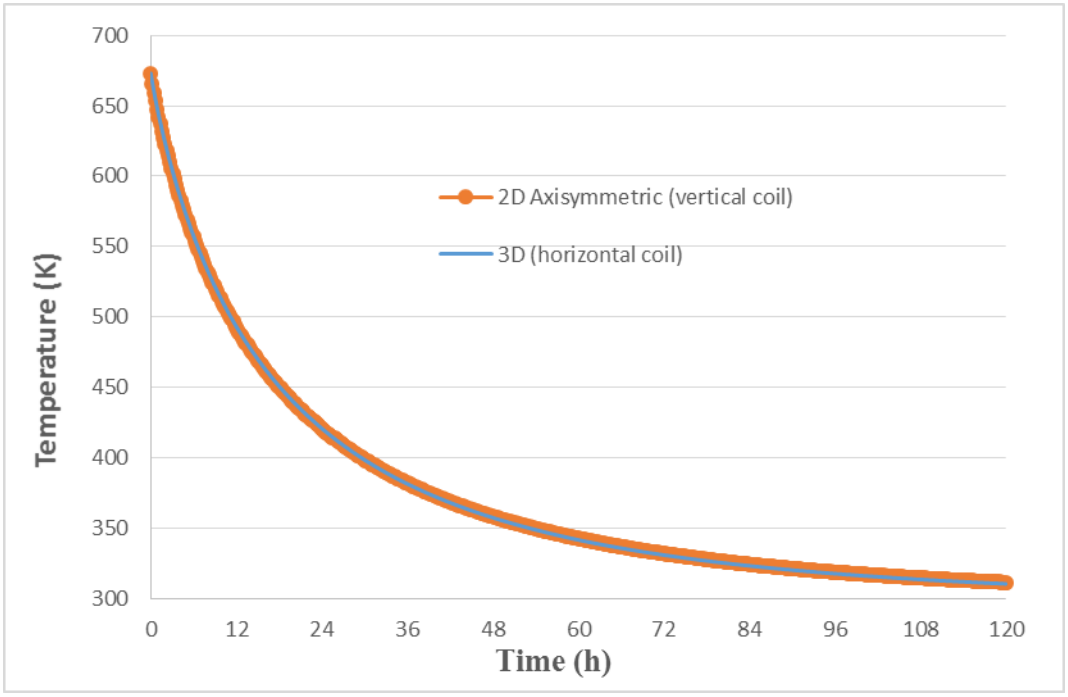

Fig. 12. Comparison of the average temperature between 2D Axisymmetric (vertical coil) and 3D (horizontal coils) models

Figure 13 shows average temperature versus time for one horizontal coil simulated with the 2D planar model compared with the 3D simulation. Initially, the cooling rate is greater for the 3D than for 2D planar model. After 5 days the average temperature is almost the same.

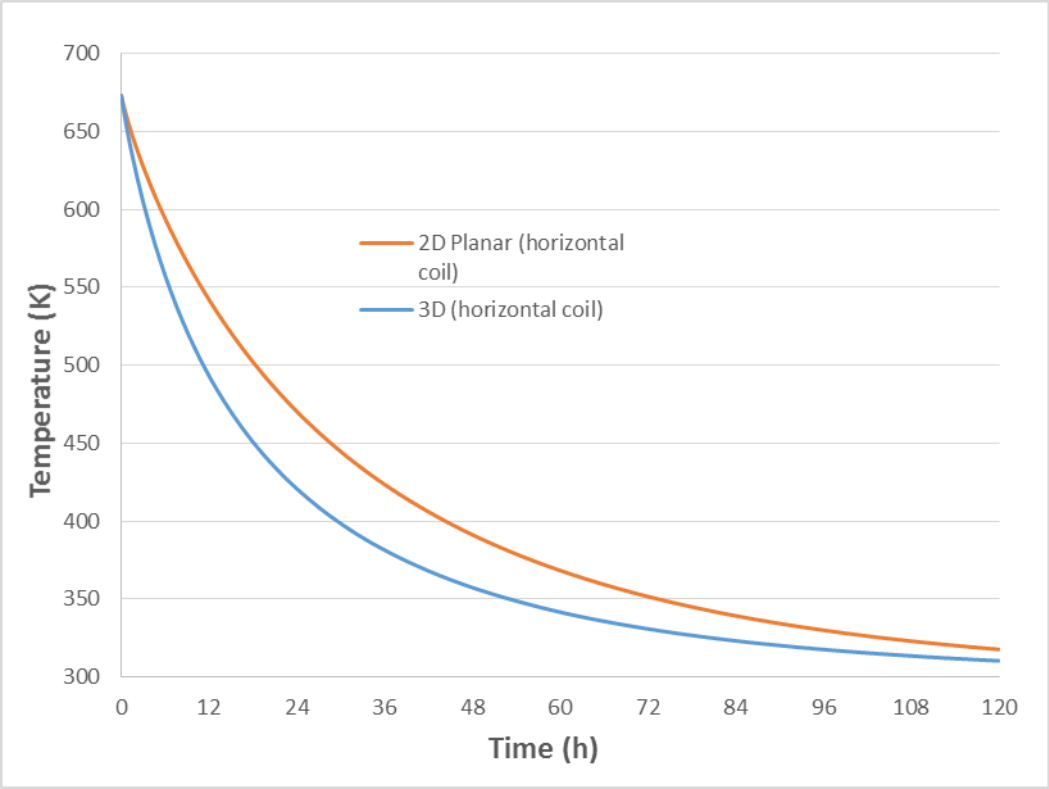

Fig. 13. Comparison between the average temperature for 2D Planar and 3D horizontal coils

3.4. Cooling simulation of three horizontal coils. 3-Dimensional model

Figure 14 shows the velocity distributions on a middle plane parallel to the symmetry axes of the coils and on a vertical plane perpendicular to the mentioned axes. It is similar to the velocity field for one coil (figure 11) and the maximum air flow is concentrated in a vertical thin layer above the coils all along their length but farther from the coils than in the case of one coil. This is coherent with the lower gradient of temperature inside the three coils (same temperature differences than for one coil but bigger distances).

Similar results to the ones obtained with the 3D simulation for one horizontal coil were obtained for three horizontal coils placed in two rows. The cooling rate is greater for the 3D simulation of one coil than the rate obtained for three coils, all along the time (Figure 15). After five days the difference is very small, but obviously the remaining temperature for three coils is a little bit greater.

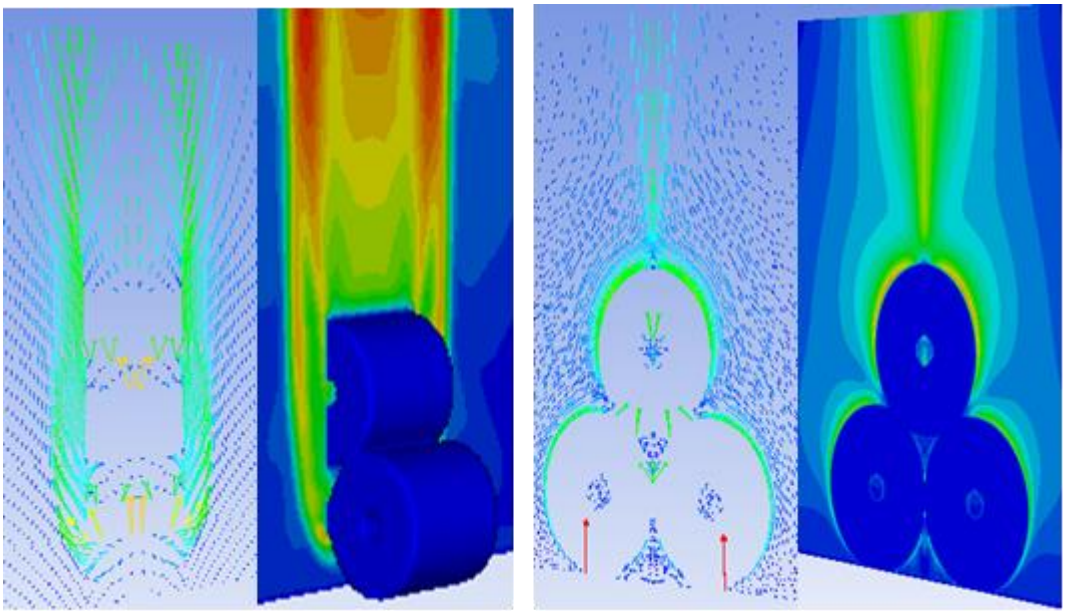

Fig.14. Velocity distributions. 3D simulation of three coils

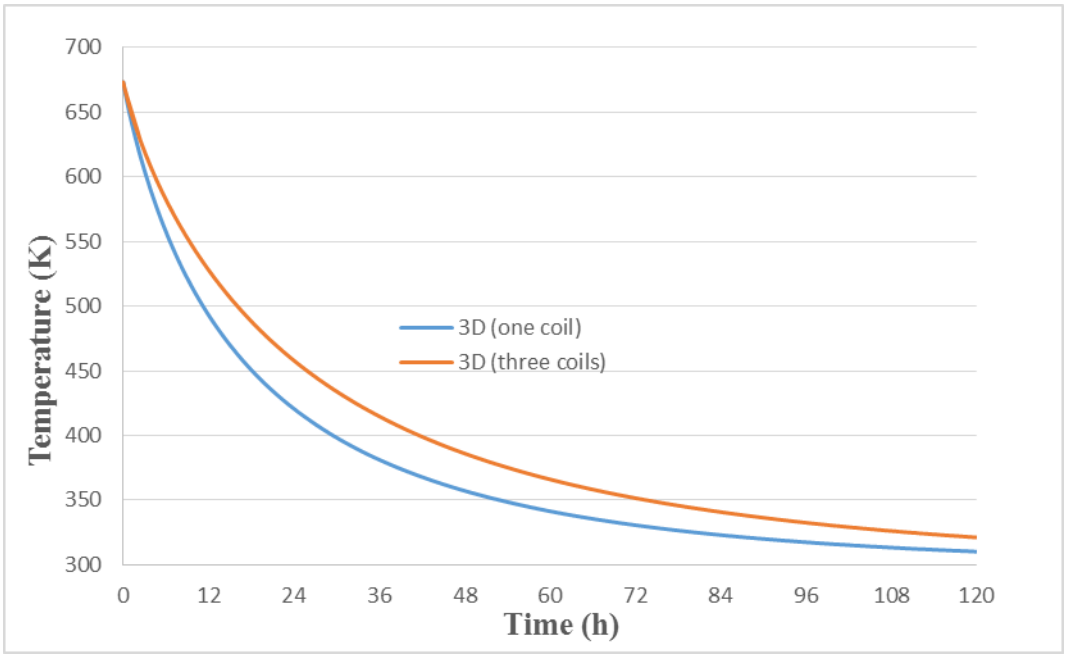

Fig.15. Comparison between the average temperature for 3D models of one and three coils (horizontally oriented).

3.5. Cooling law equation parameters

The parameter values of the equation 7 for the cases studied were obtained by the method of least squares and the goodness-of-fit was measured by the coefficient of determination (R^2). Those values are shown in table 1.

For all the models the coefficient of determination is very close to 1. It means that the equation fits very well with the data obtained with the simulations.

Parameter “a” is the coefficient affecting the natural logarithm that comes from the both mechanism: convection and radiation. This parameter has of the same order of magnitude as $(m\ C_p)/(Ah)$, which is $1/k_1$. This is coherent with the mathematical development.

Parameter “b” multiplies the function arctangent, which is a correction of the main term (natural logarithm) due to radiation. It takes into account that the heat transfer by radiation depends on the deference of the fourth powers of the absolute temperatures (according to Boltzmann’s law), and it decreases along the time of cooling. Therefore, parameter “b” is negative.

Parameter “c” accounts for the conduction inside the coil. T represents the average temperature and T+c, the temperature at the surface of the coil. Therefore, parameter “c” measures the difference between the surficial and the average temperatures. During the cooling process, parameter “c” is negative.

According to table 1, the results are coherent with the previous ones. 2D axisymmetric parameters are quite similar to the ones of the 3D simulation for one coil. For three coils, the absolute values of the parameters are greater than for one coil. Parameter “c” is greater in absolute value for three coils than for one coil, meaning that the difference between the average and the surface temperatures is greater. The cooling rate is greater when the absolute values of the parameters are lower.

Table 1. Equation parameters for the studied models

	a (x 10^{-5})	**b (x 10^{-5})**	**c**	**R^2**
2D Axisymmetric	1.296	-1.074	-4.539	0.9997
2D planar	1.552	-0.744	-1.691	0.9999
3D one coil	1.393	-1.021	-3.425	0.9999
3D three coils	1.595	-1.087	-6.771	0.9998

4. Conclusions

Steel coils must be cooled from temperatures of about 400ºC to ambient temperature to be handle and transported for sale. Coils cooling takes between four and six days depending on weather conditions. It produces unwanted stocks. The coil geometries are cylindrical and usually stored in stacks of two or three levels.

A methodology to calculate the cooling law of a coil and three coils placed in two rows is presented in this paper. The cooling law is expressed by a mathematical equation depending only on 3 parameters. The parameters have been obtained by numerical analysis with the software ANSYS – FLUENT. 2D and 3D models were used to study the heat transfer mechanisms involved in the cooling of coils and also, to characterize the temperature distributions inside the coil, as well as the temperature and velocity distributions around the coils.

The cooling law for one coil placed vertically and horizontally is almost identical but, due to space limitations, coils are placed in rows in the warehouse. It is easy to handle, transport and lock the coils horizontally. Also, the cooling rate was calculated for one coil and three coils. The cooling rate is greater for the one coil than the rate obtained for three coils.

The values of the three parameters defined by the equation of the cooling law obtained are very good because the coefficient of determination is very close to 1. Also, the values are coherent with the physical concepts of heat transfer mechanisms.

The methodology allows to quantify temperatures, times, cooling rates by means of the cooling law for the cases studied. It could be interesting to study the influence of geometrical parameters, number of coils and rows; and thermal properties of the materials by following the defined methodology for a larger number of cases, in order to be able to extrapolate the results to different cases and avoiding the simulations.

References

[1] OECD DSTI/SU/SC. The future of the steel industry: selected trends and policy issues. 73rd Steel Committee Meeting Paris, 6-7 December 2012

[2] Pardo, N., & Moya, J. A. (2013). Prospective scenarios on energy efficiency and CO2 emissions in the European iron & steel industry. Energy, 54, 113-128.

[3] Estimates of Emissions Reduction Potential for the 2015. Report. https://newclimateeconomy.report/workingpapers/wp-content/uploads/sites/5/2016/04/Estimates-Reduction-Potential-NCE-20151.pdf. (Last accessed June 2017).

[4] EC–European Commission. (2012). Directive 2012/27/EU of the European Parliament and of the Council of 25 October 2012 on energy efficiency. Official Journal of the European Union, L, 315(1).

[5] European Commission. On the Future of Carbon Capture and Storage in Europe COM (2013).

[6] Villar, A., Arribas, J. J., & Parrondo, J. (2012). Waste-to-energy technologies in continuous process industries. Clean Technologies and Environmental Policy,14(1), 29-39.

[7] Das, B., Prakash, S., Reddy, P. S. R., & Misra, V. N. (2007). An overview of utilization of slag and sludge from steel industries. Resources, conservation and recycling, 50(1), 40-57.

[8] Nobari AH, Serajzadeh S. Modeling of heat transfer during controlled cooling in hot rod rolling of carbon steels. Applied thermal engineering. 2011 Mar 31;31(4):487-92.

[9] Phadke, Sameer, Praveen Pauskar, and Rajiv Shivpuri. "Computational modeling of phase transformations and mechanical properties during the cooling of hot rolled rod." Journal of materials processing technology 150.1 (2004): 107-115.

[10] Yu, Wan-Hua, et al. "Development and application of online Stelmor controlled cooling system." Applied Thermal Engineering 29.14 (2009): 2949-2953.

[11] Czaputa, Klaus, and Brenn, Günter. "The convective drying of liquid films on slender wires." International Journal of Heat and Mass Transfer 55.1 (2012): 19-31.

[12] Le Page, Jean-François, et al. "Development of an approximate empirical-CFD model estimating coupled heat and water transfers of stacked food products placed in airflow." Journal of Food Engineering 92.2 (2009): 208-216.

[13] S.J. Park, B.H. Hong, S.C. Baik, K.H. Finite element analysis of hot rolled coil cooling, ISIJ International 38 (11) (1998) 1262– 1269.

[14] Karlberg, M. (2011). Modelling of the temperature distribution of coiled hot strip products. ISIJ international, 51(3), 416-422.

Figure captions

Tables

Table 1. Equation parameters for the studied models

Figure 1

Click here to download Figure Figure 1.jpg

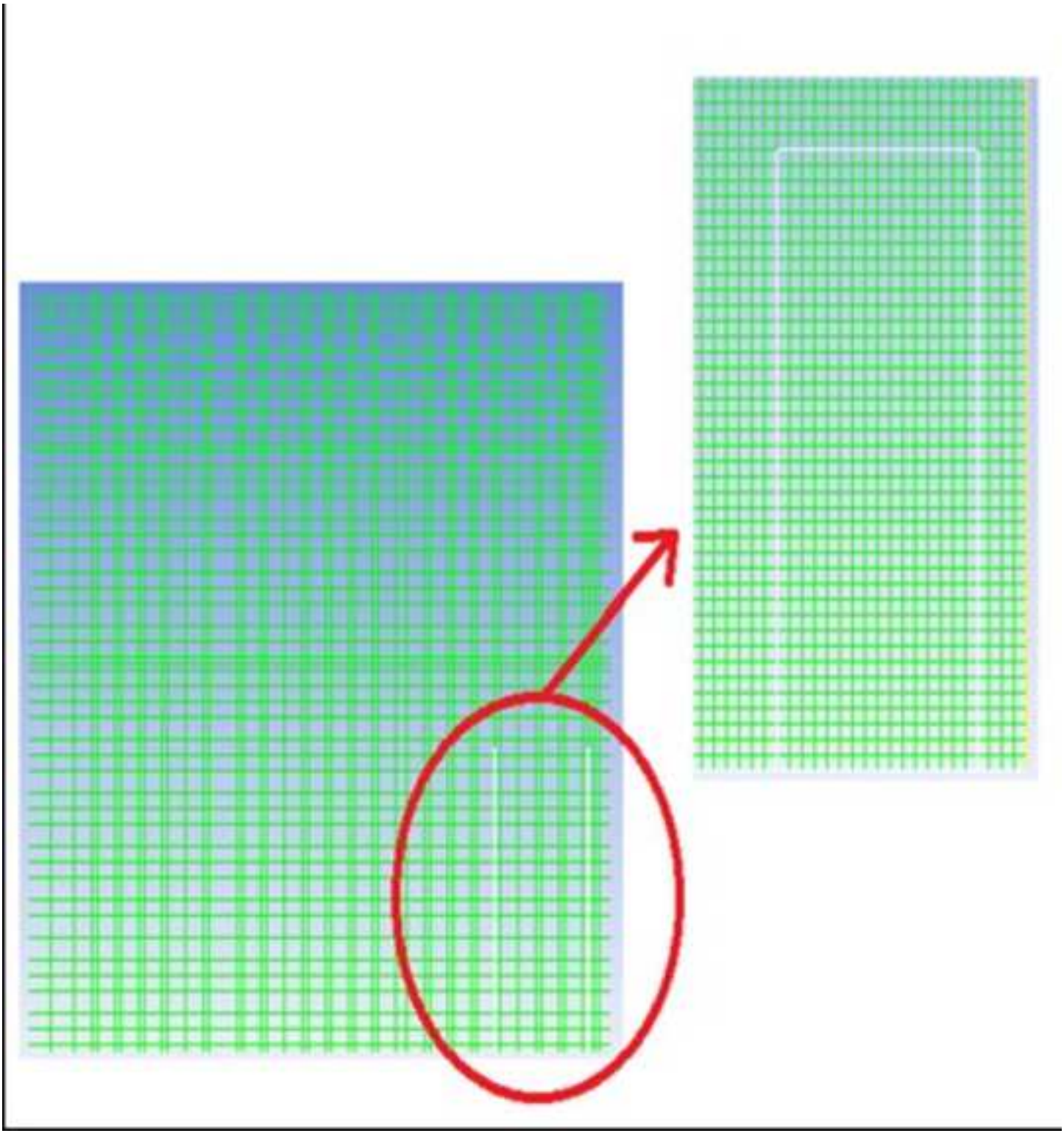

Figure 2

Click here to download Figure Figure 2.jpg

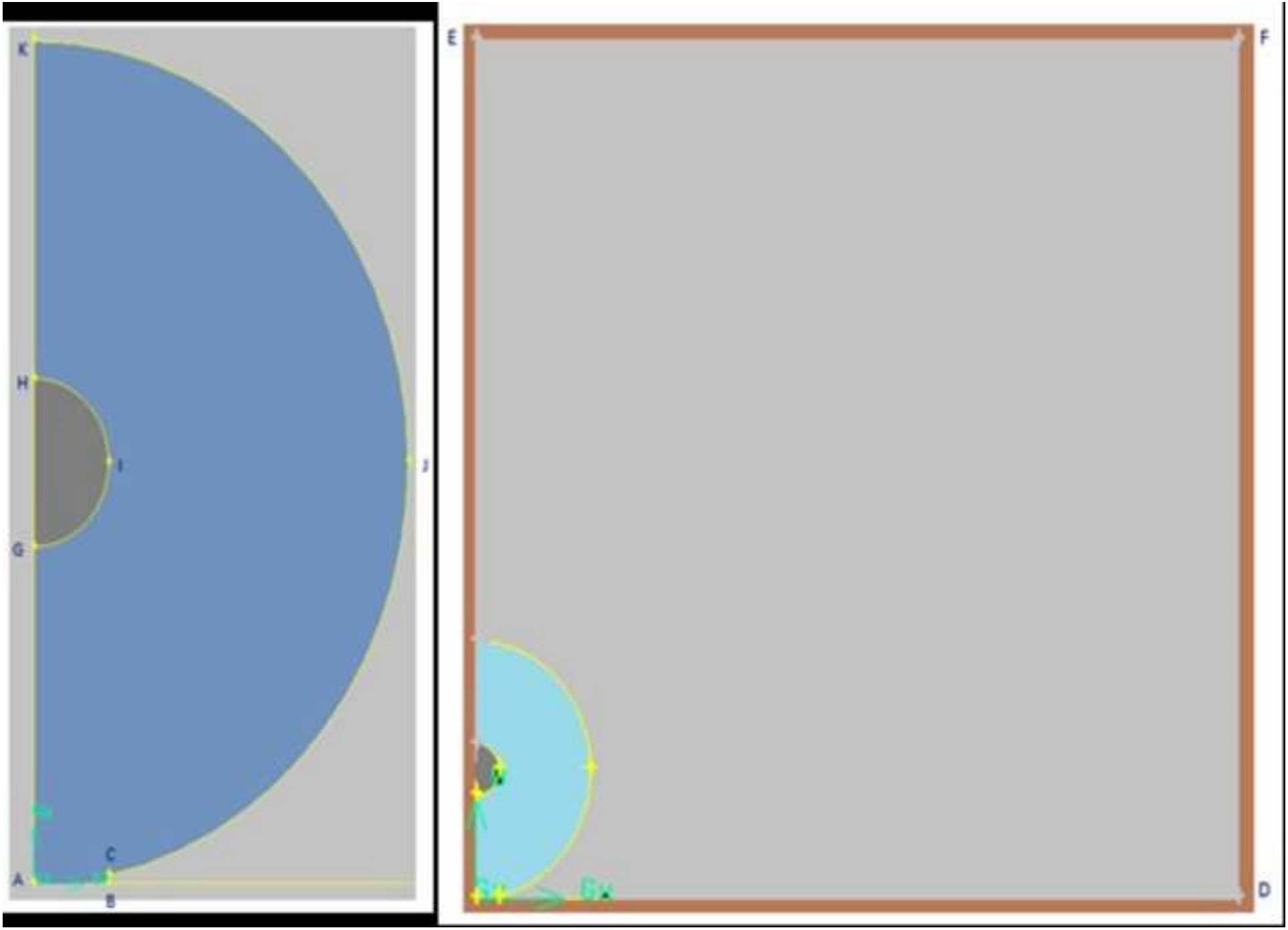

Figure 3

Click here to download Figure Figure 3.jpg

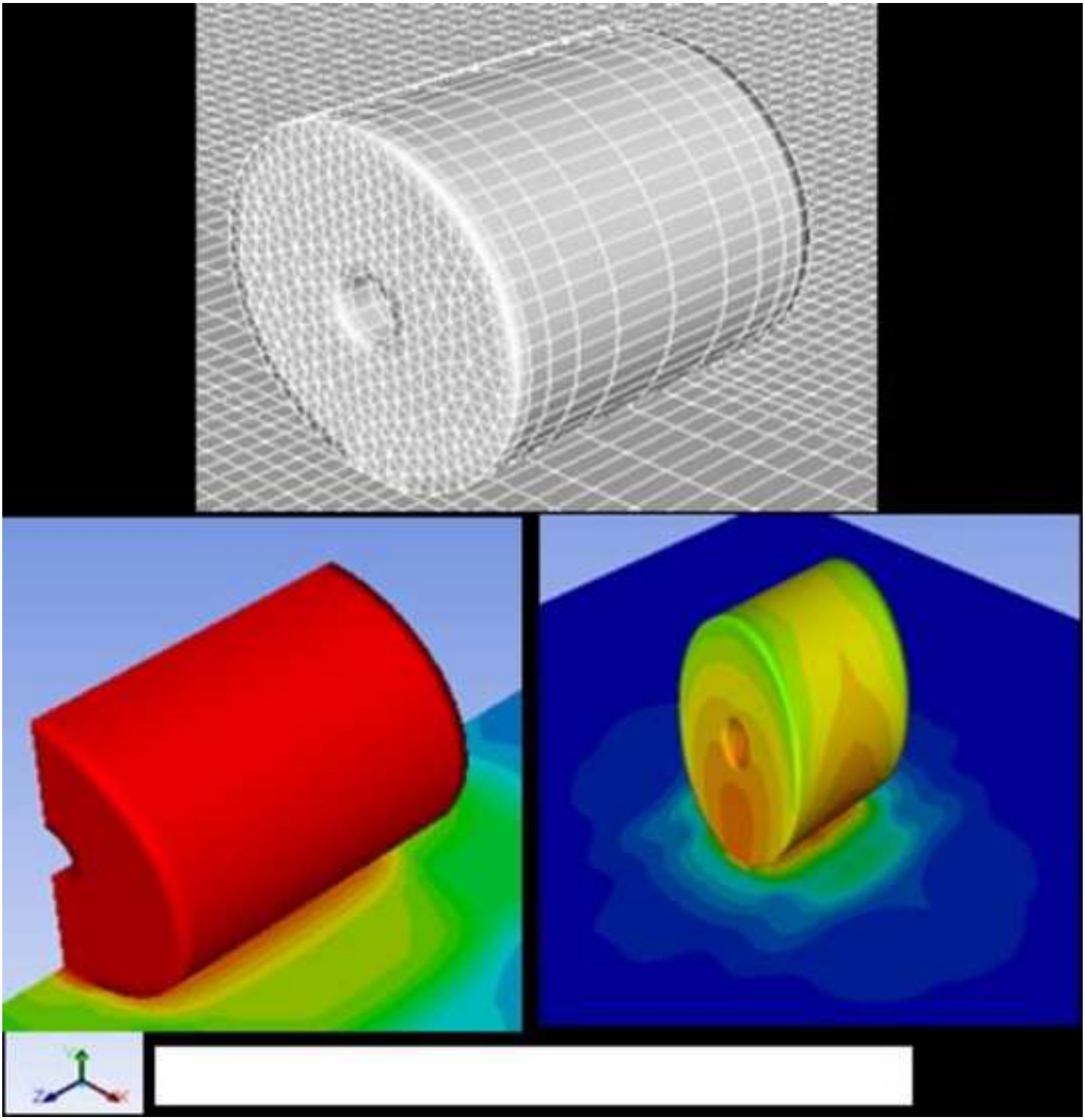

Figure 4

Click here to download Figure Figure 4.jpg

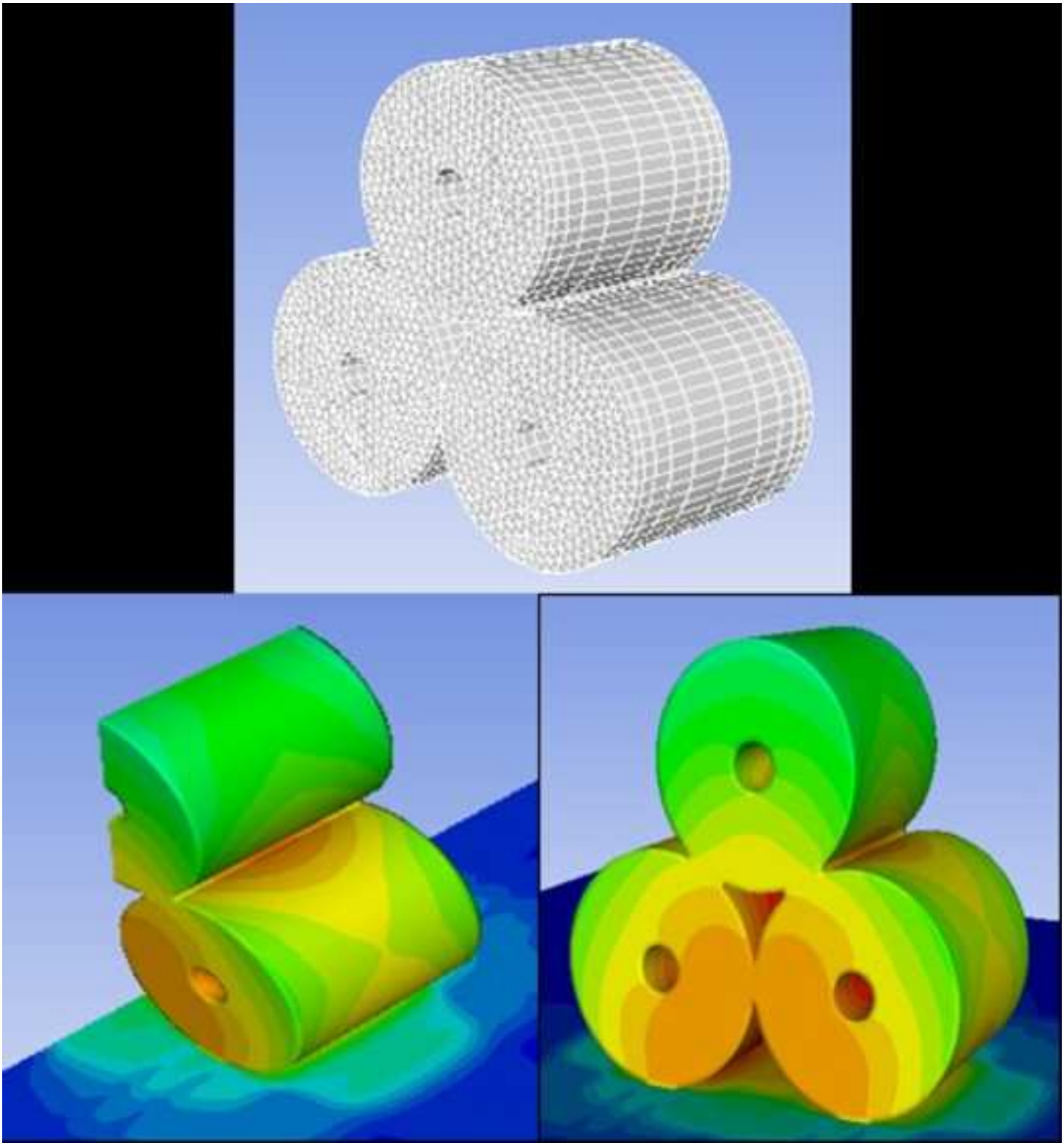

Figure 5

Click here to download Figure Figure 5.jpg

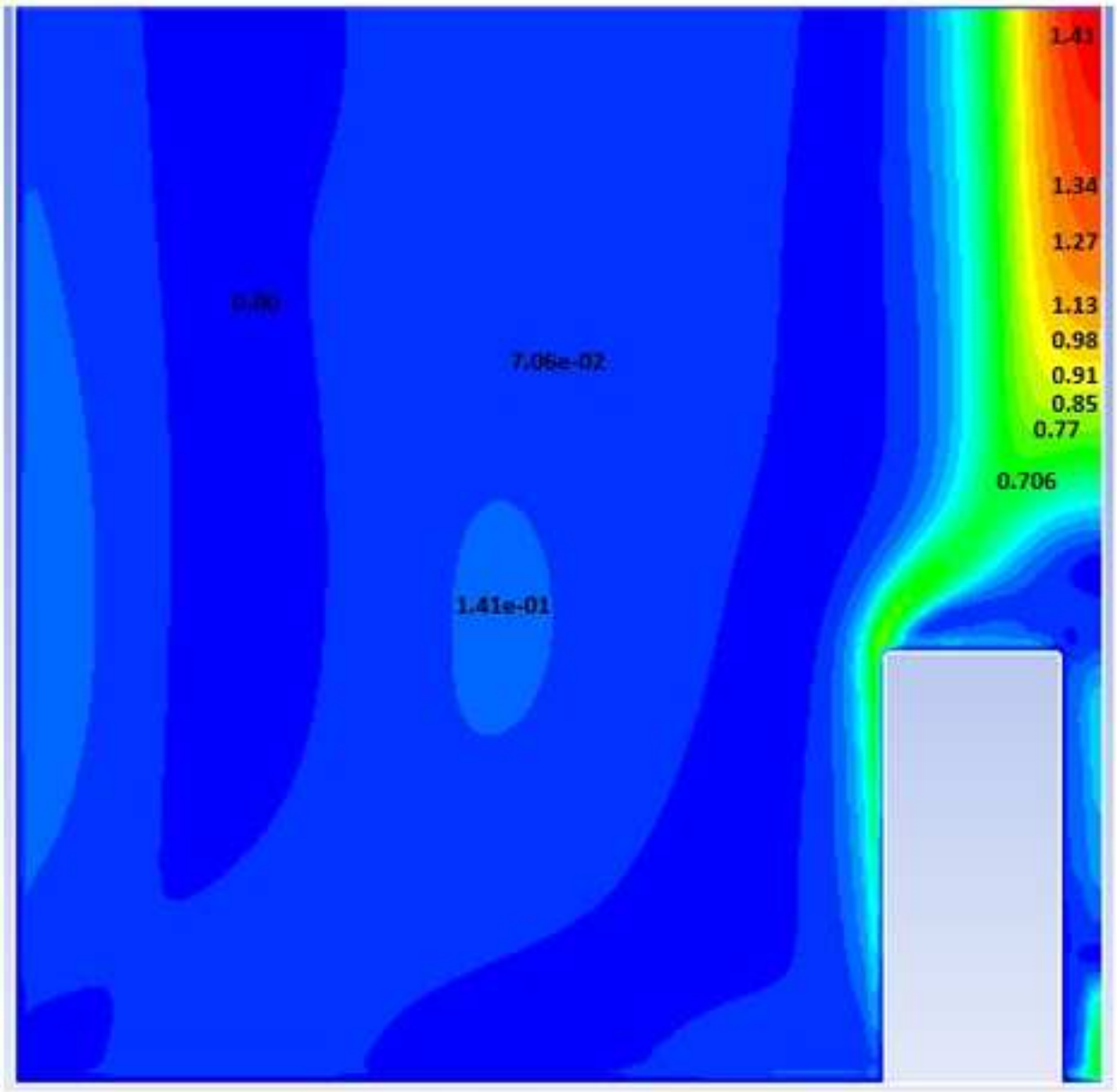

Contour of velocity

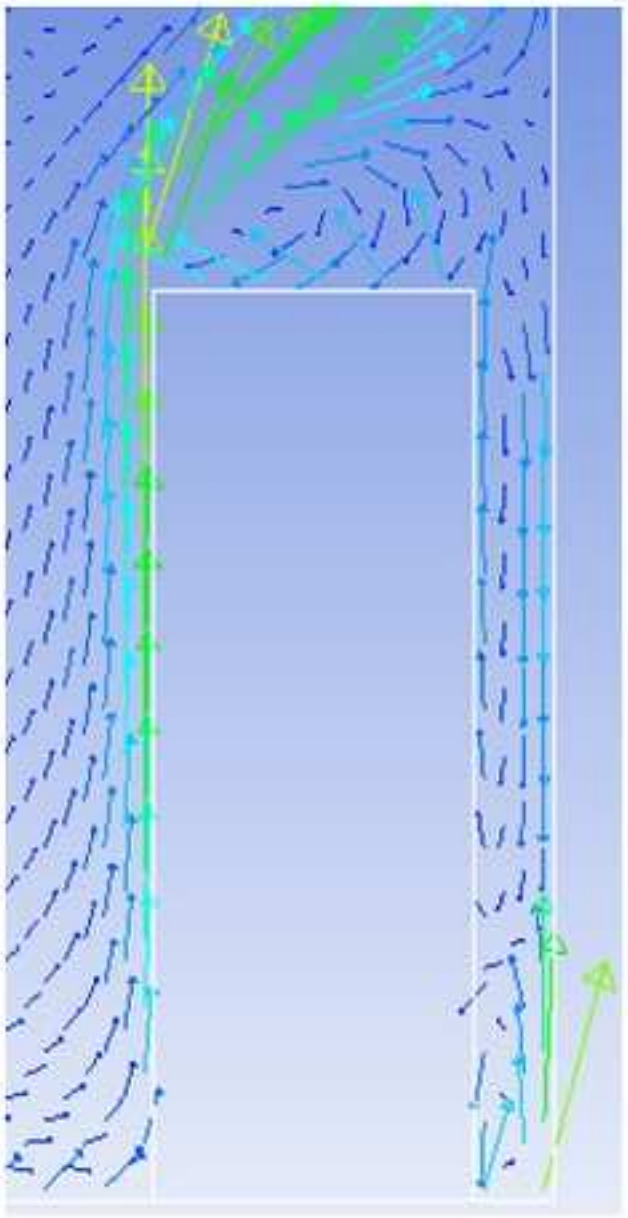

Vector velocity

Figure 6

Click here to download Figure Figure 6.jpg

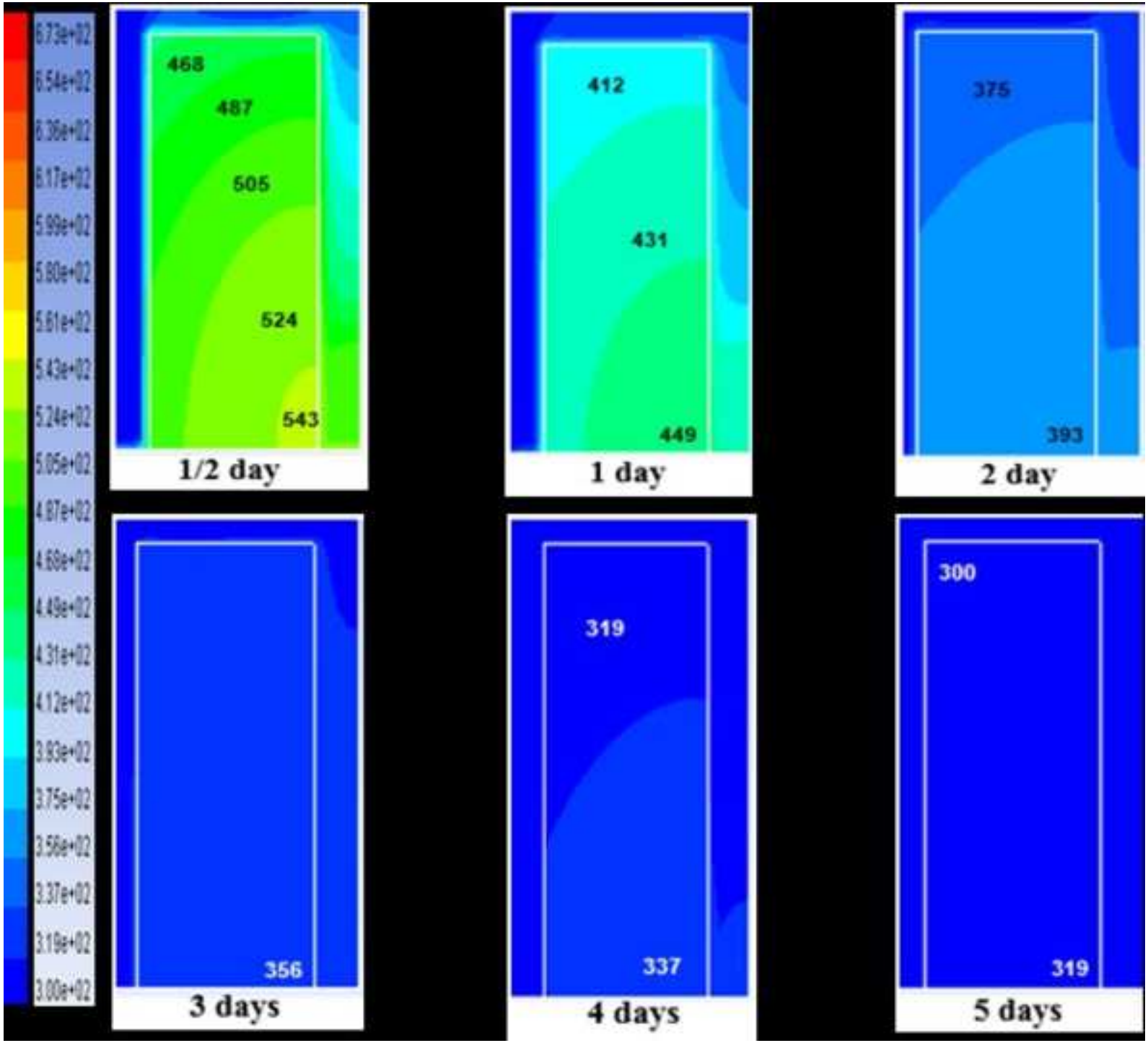

Figure 7

Click here to download Figure Figure 7.jpg

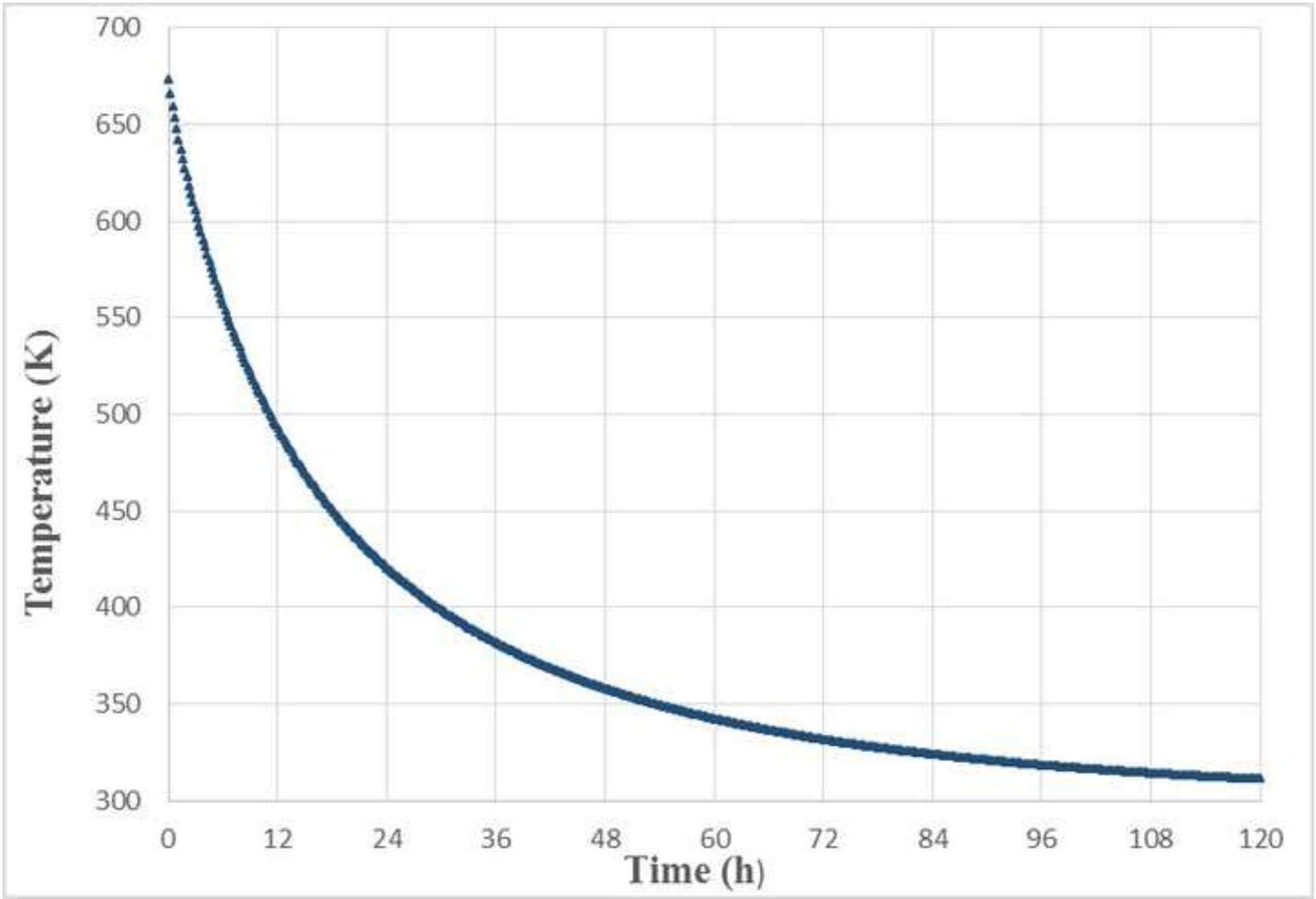

Figure 8

Click here to download Figure Figure 8.jpg

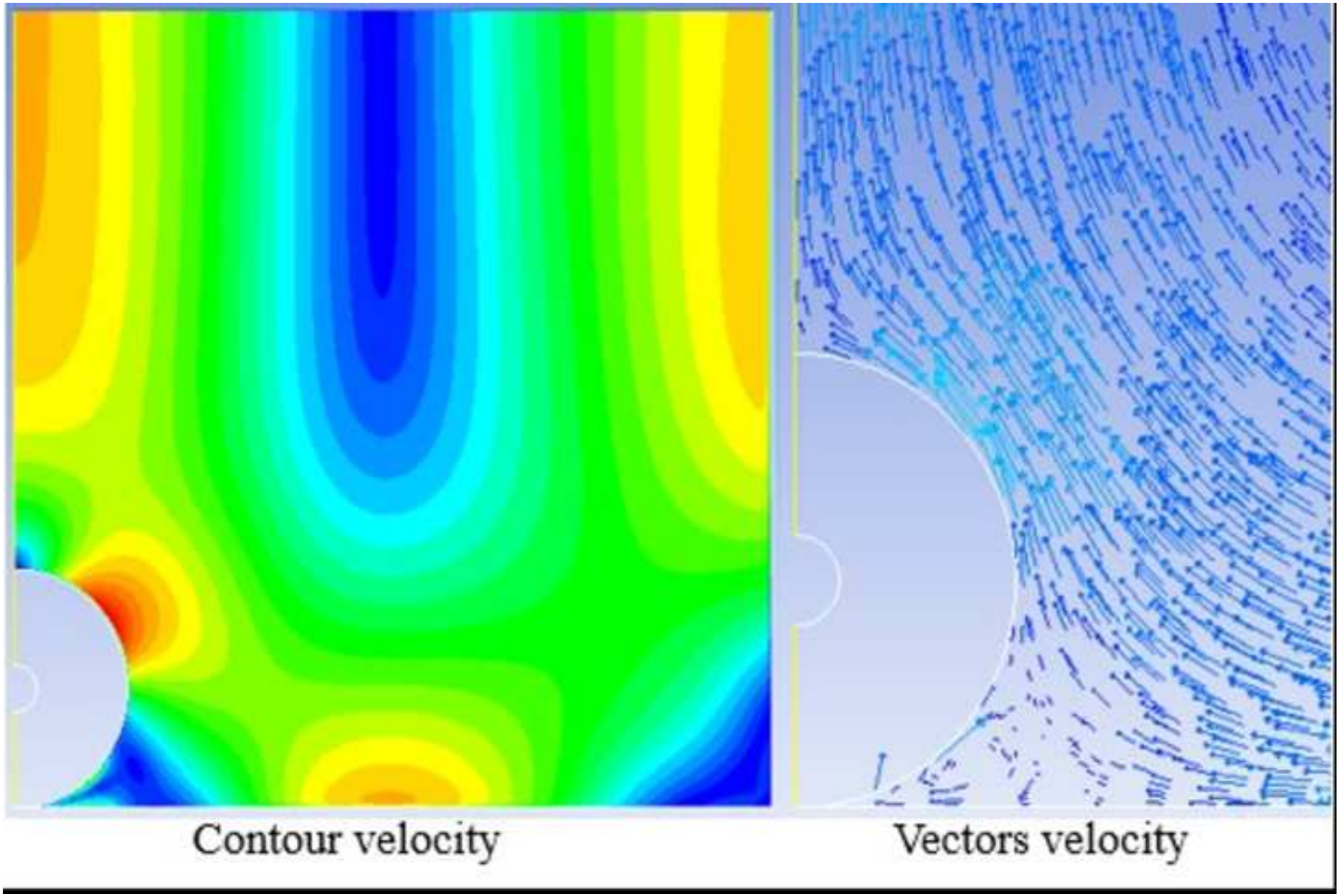

Figure 9

Click here to download Figure Figure 9.jpg

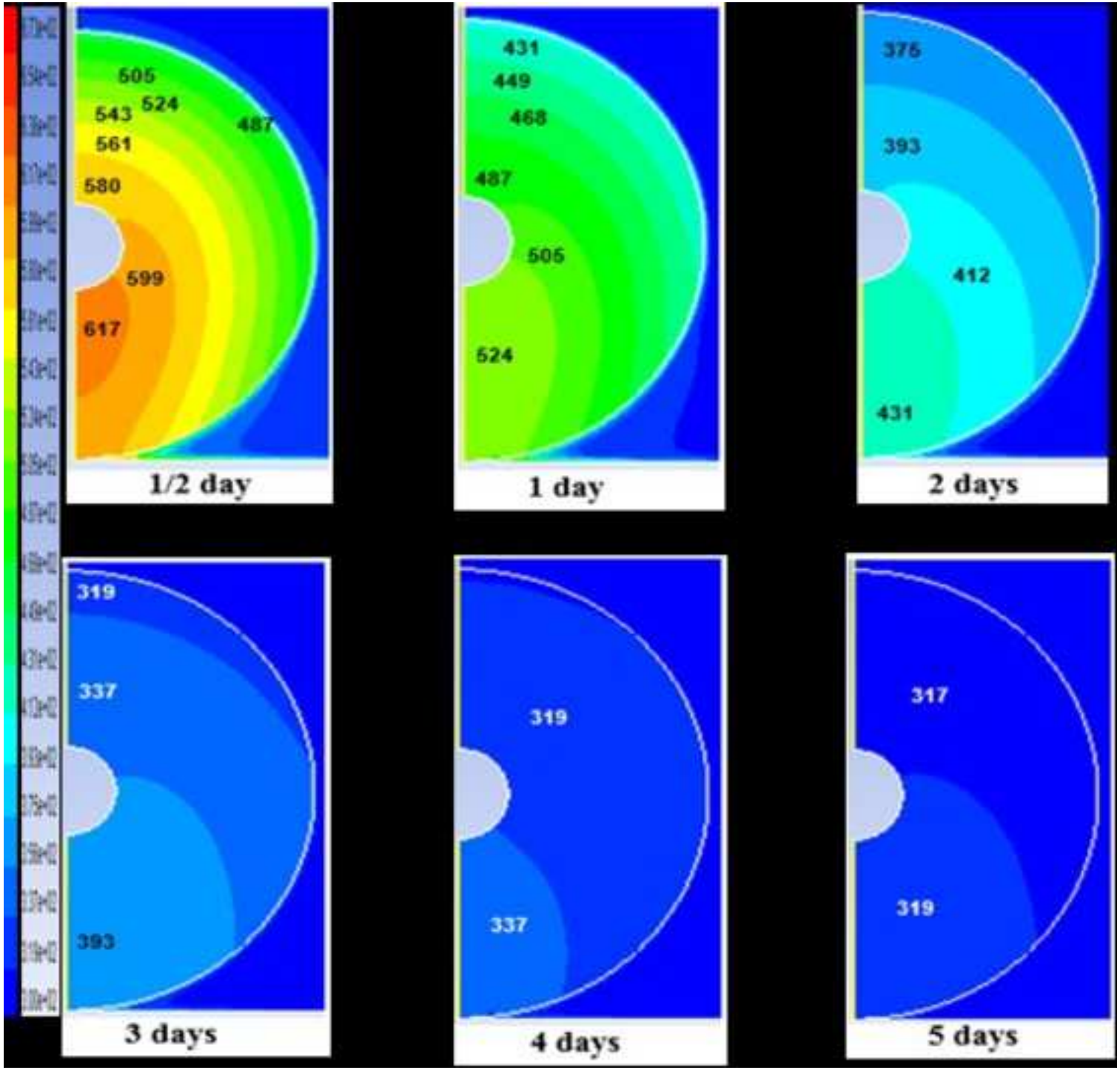

Figure 10

Click here to download Figure Figure 10.jpg

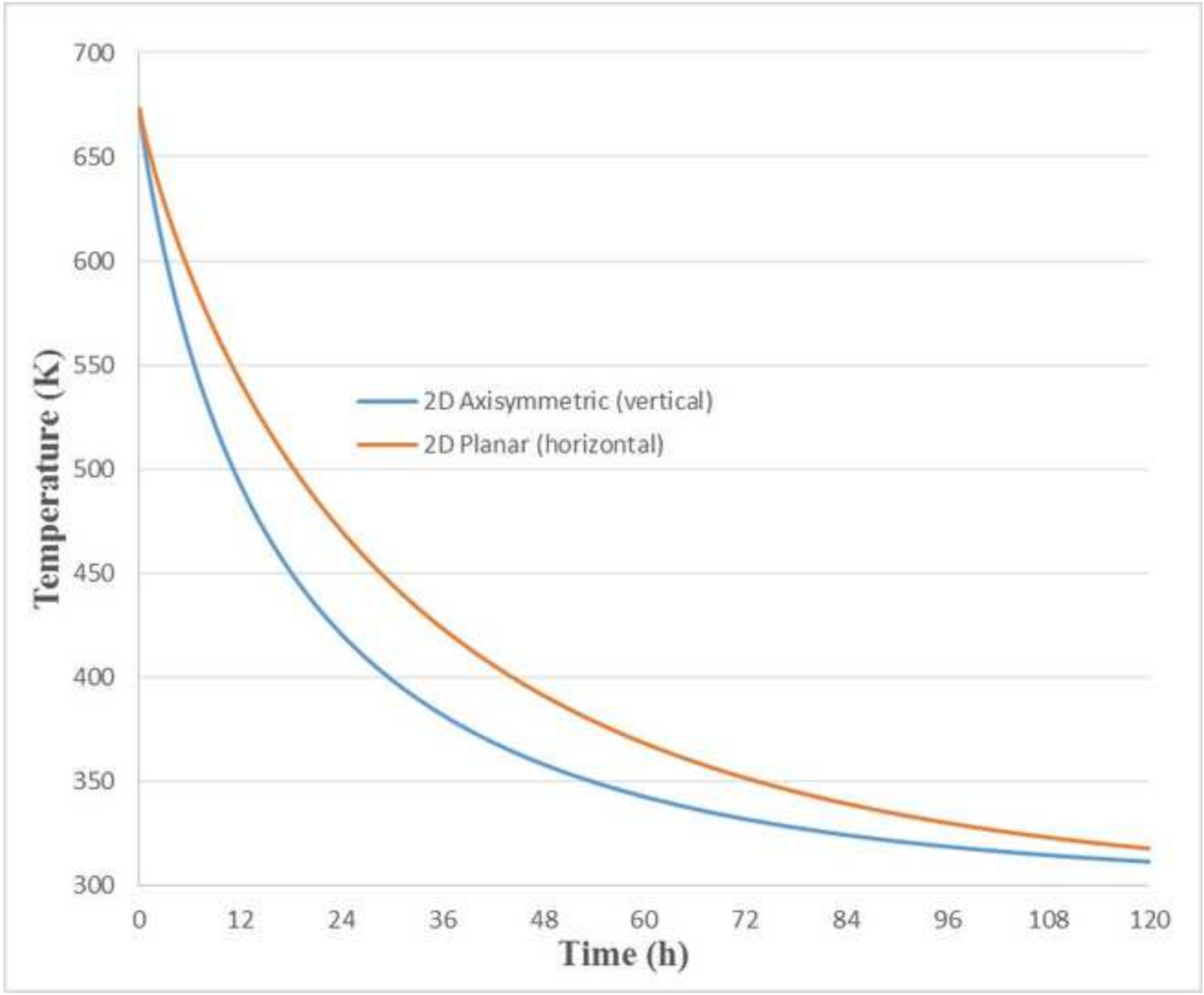

Figure 11

Click here to download Figure Figure 11.jpg

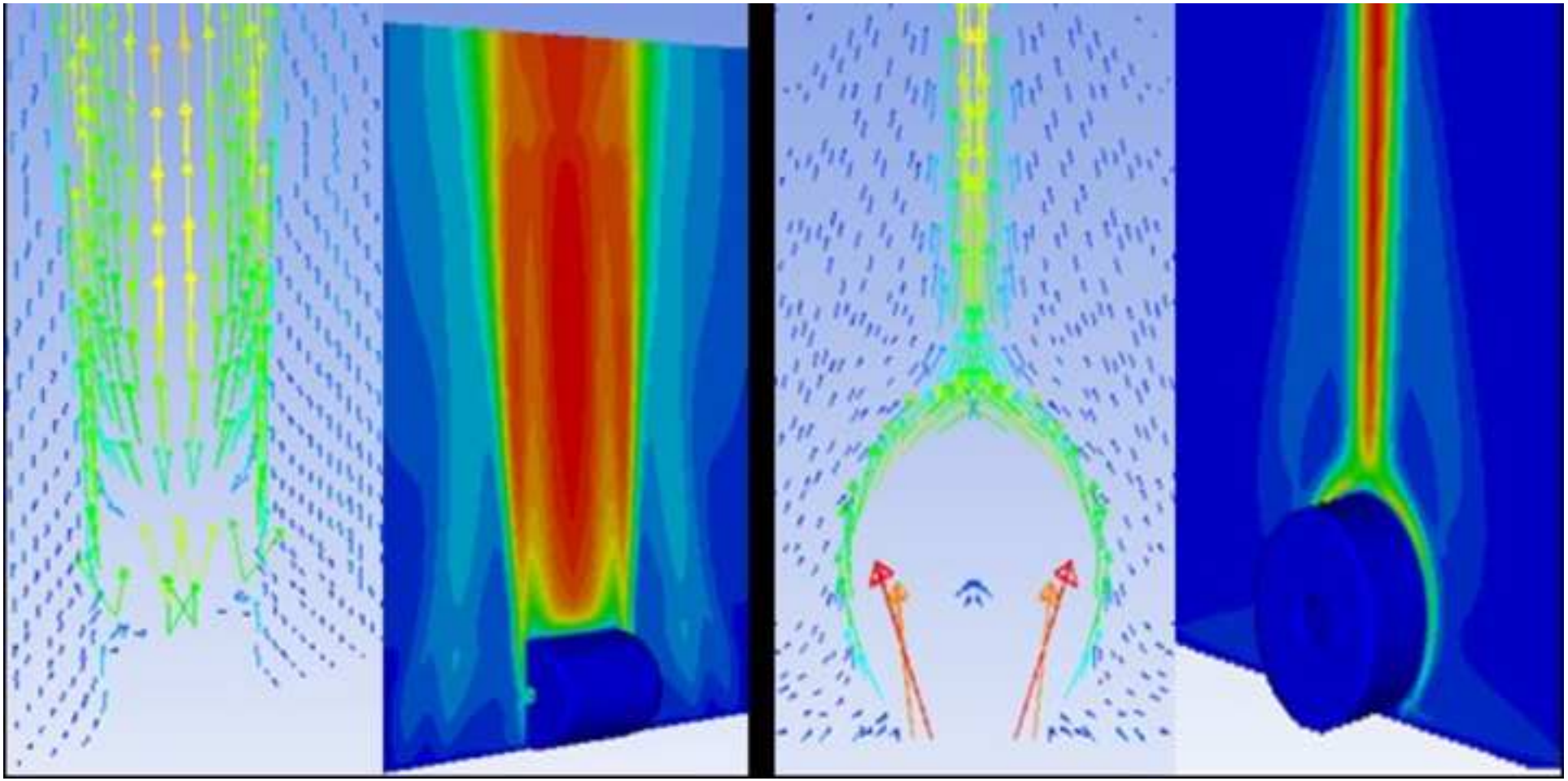

Figure 12

Click here to download Figure Figure 12.jpg

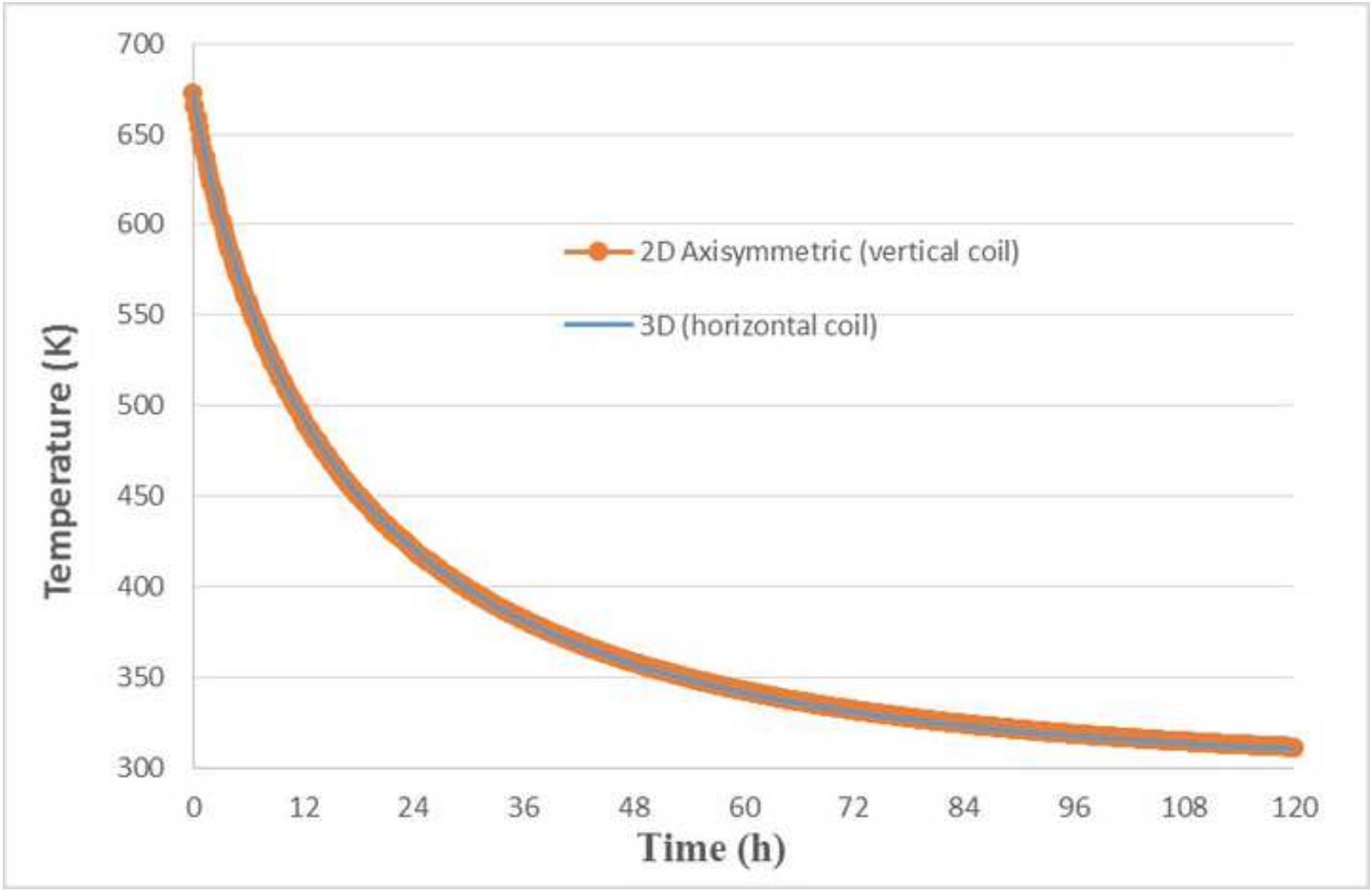

Figure 13

Click here to download Figure Figure 13.jpg

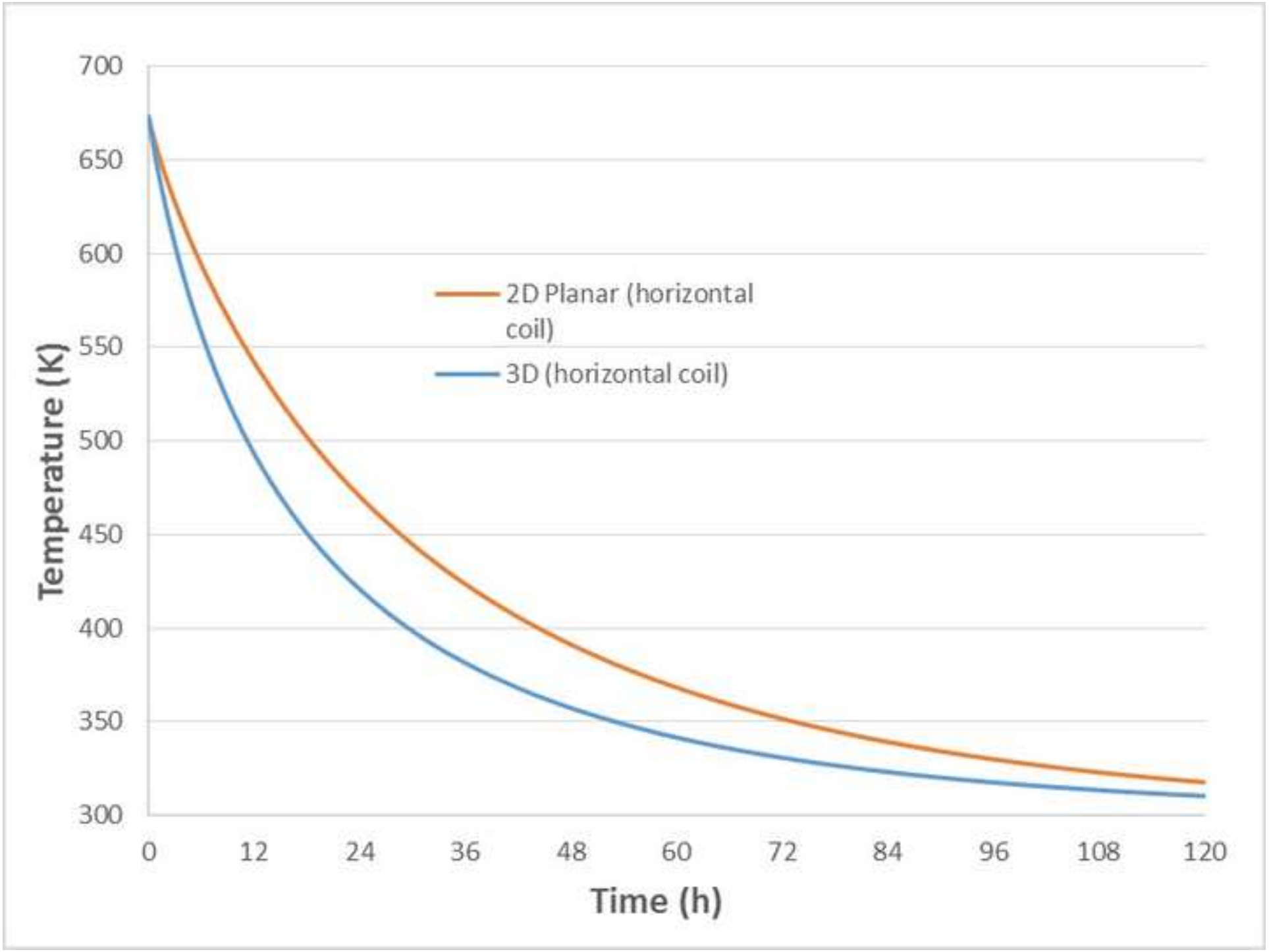

Figure 14

Click here to download Figure Figure 14.jpg

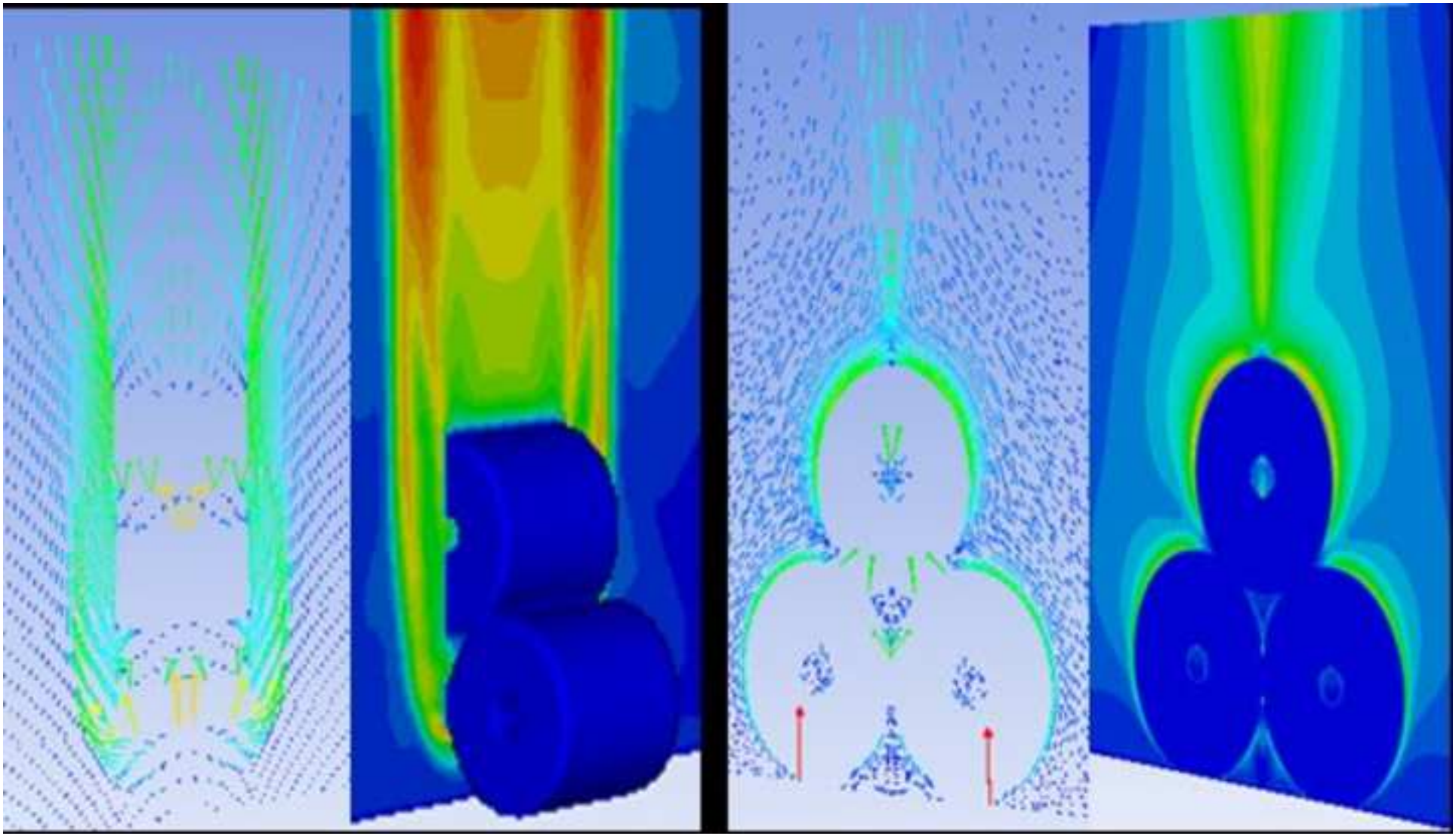

Figure 15

Click here to download Figure Figure 15.jpg

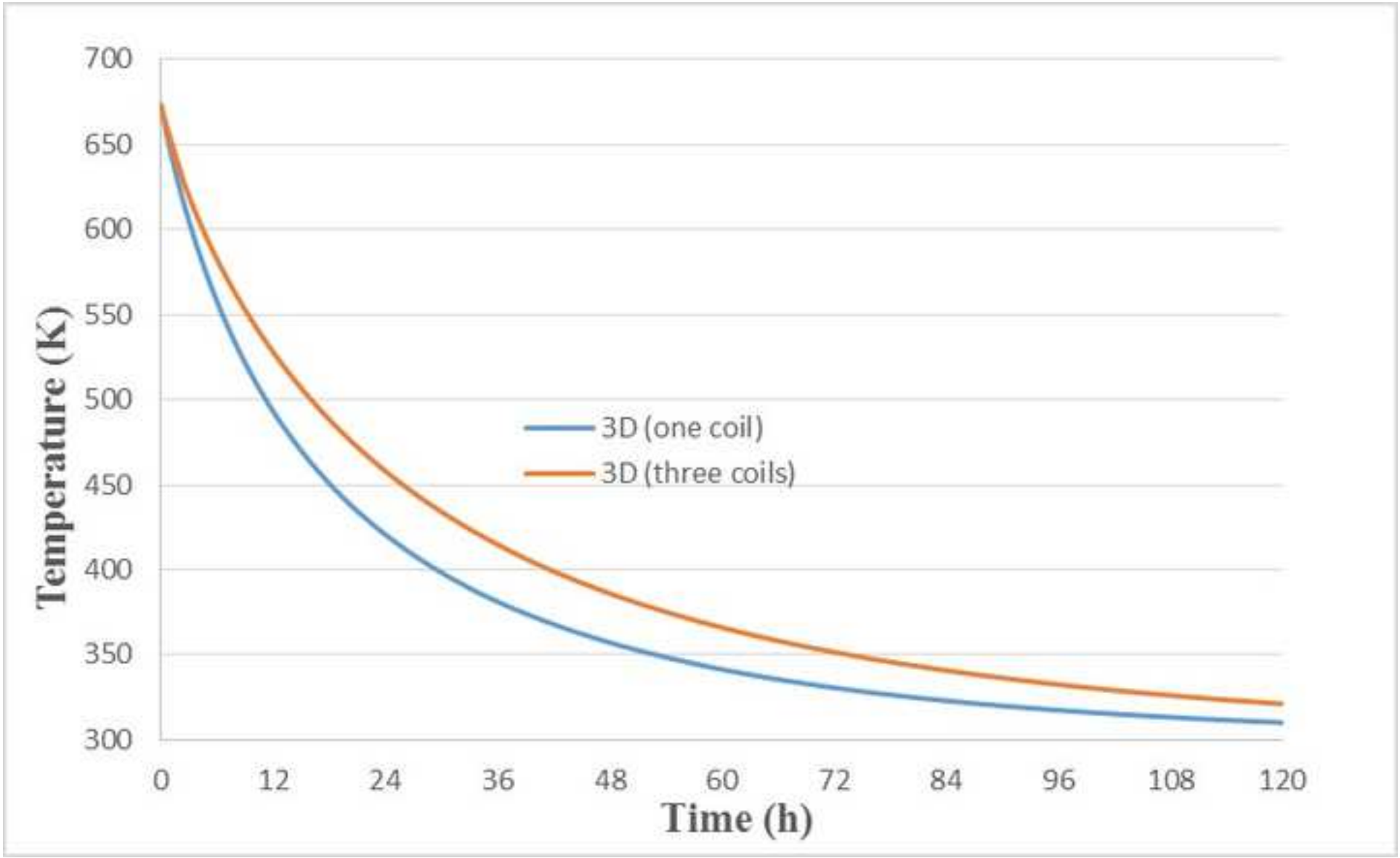

Table 1. Equation parameters for the studied models

	a (x 10^{-5})	**b (x 10^{-5})**	**c**	**R^2**
2D Axisymmetric	1.296	-1.074	-4.539	0.9997
2D planar	1.552	-0.744	-1.691	0.9999
3D one coil	1.393	-1.021	-3.425	0.9999
3D three coils	1.595	-1.087	-6.771	0.9998

International Congress

water, waste and energy management

Rome, 18-20 July 2015

Scientific Program

ISBN: 978-84-944311-5-9

Edited by: ScienceKNOW Conferences C.B.

July 2016

Modeling of Coil Cooling using 2D and 3D Computational Fluid Dynamics (CFD)

D. Irawan, A. García, A.J. Gutiérrez, E. Álvarez, E. Blanco

Energy Department

University of Oviedo, Spain

E-mail: dodi.unmuhpnk@gmail.com

1. Introduction – In metalworking, rolling is a metal forming process in which metal stock is passed through one or more pairs of rolls to reduce the thickness and to make the thickness uniform. The concept is similar to the rolling of dough. Rolling is classified according to the temperature of the metal rolled.

Image 1. Steel coil

If the temperature of the metal is above its recrystallization temperature, then the process is known as hot rolling. If the temperature of the metal is below its recrystallization temperature, the process is known as cold rolling. In terms of usage, hot rolling processes more tonnage than any other manufacturing process, and cold rolling processes the most tonnage out of all cold working processes.

Considerable researches have been devoted to research the thermal and microstructural behaviors of steels in controlled cooling process. For instance, Nobari and Serajzadeh [1] developed a mathematical model to predict temperature variations and austenite phase transformation in steel during controlled cooling. Shivpuri and co-workers [2] presented a computational approach to grain size evolution and mechanical properties of hot rolled rod. Yu et al. [3] developed an online Stelmor controlled cooling system for the stabilization of process operation. These numerical models have been successfully applied to controlled cooling process for realizing stable operation and improving product quality. Thus, in industrial practice, with more and more manipulated variables under control, the fact that the product quality varies with season and climate is more and more outstanding.

But up to now, it is no available in the literature to describe the quantitative analysis on the impacts of ambient temperature and humidity upon the cooling process of hot rolled steel. Fortunately, some investigations in the similar treatment were reported, Brenn. [4] Discussed the effects of ambient conditions on the drying process of liquid coatings on round metal wires. Page et al. [5] reported a model to analyze the effects of ambient conditions during air treatment operations of food. These research results provide base for the study of the effects of ambient conditions on the controlled cooling of hot-rolled wire rod of steel.

Steel Mills Lamination Coils Cooling, an integrated model for describing the effects of ambient conditions on the cooling performance of hot-rolled steel wire after rolling is presented. The effects of moist air on heat transfer have been derived from the theoretical and empirical models with the involved ambient conditions, and the results are used to calculate the temperature evolution and phase transformation of high-carbon steel, SWRH82B, by numerical approach. Then the predicted values of ultimate tensile strength are compared with the industrial trials to validate the model. Additionally, the inverse solution of wind speed is also discussed for realizing stable production process under different ambient conditions.

In hot-rolled steel production processes, controlled cooling after finishing rolling plays an important role on the final microstructure and mechanical properties of product. Steel coil produced at a steel mill after the laminate must be cooled from a temperature of 673.15 K to ambient temperature to be transported and sold. In this article a model to simulate and measure the rate of cooling coil is developed. The coil geometry employed is a cylinder with height between 1.6 m and 1.8 m and an outer diameter of 1.8 m. They have a few diameter co-axial hollow centre. The coils cooling take between 4 and 6 days depending on weather conditions. Usually the cold coil will be stored in a warehouse.

It produces unwanted stocks and thus represents a "bottleneck" in the marketing process. In this study, the process of coils cooling is studied using CFD techniques. To do so, 2D (two-dimensional) axisymmetric and 3D (three dimensional) transient models were used. The objective is to obtain the optimal rate of temperature decrease depending on the geometry and the orientation (horizontal or vertical arrangement) of the coils.

2. Material and methods – The geometry of the coils is cylindrical with an inner diameter of 0.18 m and outside diameter of 0.9 m and 1.8 m high. The coil is assumed to be located in a spacious room measuring 4.5 m x 4.5 m for 2D axisymmetric and 6 m x 6 m x 6 m for 3D model. Natural convection process for cooling was considered. In the present study, the geometry are performed using Gambit 2.4.6 Fluent Inc. USA and CFD package ANSYS FLUENT 16.0.0. for the simulations. To study vertical and horizontal coils cooling, 2D axisymmetric and 3D transient models were used respectively.

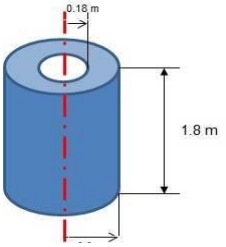

Image 2. Steel coil dimensions


Image 3. 2D Axisymmetric models 10,000 cells

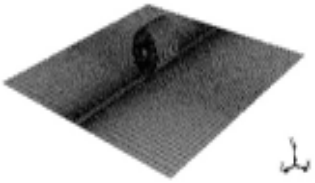
Image 4. 3D model 230826 cells

The 2D energy equation is as follows:

$$\frac{\partial}{\partial x}\left(k\frac{\partial T}{\partial x}\right)+\frac{\partial}{\partial y}\left(k\frac{\partial T}{\partial y}\right)+\dot{q}=\rho C_p\frac{\partial T}{\partial t} \quad (1)$$

where T and t are temperature and time.

3D ANSYS FLUENT solves the energy equation in the following form:

$$\frac{\partial y}{\partial t}(\rho E)+\nabla.\left(\vec{v}(\rho E+p)\right)=\nabla\left(k_{eff}\nabla T-\sum_j h_j\vec{J}_j+(\bar{\bar{\tau}}_{eff}.\vec{v})\right)+S_h \quad (2)$$

Where k_{eff} is the effective conductivity ($k+k_t$ where k_t is the turbulent thermal conductivity, defined according to the turbulence model being used), AND $\vec{J}_J$ is diffusion flux of species, *j*. The first three terms on the right hand-side represent energy transfer due to conduction, species diffusion, and viscous dissipation, respectively. S_h Includes the heat of chemical reaction, and any other volumetric heat sources:

$$E=h\frac{p}{\rho}+\frac{v^2}{2} \quad (3)$$

Where sensible enthalpy *h* is defined for ideal gas as

$$\boldsymbol{h}=\sum_j \boldsymbol{Y_j}\,\boldsymbol{h_j} \quad (4)$$

And for incompressible flow as

$$\boldsymbol{h}=\sum_j \boldsymbol{Y_j}\,\boldsymbol{h_j}+\frac{\boldsymbol{p}}{\boldsymbol{\rho}} \quad (5)$$

Y_j is the mass fraction of species *j* and

$$h_j=\int_{T_{ref}}^{T} C_p.jdT \quad (6)$$

The value used for T_{ref} in the sensible enthalpy calculation depends on the solver and model in use.

For transport equations model we using the standard $k-\varepsilon$, the turbulence kinetic energy *k* and its rate of dissipation, ε are obtained from the following transport equations:

$$\frac{\partial}{\partial t}(\rho k)+\frac{\partial}{\partial x_i}(\rho k u_i)=\frac{\partial}{\partial x_j}\left[\left(\mu+\frac{\mu_t}{\sigma_k}\right)\frac{\partial k}{\partial x_j}\right]+G_k+G_b-\rho\varepsilon-Y_M+S_k \quad (7)$$

$$\frac{\partial y}{\partial t}(\rho\varepsilon)+\frac{\partial}{\partial x_i}(\rho\varepsilon u_i)=\frac{\partial}{\partial x_j}\left[\left(\mu+\frac{\mu_t}{\sigma_\varepsilon}\right)\frac{\partial \varepsilon}{\partial x_j}\right]+C_{1\varepsilon}\frac{\varepsilon}{k}+(G_k+C_{3\varepsilon}G_b)-C_{2\varepsilon}\rho\frac{\varepsilon^2}{k}+S_\varepsilon \quad (8)$$

Standard wall function, Momentum boundary condition based on launder-Spaulding law-of-the wall velocity yields:

$$U^* = \frac{1}{k}\ln(Ey^*) \tag{9}$$

where:

$$U^* \equiv \frac{U_P C_\mu^{1/4} K_P^{1/2}}{\tau_w/\rho} \tag{10}$$

$$y^* \equiv \frac{\rho C_\mu^{1/4} K_P^{1/2} y_P}{\mu} \tag{11}$$

The equation for radiation model (DO) is:

$$\nabla.(I(\vec{r},\vec{s})\,\vec{s}\,) + (a+\sigma_s)I(\vec{r},\vec{s}) = an^2\frac{\sigma T^4}{\pi} + \frac{\sigma_s}{4\pi}\int_0^{4\pi} I\,(\vec{r},\vec{s}')\Phi(\vec{s},\vec{s}')d\Omega' \tag{12}$$

Natural cooling process is considered for both 2D axisymmetric and 3D models.
The selected Solver was pressure based, transient, and absolute.

a) Models use Energy equation, k-epsilon standard turbulence model, near-wall treatment and standard wall function.
b) Radiation model was DO (Discrete Ordinate)

Boundary conditions:

a) Bottom wall. It has been used calcium carbonate for assumption in the floor. Temperature 300 K.
b) Coils wall. Coupled was selected because thermal conditions were specified on the inner surface of the thin wall.
c) Left hand-side. The thermal condition that combines the convection and radiation boundary conditions by selecting the mixed option. With this thermal condition to set heat transfer coefficient, free stream temperature, external surface emissivity, and external radiation temperature is needed.
d) Upper. Set up radiation with specified external temperature.

3. Results and Discussion - To simulate the process, a transient simulations with different time steps were used. A sensitivity analysis demonstrated that the optimal time step is 800 s.
Table 1 and Image 5 show cooling coil mean temperature versus time comparison between 2D axisymmetric and 3D models. They are quite similar and almost identical from 3 to 5 days. Images 6 to 9 present the temperature and velocity maps for both models. They are coherent and show how the coils are cooling by natural convection and the most homogeneous temperature distribution corresponds to the horizontal arrangement of the coil (3D simulation).

Table 1. Cooling coils average temperature (K)

Days	2D Axisymmetric	3D
0	673.15	673.15
1/2	502.28	520.86
1	431.15	448.39
1.5	390.36	404.86
2	364.93	376.47
2.5	347.97	357.01
3	336.15	343.15
3.5	327.66	333.05
4	321.43	325.55
4.5	316.77	319.89
5	313.23	315.56

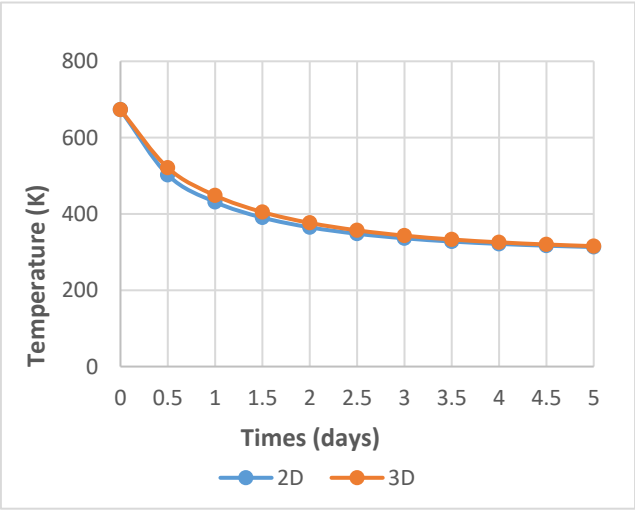

Image 5. Coil average temperature versus time

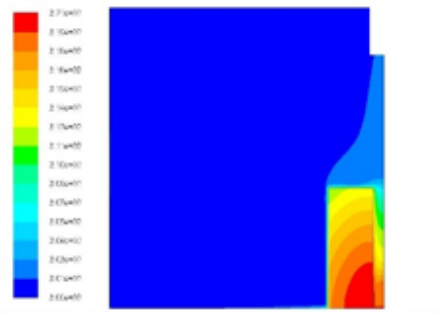

Image 6. Static temperature - 2D axisymmetric model

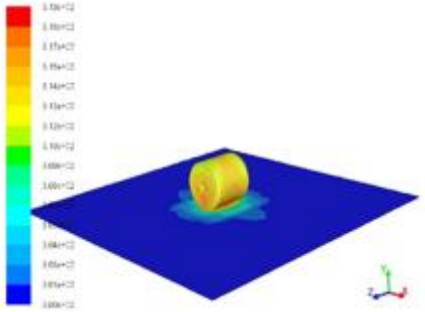

Image 7. Static temperature - 3D model

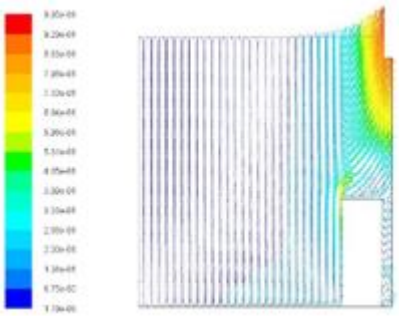

Image 8. Velocity vectors - 2D axisymmetric model

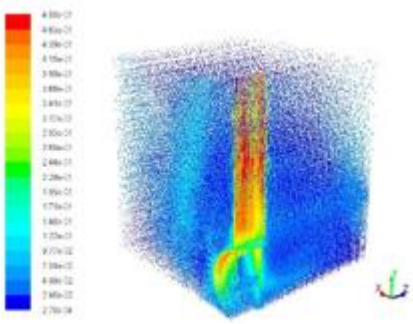

Image 9. Velocity vectors - 3D model

4. Conclusions - 2D axisymmetric and 3D simulation models have been used to study steel coils natural cooling. Both models are consistent and the results obtained are quite similar. It takes 5 days for a steel coil to be cooled from 673.15 K to ambient temperature; and relationship between average coils temperature and time is nearly equal. The most homogeneous temperature distribution corresponds to the horizontal arrangement of the coil.
In future works, cooling considering several rows of coils and optimal spatial arrangement will be studied, as well as the possibility of forced flow.

Acknowledgement
This work has been realized under Erasmus Mundus Swap and Transfer project, at the Department of Energy University of Oviedo, Spain.

5. References

[1] Nobari AH, Serajzadeh S. Modeling of heat transfer during controlled cooling in hot rod rolling of carbon steels. Applied thermal engineering. 2011 Mar 31;31(4):487-92.
[2] Phadke, Sameer, Praveen Pauskar, and Rajiv Shivpuri. "Computational modeling of phase transformations and mechanical properties during the cooling of hot rolled rod." *Journal of materials processing technology* 150.1 (2004): 107-115.
[3] Yu, Wan-Hua, et al. "Development and application of online Stelmor controlled cooling system." *Applied Thermal Engineering* 29.14 (2009): 2949-2953.
[4] Czaputa, Klaus, and Günter Brenn. "The convective drying of liquid films on slender wires." *International Journal of Heat and Mass Transfer* 55.1 (2012): 19-31.
[5] Le Page, Jean-François, et al. "Development of an approximate empirical-CFD model estimating coupled heat and water transfers of stacked food products placed in airflow." *Journal of Food Engineering* 92.2 (2009): 208-216.
[6] ANSYS FLUENT 14.5 Theory Guide, ANSYS Inc.